Experimental and theoretical studies of Notch signaling–mediated spatial pattern

Thesis by

Amit Lakhanpal

In Partial Fulfillment of the Requirements

for the Degree of

Doctor of Philosophy

California Institute of Technology

Pasadena, California

2014

(Defended July 2013)

For Mama, Papa, and Niti

Acknowledgments

Nothing of this work would have been possible without the support of my adviser, Michael Elowitz, for which I am very grateful. More than just that, his mentorship has been invaluable, including the excellent opportunity to work on all stages of the research process — finding a good problem, working out a program, grantwriting, working through iterations of experiments and analysis, writing up papers, going through peer review — and benefit from his expertise in each of them. I also owe a great debt of gratitude to David Sprinzak, who was in essence as a second adviser to me while he was a postdoc in the lab, and remained a strong source of support throughout. Their example is one from which I am very glad to have had the opportunity to learn.

It has also been my good fortune to have shared my time in the lab with some extraordinary people. Among them is our "Delta Force" of Lauren LeBon, Sandy Nandagopal, and Leah Santat, a group with which I am proud to have worked so closely and for whose advice and support over the years I am thankful. Joe Levine, Fred Tan, and Jon Young, even if their tastes in model systems tended to run in different directions, were particularly good partners in fun-for-fun's-sake to lighten the atmosphere on occasion.

Outside of the lab, I truly appreciated the the warm and welcoming TACIT community through which I had the chance to meet some truly fantastic people who were a source of tremendous support.

Finally, my graduate studies have been supported by the Fannie and John Hertz Foundation, for which I am very grateful.

Abstract

Notch signaling acts in many diverse developmental spatial patterning processes. To better understand why this particular pathway is employed where it is and how downstream feedbacks interact with the signaling system to drive patterning, we have pursued three aims: (i) to quantitatively measure the Notch system's signal input/output (I/O) relationship in cell culture, (ii) to use the quantitative I/O relationship to computationally predict patterning outcomes of downstream feedbacks, and (iii) to reconstitute a Notch-mediated lateral induction feedback (in which Notch signaling upregulates the expression of Delta) in cell culture. The quantitative Notch I/O relationship revealed that in addition to the *trans*-activation between Notch and Delta on neighboring cells there is also a strong, mutual *cis*-inactivation between Notch and Delta on the same cell. This feature tends to amplify small differences between cells. Incorporating our improved understanding of the signaling system into simulations of different types of downstream feedbacks and boundary conditions lent us several insights into their function. The Notch system converts a shallow gradient of Delta expression into a sharp band of Notch signaling without any sort of feedback at all, in a system motivated by the *Drosophila* wing vein. It also improves the robustness of lateral inhibition patterning, where signal downregulates ligand expression, by removing the requirement for explicit cooperativity in the feedback and permitting an exceptionally simple mechanism for the pattern. When coupled to a downstream lateral induction feedback, the Notch system supports the propagation of a signaling front across a tissue to convert a large area from one state to another with only a local source of initial stimulation. It is also capable of converting a slowly-varying gradient in parameters into a sharp delineation between high- and low-ligand populations of cells, a pattern reminiscent of smooth muscle specification around artery walls. Finally, by implementing a version of the lateral induc-

tion feedback architecture modified with the addition of an autoregulatory positive feedback loop, we were able to generate cells that produce enough *cis* ligand when stimulated by *trans* ligand to themselves transmit signal to neighboring cells, which is the hallmark of lateral induction.

Contents

Chapter 1

Introduction

Integral to most modern definitions of 'life' is the capacity to reproduce. Complex multicellular organisms, in order to satisfy this imperative, cycle between the single-cell zygotic state and the adult form. Developmental biology addresses the mechanisms by which a single cell under suitably supportive conditions can reliably proceed to generate a functional, fully-formed multicellular organism. The developmental trajectory must include growth in the number of cells by division, specialization of cellular function by differentiation, and proper ordering of those processes in space and time by means of some regulation. Such regulation frequently arises from communication between initially equivalent cells which, under the influence of a feedback network, coordinate to achieve a spatially patterned outcome. Our primary interest in this work is to understand the basis of spatial patterning by studying the interactions between intercellular signaling systems and intracellular feedback networks, using both *in silico* computation and *in vitro* experimental methods.

The modern body of knowledge in a wide variety of developmental spatial and temporal patterns is vast, with ancient origins in the description of macroscopically-discernible stages of embryological development [1]. Over time advances in the state of technology allowed progressively more refined observational and eventually experimental approaches. Microscopy and the cell theory of biology made visible early steps in establishing body plan [2], and transplantation experiments [3] began to reveal the important role of interactions between different types of cells in initiating patterning processes. Eventually knowledge of the genetic basis of biological activity led to the search for genetic influences on development [4]. Classical genetic approaches involved careful observation of normal

wild type patterning outcomes, so that the outcome of mutagenesis can be compared against normal. Screens involving visible features (such as the number and polarity of segments in an embryo in the seminal *Drosophila* work of Nüsslein-Volhard and Wieschaus [5]) identified many determinants of spatial pattern, and have been complemented over time with improvements in imaging techniques allowing more detailed probes of structure formation processes. This has been especially crucial with respect to dynamic patterns of gene expression that were inaccessible in realtime (or otherwise) before effective fluorescent imaging. In addition, progressively greater sophistication in manipulating the genomes of model organisms has enabled a wider spectrum of genetic perturbations, allowing control over the timing, spatial distribution, and strength of mutant alleles that has been critical in understanding how components of signaling systems and regulatory networks interact to drive spatial pattern.

As much as approaches to studying development have evolved over time, they remain fundamentally tied to studying patterns in the context where they arise naturally. This has many advantages, especially with respect to physiological relevance, but there are also important limitations. When manipulating an endogenous pathway it is not possible to make claims of sufficiency for any proposed mechanism, because in natural systems every component is embedded in a dense interaction network. The specificity of a phenomenon to a particular organism, or its generality across species, cannot be rigorously assessed exclusively in natural systems. Especially in development, when a process of interest might be one of many occurring simultaneously in a highly dynamic environment, the natural context may be exceedingly difficult to measure or manipulate. Part of the promise of synthetic approaches to biology is to overcome such challenges [6]. If a proposed mechanism for a phenomenon, such as reasonably stable oscillations, can successfully capture the desired behavior when implemented using components orthogonal to the host organism [7,8], it constitutes a proof of sufficiency. Successfully transplanting a proposed regulatory network architecture into an *in vitro* system also offers support for cross-species generality. Synthetic approaches to reconstruct behaviors have been recently employed beyond prokaryotes in mammalian cell culture [9]. These motivations drive our intention to gain insight into developmental pattern formation by synthetically

reconstituting putative minimal regulatory networks in mammalian cell culture.

As mentioned earlier, communication between cells is required for the kind of bottom-up spatial patterning events observed throughout development. A small number of signaling pathways are employed for this purpose in development, among which is the Notch signaling pathway [10]. The first observed phenotype due to a mutation in the gene that would come to be known as Notch arose in *Drosophila*, where the allele in question generated malformed wings with notches along their margin [11,12]. Further studies of *Drosophila* with mutant Notch alleles showed an effect on the distribution of cell types [13], in particular between neurons and ectoderm, suggesting a role in cell fate determination. Work in what would prove to be the Notch ortholog in *C. elegans* [14], lin-12, provided evidence that the action of Notch was partly cell non-autonomous [15] — that it normally depended on interactions with a neighboring cell. Searches in *Drosophila* for mutations in other genes with similarity to the Notch phenotype proved successful, including the identification of Delta (so named for the thickening of wing veins in Delta heterozygotes). Delta was established to be a ligand for Notch by a variety of evidence including gene dosage mosaic analysis [16]. From these early experiments elucidating the roles of Notch signaling in specific model systems, knowledge of the signaling system's importance due to its frequent use throughout development, its conservation across species, and its complexity via additional regulators of signaling has grown considerably [10,17].

Notch refers to a family of single-pass transmembrane receptors (ranging from one member in *Drosophila* to four in mammals) with a series of EGF-like repeats in the extracellular part and an intracellular part containing nuclear localization signals and a trans-activating domain [18]. The canonical partners of the Notch family are the transmembrane DSL (Delta/Serrate/Lag-2) ligands — Delta and Serrate in *Drosophila*, Delta-like(Dll)1/3-4 and Jagged1-2 in mammals [18]. The extracellular EGF-like repeats of Notch receptors and DSL ligands interact in *trans* on the surfaces of neighboring cells, which generates a force [19] exposing a site on the receptor to a cleavage event that ultimately leads to release of the receptor intracellular domain and its trafficking into the nucleus, where it regulates downstream genes. A receptor and a ligand on the surface of the same

cell can also bind in *cis*, which has an inhibitory effect on signaling [20].

Notch signaling is implicated in a wide variety of spatial patterning processes including the specification of neural and epidermal cells from neuroectoderm [21], organization of sensory regions in the inner ear [22], wing vein boundary sharpening in *Drosophila* [23], and smooth muscle specification surrounding artery walls [24]. In neural specification the Notch system engages a type of feedback known as 'lateral inhibition' in which Notch signaling downregulates Delta expression, which leads to an alternating spatial pattern of Notch activity (referred to as a lateral inhibition pattern). In the *Drosophila* wing vein, the boundary between vein and intervein cells is sharpened in a Notch-dependent process. The specification of smoooth muscle surrounding the walls of some arteries is a 'lateral induction' process, in which Notch signaling activates expression of ligand. In each of these cases, the combination of (i) a signaling system, (ii) a downstream regulatory feedback, and (iii) specific initial conditions drive the system to a patterned outcome.

Our first step toward synthetically reconstituting developmental spatial pattern was to choose a signaling system and characterize its properties relevant to patterning. We chose the Notch signaling system, and decided that in order to gain insight into why the Notch system is used in specific natural patterning processes and to rationally compose synthetic pattern-generating feedbacks it was necessary to quantitatively understand the relationship between ligand levels (in *cis* and in *trans*) and the system's signal output. In spite of the system's developmental importance and the vast literature relating to it, such a measurement had not been reported. The results of our measurement of the system input/output relationship for the Notch1/Dll1 pair have been published [25], and appear as Chapter 2 of this thesis. My contributions to the work were principally in data analysis and computations relating to the interpretation of the data, including its potential developmental relevance.

Second, we have taken the insights into the Notch system from its ligand response profile and applied them to a variety of spatial patterns known to employ Notch signaling. This computational work comprises the content of Chapter 3. Its first section, published with my contribution as equal first author [26], reports on our findings regarding the effect of *cis*-inhibition in models of boundary

formation and lateral inhibition motivated by specific developmental processes. The second section expands on an exceptionally elegant mechanism for lateral inhibition that I conceived during our analysis of the Notch signaling response function data [27]. Lastly, the third section presents my unpublished work on the potential for patterning with a lateral induction feedback.

Third, we have sought to implement a pattern-forming feedback downstream of the Notch signaling system in mammalian cell culture. Chapter 4 describes an attempt to synthetically reconstitute lateral induction signaling in CHO-K1 cells, a standard mammalian cell culture line. It also reports on the effect of rewiring the feedback circuit to incorporate an additional auto-activating positive feedback. Ultimately, taken together we quantitatively characterize the signaling behavior of the Notch system, computationally assess the significance of this behavior combined with feedbacks in spatial patterning processes, and attempt to reconstitute the lateral induction behavior in cell culture.

References

1. Needham, J. *A History of Embryology.* (The University Press, Cambridge, UK, 1959).

2. De Felici, M. & Siracusa, G. The rise of embryology in Italy: from the Renaissance to the early 20th century. *Int J Dev Biol* **44**, 515-521 (2000).

3. De Robertis, E.M. Spemann's organizer and self-regulation in amphibian embryos. *Nat Rev Mol Cell Biol* **7**, 296-302 (2006).

4. Ernst, S.G. Offerings from an Urchin. *Developmental Biology* **358**, 285-294 (2011).

5. Nüsslein-Volhard C. & Wieschaus E. Mutations affecting segment number and polarity in Drosophila. *Nature* **287**, 795-801 (1980).

6. Sprinzak, D. & Elowitz, M.B. Reconstruction of genetic circuits. *Nature* **438**, 443-448 (2005).

7. Stricker J. *et al.* A fast, robust and tunable synthetic gene oscillator. *Nature* **456**, 516-519 (2008).

8. Elowitz, M.B. & Leibler, S. A synthetic oscillatory network of transcriptional regulators. *Nature* **405**, 335-338 (2000).

9. Weber W. & Fussenegger M. Synthetic gene networks in mammalian cells. *Curr Opin Biotechnol* **21**, 690-696 (2010).

10. Bray S.J. Notch signaling: a simple pathway becomes complex. *Nat Rev Mol Cell Bio* **7**, 678-689 (2006).

11. Dexter, J.S. The analysis of a case of continuous variation in Drosophila by a study of its linkage. *The American Naturalist* **48**, 712-758 (1914).

12. Morgan, T.H. & Bridges C.B. *Sex-linked inheritance in Drosophila.* (Carnegie Institution, Washington D.C., 1916).

13. Poulson D.F. Chromosomal deficiencies and the embryonic development of Drosophila melanogaster. *PNAS* **23**, 133-137 (1937).

14. Greenwald, I. lin-12, a nematode homeotic gene, is homologous to a set of mammalian proteins that includes epidermal growth factor. *Cell* **43**, 583-590 (1985).

15. Greenwald, I. Notch and the awesome power of genetics. *Genetics* **191**, 655-669 (2012).

16. Heitzler, P. & Simpson, P. The choice of cell fate in the epidermis of Drosophila. *Cell* **64**, 1083-1092 (1991).

17. Guruharsha, K.G., Kankel M.W. & Artavanis-Tsakonas S. The Notch signaling system: recent insights into the complexity of a conserved pathway. *Nat Rev Gen* **13**, 654-666 (2012).

18. Radtke, F., Schweisguth, F. & Pear, W. The Notch 'gospel'. *EMBO Rep* **6**, 1120-1125 (2005).

19. Musse, A.A., Meloty-Kapella, L. & Weinmaster, G. Notch ligand endocytosis: Mechanistic basis of signaling activity. *Seminars in Cell & Developmental Biology* **23**, 429-436 (2012).

20. D'Souza, B., Meloty-Kapella, L. & Weinmaster, G. Canonical and Non-Canonical Notch Ligands. *Current Topics in Developmental Biology* **92**, 73-129 (2010).

21. Kunisch M., Haenlin M., & Campos-Ortega J.A. Lateral inhibition mediated by the Drosophila neurogenic gene delta is enhanced by proneural proteins. *PNAS* **91**, 10139-10143 (1994).

22. Kiernan A.E. Notch signaling during cell fate determination in the inner ear. *Semin Cell Dev Biol* **24**, 470-479 (2013).

23. Huppert, S.S., Jacobsen, T.L. & Muskavitch, M.A. Feedback regulation is central to Delta-Notch signalling required for Drosophila wing vein morphogenesis. *Development* **124**, 3283 -3291 (1997).

24. Manderfield, L.J. *et al.* Notch activation of Jagged1 contributes to the assembly of the arterial wall. *Circulation* **125**, 314-323 (2012).

25. Sprinzak, D. *et al.* Cis-interactions between Notch and Delta generate mutually exclusive signalling states. *Nature* **465**, 86-90 (2010).

26. Sprinzak, D., Lakhanpal, A., LeBon, L., Garcia-Ojalvo, J. & Elowitz, M.B. Mutual Inactivation of Notch Receptors and Ligands Facilitates Developmental Patterning. *PLoS Comput Biol* **7**, e1002069 (2011).

27. Lakhanpal, A., Sprinzak, D., & Elowitz, M.B. Mutual inactivation of Notch and Delta permits a simple mechanism for lateral inhibition patterning. *arXiv*:1005.4301v1 (2010).

Chapter 2

Cis-interactions between Notch and Delta generate mutually exclusive signalling states

This chapter has been published[1] in identical form, save for differences between journal and thesis formatting requirements. My contribution as described in the published manuscript was to the data analysis, and in providing input for writing the paper. I also contributed significantly to the analysis of the potential pattern-related consequences of the *cis*-inhibition feature reported in the paper.

Abstract

The Notch-Delta signalling pathway allows communication between neighbouring cells during development [1]. It has a critical role in the formation of 'fine-grained' patterns, generating distinct cell fates among groups of initially equivalent neighbouring cells and sharply delineating neighbouring regions in developing tissues [2-5]. The Delta ligand has been shown to have two activities: it transactivates Notch in neighbouring cells and *cis*-inhibits Notch in its own cell. However, it remains unclear how Notch integrates these two activities and how the resulting system facilitates pattern formation. Here we report the development of a quantitative time-lapse microscopy platform for analysing Notch-Delta signalling dynamics in individual mammalian cells, with the aim of addressing these issues. By controlling both *cis*- and *trans*-Delta concentrations, and monitoring

[1]Sprinzak, D., Lakhanpal, A., LeBon, L., Santat, L.A., Fontes, M.E., Anderson, G.A., Garcia-Ojalvo, J., & Elowitz, M.B. Cis-interactions between Notch and Delta generate mutually exclusive signalling states. *Nature* **465**, 86-90 (2010).

the dynamics of a Notch reporter, we measured the combined *cis*-*trans* input-output relationship in the Notch-Delta system. The data revealed a striking difference between the responses of Notch to *trans*- and *cis*- Delta: whereas the response to *trans*-Delta is graded, the response to *cis*-Delta is sharp and occurs at a fixed threshold, independent of *trans*-Delta. We developed a simple mathematical model that shows how these behaviours emerge from the mutual inactivation of Notch and Delta proteins in the same cell. This interaction generates an ultrasensitive switch between mutually exclusive sending (high Delta/low Notch) and receiving (high Notch/low Delta) signalling states. At the multicellular level, this switch can amplify small differences between neighbouring cells even without transcription-mediated feedback. This Notch-Delta signalling switch facilitates the formation of sharp boundaries and lateral-inhibition patterns in models of development, and provides insight into previously unexplained mutant behaviours.

Letter

Notch and Delta are single-pass transmembrane protein families found in metazoan species. Delta in one cell can bind to, and transactivate, Notch in a neighbouring cell. This interaction results in proteolytic release of the Notch intracellular domain, which translocates to the nucleus and activates target genes6 (Fig. 1a). Delta also has a second role, inhibiting Notch activity in its own cell (*cis*-inhibition) [7-10]. *Cis*-inhibition has been shown to involve direct interaction of the two proteins [11], but current understanding is incomplete [12].

To understand how concentrations of *cis*- and *trans*-Delta are integrated by the Notch pathway (Fig. 1b), we constructed cell lines that allowed us to modulate the concentrations of *cis*- and *trans*-Delta independently, and to monitor quantitatively the transcriptional response of a Notch reporter (Fig. 1c and Supplementary Fig. 1). These cell lines stably expressed Notch receptors and corresponding yellow fluorescent protein (YFP) reporters of Notch activity (Supplementary Figs 1 and 2). They also contained a doxycycline-inducible chimaeric rat Dll1-mCherry fusion gene (Delta-mCherry; Supplementary Fig. 3). In our main cell line, hN1G4^{esn}, the intracellular domain of human NOTCH1 was replaced with a minimal variant of the transcriptional activator Gal4, denoted Gal4^{esn}

[13], to avoid activation of endogenous Notch targets [14-16]. A second cell line, hN1, containing the full-length human NOTCH1 was analysed as a control (Supplementary Fig. 1). Notch messenger RNA expression levels in these cells were comparable to those observed in early T-cell progenitors where Notch is active [17] (Supplementary Information).

We first asked how Notch activity depends on the concentration of *trans*-Delta. We adsorbed fusion proteins, consisting of immunoglobin-G (IgG) fused to the extracellular domain of human DLL1 ($\text{Delta}^{\text{ext}}$), to the surface of plates at different concentrations, denoted D_{plate} (Fig. 2a and Supplementary Fig. 4) [18,19], and recorded time-lapse movies of Notch activation. Before the start of each movie ($t < 0$), we inhibited Notch activation using the γ-secretase inhibitor *N*-[*N*-(3,5-difluorophenacetyl)-L-alanyl]- *S*-phenylglycine t-butyl ester (DAPT). At $t = 0$, DAPT was washed out, allowing the fluorescent reporter to accumulate at a rate determined by Notch activity (Fig. 2b, c and Supplementary Movie 1). The YFP production rate showed a graded response to D_{plate}, well-fitted by a Hill function with a modest Hill coefficient (Fig. 2d).A similar response was observed in the hN1 cell line (Supplementary Figure 1). This graded response was not due to the use of plate-bound ligands: when cells expressing only Delta were co-cultured with cells expressing only Notch, we observed a similarly graded dependence of Notch activity on the level of Delta expression, but with greater variability (Supplementary Fig. 5).

We next set out to quantify the response of Notch to varying concentrations of *cis*-Delta in the $\text{hN1G4}^{\text{esn}}$ cell line. We used a scheme in which Delta-mCherry was expressed in a pulse before the start of the movie and subsequently allowed to dilute, effectively titrating its concentration [20] (Fig. 3a). These experiments were performed at low cell density, where relatively weak inter-cellular activation of Notch is observed (Supplementary Fig. 6), and transactivation was induced predominantly by D_{plate}. At the beginning of the movie, Notch reporter expression was fully inhibited by high Delta- mCherry concentrations (Fig. 3b and Supplementary Movie 2). Subsequently, Delta-mCherry concentrations gradually declined on a timescale of $\tau_D = 32 \pm 2.5$ h, consistent with dilution by cell growth and division (Fig. 3c). At $t_{\text{on}} \approx 40$ h, we observed a sharp onset of reporter expression in the median response of the population (Fig. 3c). Even sharper responses were evident

in individual cell lineages (Fig. 3d-f and Supplementary Fig. 13). Similar behaviour was observed in the hN1 cell line (Supplementary Fig. 7)

To quantify the sharpness of *cis*-inhibition, we computed the rise time, denoted τ_{rise}, required for Notch activity to increase by a factor of e in individual cells (Fig. 3e and Fig. 3a, inset). The distribution of τ_{rise} showed a median of 2.6 h, which is considerably less than τ_{D} (Fig. 3f). For comparison, an equivalently sharp Hill function of *cis*-Delta would require a Hill coefficient of $\tau_{\text{D}}/\tau_{\text{rise}} < 12$.

We repeated the experiment for a variety of D_{plate} values, allowing us to directly measure the integrated response of Notch across the two-dimensional input space of *cis*- and *trans*-Delta concentrations (Fig. 3g and Supplementary Fig. 14). Activation occurred at a similar value of t_{on} and, therefore, a similar *cis*-Delta concentration, regardless of D_{plate}, as indicated by the fixed position of the transition from black to green points in Fig. 3g. In addition, the activation remained sharp at all D_{plate} values for which it could be clearly measured.

Thus, an explanation for the observed *cis*- and *trans*-signal integration must simultaneously account for the three key features of the experimental data: a graded response to *trans*-Delta (Fig. 2d), a sharp response to *cis*-Delta (Fig. 3c-f) and a fixed threshold for *cis*-inhibition across varying concentrations of *trans*-Delta (Fig. 3g). We show here that a simple model can explain these observations in a unified way (Box 1 and Fig. 3h). The model's key assumption is that Notch and Delta in the same cell mutually inactivate each other. As shown in Box 1, strong enough mutual inactivation can produce an ultrasensitive switch between two mutually exclusive signalling states: cells can be in a predominantly 'sending' state, with high Delta concentration and low Notch concentration, or a 'receiving' state, with high Notch concentration and low Delta concentration, but cannot be in both states at the same time. Alternative models that do not include mutual inactivation fail to account for the observed data (Supplementary Fig. 8).

The three features described above emerge naturally in this model. First, in the absence of *cis*-Delta, the rate of Notch activation is proportional to the *trans*-Delta concentration, generating a graded response. Second, a sharp response to *cis*-Delta results from mutual inactivation, which

causes an excess of either protein to strongly diminish the activity of the other. Finally, the switching point occurs when Notch and *cis*-Delta concentrations are comparable, and is therefore only weakly dependent on *trans*-Delta.

The mutual-inactivation model predicts cis-inhibition, not just of Notch by Delta but also of Delta by Notch. This interaction is supported by results in other systems [12,21,22]. We tested this prediction in our system using a transactivation assay based on co-culture of Delta-expressing sending cells with Notch reporter cells. Expression of Notch in the Delta-expressing cells reduced their ability to transactivate, as predicted (Supplementary Fig. 9). The exact biochemical mechanism of mutual inactivation remains unclear, but we observed no sharp drop in the total cellular Delta-mCherry fluorescence during switching, suggesting that the inactive complex may be stable in these conditions (Fig. 3c, d).

This signalling switch has important implications for multicellular patterning. To understand these implications, consider two neighbouring cells that produce Notch and Delta at constant rates (Fig. 4a). A slight excess of Notch production in one cell and a slight excess of Delta production in its neighbour can generate a strong signalling bias in one direction: the first cell becomes a receiver and the second becomes a sender. In this way, a small difference in production rates between cells is amplified into a much larger difference in Notch activity (Fig. 4b). This amplification does not require transcriptional regulation or feedback.

The send-receive signalling switch can facilitate formation of sharp boundaries. For example, in Drosophila Notch and Delta sharply delineate wing vein boundaries [4,5]. In this system, Delta production is initially expressed in a graded profile transverse to the vein. Eventually, Notch signalling is restricted to two sharp side bands on either side of the vein axis.

As a simplified model, we simulated the development of a field of cells with a graded rate of Delta production and a uniform rate of Notch production (Fig. 4c). The mutual-inactivation model generated sharply defined side bands of Notch signalling at positions where the two production rates intersect, that is, where sender and receiver cells are next to each other (Fig. 4c). Moreover, this model explains a striking mutant behaviour that occurs in the *Drosophila* wing vein system.

Although Notch and Delta are individually haploinsufficient (causing thicker veins), the Notch$^{+/-}$ Delta$^{+/-}$ double mutant restores the wild-type phenotype [23]. This suppression of the single-mutant phenotypes in the double mutant emerges automatically in the model because proportional rescaling of the Notch and Delta production rates does not move their intersection points (Fig. 4d). This suppression is maintained across a broad range of parameter values and persists even with additional feedbacks (Supplementary Fig. 10c), but is difficult to explain in other models (Supplementary Fig. 10a and Supplementary Information).

The send-receive signalling switch can also facilitate lateral-inhibition patterning. When Notch transcriptionally downregulates Delta expression, the resulting intercellular positive-feedback loop can generate 'checkerboard' patterns of Notch activity [24,25] (Fig. 4e). Without mutual inactivation, pattern formation requires a minimum Hill coefficient of $n = 2$, or higher, in the regulatory feedback loop (Fig. 4f, left, and Supplementary Information). Although we cannot rule out such cooperativity, or additional feedback loops, no evidence for strongly cooperative transactivation was observed here or previously (Fig. 2d and Supplementary Fig. 1). In contrast, mutual inactivation allows patterning even without cooperativity, by introducing a sharp response to changes in Delta expression (Fig. 4f, right). In addition, for strong enough *cis*-inhibition, mutual inactivation allows cells with high Delta concentrations to coexist next to one another in the steady state, leading to a broader range of possible patterns (Supplementary Fig. 17). Finally, we note that low concentrations of free Notch and Delta exist in sender and, respectively, receiver cells for finite mutual-inactivation strengths (Supplementary Fig. 11). The resulting signalling between like cells (senders or receivers) can have a role in lateral-inhibition patterning dynamics.

Modeling Box

Here we describe a simple model of Notch-Delta interactions that explains the experimental data and provides insight into developmental patterning processes. The model involves several reactions. First, during intercellular signalling, Notch in one cell binds to extracellular Delta, of concentration D_{trans}, leading to release of the Notch intracellular domain and degradation of its extracellular

domain [6]. Similarly, Notch in a neighbouring cell, N_{trans}, can bind to Delta. Second, Notch binds irreversibly to Delta in the same cell to form a stable, inactive, complex, which is effectively removed from the system [12]. Finally, Notch and Delta are produced at constant rates, and degraded and/or diluted at a constant rate, in addition to being removed through the interactions described above.

These reactions can be expressed as a set of ordinary differential equations for the concentrations of free Notch, N, and free Delta, D, in an individual cell. An additional equation represents the intracellular domain of Notch, S, which activates expression of the fluorescent reporter gene:

$$\begin{aligned}
\frac{dN}{dt} &= \beta_N - \gamma N - \frac{DN}{k_c} - \frac{D_{trans}N}{k_t} \\
\frac{dD}{dt} &= \beta_D - \gamma D - \frac{DN}{k_c} - \frac{DN_{trans}}{k_t} \\
\frac{dS}{dt} &= \frac{D_{trans}N}{k_t} - \gamma_S S
\end{aligned}$$

Here D_{trans} represents $\mathrm{D_{plate}}$ in Figs 2 and 3, but could also represent Delta concentration in one or more neighbouring cells (Supplementary Information). Similarly, D in these equations corresponds to *cis*-Delta in the experiments, and β_N and β_D denote the production rates of Notch and Delta, respectively. The combined degradation and dilution rate, γ, is assumed for simplicity to be the same for Notch and Delta, and γ_S is the rate of decay of S. We write k_c and k_t to denote the strengths of *cis*-inhibition and transactivation, respectively. See Supplementary Information for a more detailed description.

In the steady state, mutual inactivation leads to a switch between two qualitatively distinct behaviours, depending on the relative production rates of Delta and Notch. When $\beta_D > \beta_N$, excess Delta effectively inactivates almost all Notch, allowing cells to send, but not efficiently receive, signals. Conversely, when $\beta_D < \beta_N$, excess Notch effectively inactivates Delta, allowing cells to receive, but not efficiently send, signals. Thus, the system approaches two mutually exclusive signalling states: high Delta/low Notch ('sending'; pink shading in Figure), and high Notch/low Delta ('receiving'; blue shading in Figure). We note that this switch is not bistable.

In the steady state, the transition between the two regimes is ultrasensitive: near the threshold,

a relatively small change in β_D or β_N can lead to a much larger change in signalling (Supplementary Fig. 11). Related biochemical kinetics occur in bacterial small RNA and protein sequestration [27-29]. In Fig. 3, ultrasensitivity occurs dynamically in response to the decay of the total Delta concentration (Supplementary Information).

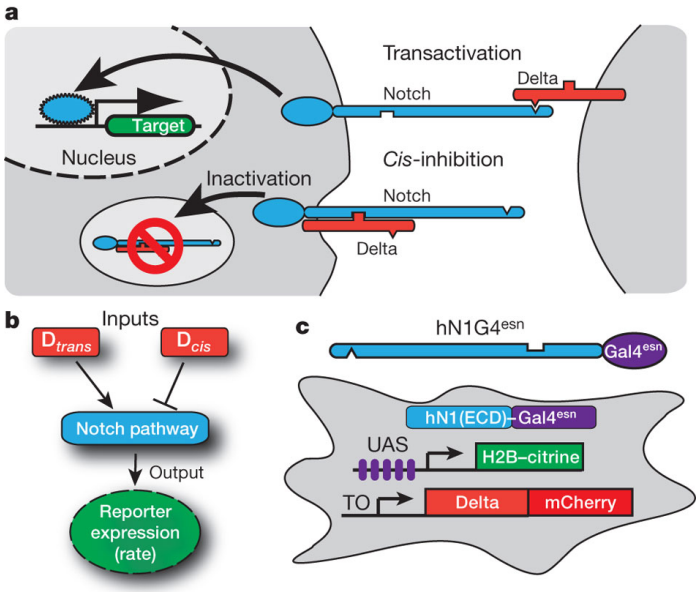

Figure 1: System for analyzing signal integration in the Notch-Delta pathway. a, Notch (blue) and Delta (red) interactions are indicated schematically. b, Notch activity integrates *cis*-and *trans*-Delta. c, T-REx-CHO-K1 cell line for analysing Notch activity. The hN1G4^{esn} cell line stably incorporates a variant of human NOTCH1 in which the activator Gal4^{esn} replaces the Notch intracellular domain (here hN1(ECD) is the extracellular domain of hN1). This cell line also contains genes for histone 2B (H2B)citrine (YFP) reporter controlled by an upstream activating sequence (UAS) promoter, a tetracycline-inducible (TO) DeltamCherry fusion protein and a constitutively expressed H2Bcerulean (cyan fluorescent protein, or CFP) for image segmentation (not shown). A similar cell line expressing full-length human NOTCH1 (the hN1 cell line) was also analysed (Supplementary Figs 1 and 2). These cells exhibit no detectable endogenous Notch or Delta activities. NotchDelta interactions are indicated schematically and do not represent molecular interaction mechanisms [11].

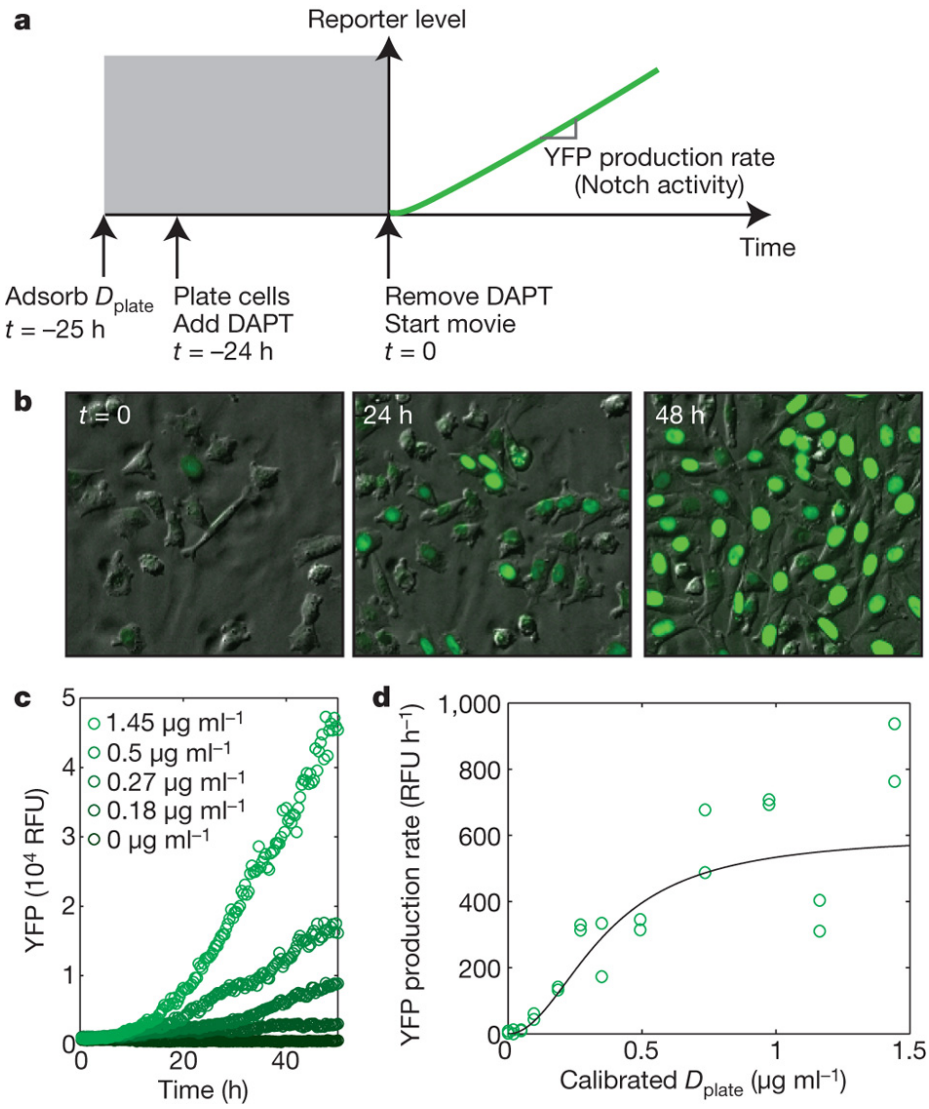

Figure 2: Transactivation of Notch occurs in a graded fashion. a, Experimental design. The rate of increase of fluorescence (slope of green line) is a measure of Notch activity. b, Typical hN1G4^{esn} filmstrip showing activation of Notch reporter (green), with $D_{plate} = 1.16$ μg ml^{-1} and frame times as indicated (Supplementary Movie 1; compare with Supplementary Fig. 6). c, hN1G4^{esn} cells respond in a graded manner to variations in D_{plate}. The data show the median fluorescence of individual cells within a single field of view for the indicated values of D_{plate} (see Supplementary Fig. 15 for distributions). RFU, relative fluorescence unit. d, The relationship between D_{plate} and Notch activity (in RFU per hour, from the linear regime in c). The Hill-function fit is indicated by the black line, which has Hill coefficient $n = 1.7$ (95% confidence interval, $n = 0.8 - -2.7$). Similar results were obtained using the hN1 cell line (Supplementary Fig. 1). We note that doxycycline does not directly affect Notch activation or cell growth, nor does D_{plate} affect cell growth (Supplementary Fig. 12).

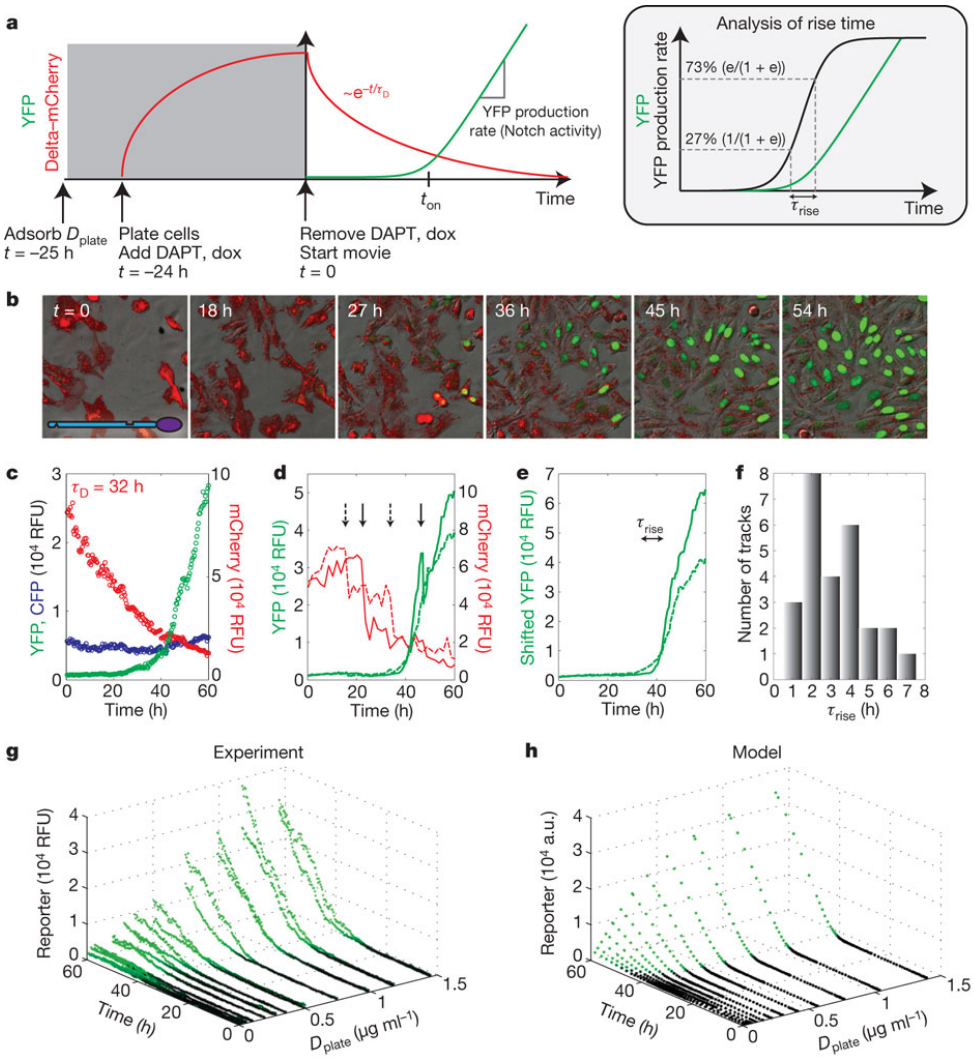

Figure 3: *Cis-trans* signal integration by Notch. a, Experimental protocol. Inset, the rise time, τ_{rise}, is the time required for Notch activity (black line or slope of green line) to change by a factor of e. dox, doxycycline. b, Filmstrip of hN1G4$^{\mathrm{esn}}$ cells, with $D_{plate} = 1.45$ μg ml^{-1} (Supplementary Movie 2), showing Delta-mCherry fluorescence (red) and concomitant activation of Notch reporter (green) at the indicated times (compare with Supplementary Fig. 6). c, Population average (median) response for the same movie shows a slow decay of Delta-mCherry fluorescence (red data), but a sharp response of reporter expression (green data). Constitutively expressed pCMV-H2B-cerulean (blue data) remains constant (control). Compare with the single-cell tracks in Supplementary Fig. 13 and the response to modulation of doxycycline in Supplementary Fig. 14. d, Single-cell response for two individual cells (solid and dashed lines, colours as in c). Black arrows mark cell divisions. e, Single-cell traces in d replotted, but shifted up after each cell division event to 'add back' sister-cell fluorescence, to show the continuity of Notch activity (see also Supplementary Fig. 13). f, Histogram of τ_{rise} from 26 non-overlapping cell lineages (Supplementary Fig. 13). g, Notch response to both *cis*- and *trans*-Delta. Data shown are from two duplicate movies acquired at each of 12 D_{plate} values for hN1G4$^{\mathrm{esn}}$ cells. Green colouring indicates data that exceed a detection threshold. Note that onset (the black-to-green transition) occurs at approximately the same time for all D_{plate} values. h, Simulations based on the model in Box 1 are qualitatively similar to data in g (see Supplementary Information and Supplementary Fig. 16 for model details). a.u., arbitrary units.

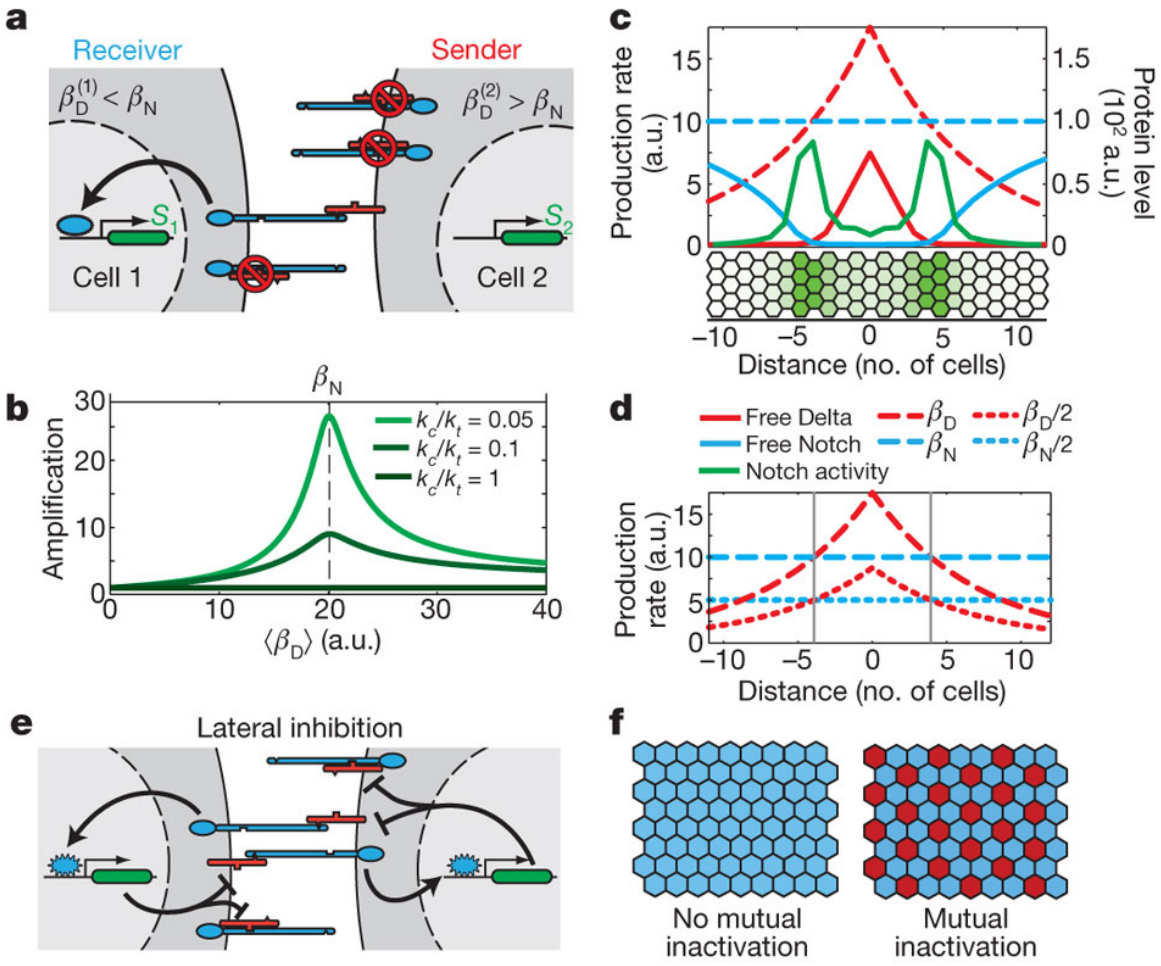

Figure 4: The mutual-inactivation model in multicellular patterning. a, Signal amplification. The two interacting cells have the same amount of Notch (here, two molecules) but different amounts of Delta (one or three molecules). Owing to the *cis*-interaction between Notch and Delta, signalling is strongly biased to cell 1. b, Notch amplifies differences between cells. Signal amplification, $(S_1/S_2 - 1)/(\beta_D^{(2)}/\beta_D^{(1)} - 1)$, for two interacting cells, with different Delta production rates, $\beta_D^{(2)} = 1.35\beta_D^{(1)}$ (see model in Supplementary Information). The x axis shows the average Delta production rate, $\langle\beta_D\rangle = (\beta_D^{(2)} + \beta_D^{(1)})/2$. Maximum amplification occurs when Delta production rates flank β_N (vertical dashed line). Stronger mutual inactivation (smaller k_c/k_t) increases signal amplification. c, d, Sharp boundary formation in response to a gradient of Delta production. c, Simulation of a field of interacting cells in which Delta production rates decay exponentially from the centre, according to $\beta_D(x) = \beta_D^0 \exp(-x/x_0)$ with $x_0 = 7$ cells (dashed red line). The Notch production rate, β_N, is constant (dashed blue line). The resulting free Notch and Delta protein levels are indicated (solid lines). Notch activation occurs in two sharply defined columns of cells (green line in plot and green cells in cellular diagram). d, Suppression of mutant phenotypes is explained by the mutual-inactivation model. Grey lines indicate positions where $\beta_N = \beta_D(x)$, leading to Notch activity peaks. Simultaneous reduction of both Notch and Delta production rates by half maintains boundary positions (dotted lines) (Supplementary Fig. 10). e, f, Mutual inactivation facilitates lateralinhibition patterning (e). In the absence of cooperativity in regulatory feedback, a standard lateral-inhibition model [24] cannot pattern (f, left) but a model of lateral inhibition with mutual inactivation can (f, right).

Methods Summary

We assembled genetic constructs and cell lines by standard methods (Supplementary Table 1). All cell lines used in the main text (Supplementary Table 2) were derived from T-REx-CHO-K1(Invitrogen). Cell lines were constructed by sequential rounds of Lipofectamine 2000 (Invitrogen) transfection and selection. We isolated stably transfected clones by limiting dilution or FACS.

Time-lapse microscopy was performed with cells plated on 24-well glass-bottom plates (MatTek). For plate-bound Delta experiments, IgG-Delta$^{\mathrm{ext}}$ was adsorbed to the plate together with 5 μg ml^{-1} hamster fibronectin (Innovative Research) before cell plating. Before imaging, cells were switched to a low-fluorescence medium, consisting of 5% FBS in αMEM lacking riboflavin, folic acid, phenol red and vitamin B12. Movies were acquired using an Olympus IX81-ZDC microscope, equipped with an environmental chamber at 37°C supplying 5% CO_2, a $\times$20, numerical-aperture-0.7 objective, and automated acquisition software (METAMORPH (version 7.5.6.0), Molecular Devices).

We obtained western blots for Gal4 using standard protocols. Blots were probed using rabbit anti-Gal4 DBD primary antibody (sc-577, Santa Cruz Biotechnology; 1:200) followed by incubation with horseradish peroxidaselabelled anti-rabbit IgG secondary antibody (Amersham; 1:2,000). Bands were quantified using a VersaDoc gel imaging system (Bio-Rad). Quantitative PCR with reverse transcription was performed using standard protocols based on the RNeasy kit (Qiagen) and the iScript cDNA synthesis kit (Bio-Rad).

We analysed co-culture experiments for YFP fluorescence using a FACScalibur flow cytometer (Becton Dickinson) and standard protocols. Movies were analysed in several stages. First, individual cell nuclei were identified in CFP images using a custom algorithm (MATLAB, MathWorks R2007a) based on edge detection and thresholding of constitutively expressed H2B-cerulean fluorescence. Then, for analysis of single-cell expression trajectories, individual nuclei were tracked across frames using custom software (MATLAB, C) based on the softassign algorithm (Supplementary Information). All single-cell trajectories were validated manually. For further details, see Supplementary Information.

References

1. Artavanis-Tsakonas, S., Rand, M. D. & Lake, R. J. Notch signaling: cell fate control and signal integration in development. *Science* **284**, 770-776 (1999).

2. Goodyear, R. & Richardson, G. Pattern formation in the basilar papilla: evidence for cell rearrangement. *J. Neurosci.* **17**, 6289-6301 (1997).

3. Heitzler, P. & Simpson, P. The choice of cell fate in the epidermis of Drosophila. *Cell* **64**, 1083-1092 (1991).

4. Huppert, S. S., Jacobsen, T. L. & Muskavitch, M. A. Feedback regulation is central to Delta-Notch signalling required for Drosophila wing vein morphogenesis. *Development* **124**, 3283-3291 (1997).

5. de Celis, J. F., Bray, S. & Garcia-Bellido, A. Notch signalling regulates veinlet expression and establishes boundaries between veins and interveins in the Drosophila wing. *Development* **124**, 1919-1928 (1997).

6. Bray, S. J. Notch signalling: a simple pathway becomes complex. *Nature Rev. Mol. Cell Biol.* **7**, 678-689 (2006).

7. de Celis, J. F. & Bray, S. Feed-back mechanisms affecting Notch activation at the dorsoventral boundary in the Drosophila wing. *Development* **124**, 3241-3251 (1997).

8. Micchelli, C. A., Rulifson, E. J. & Blair, S. S. The function and regulation of cut expression on the wing margin of Drosophila: Notch, Wingless and a dominant negative role for Delta and Serrate. *Development* **124**, 1485-1495 (1997).

9. Klein, T., Brennan, K. & Arias, A. M. An intrinsic dominant negative activity of serrate that is modulated during wing development in Drosophila. *Dev. Biol.* **189**, 123-134 (1997).

10. Miller, A. C., Lyons, E. L. & Herman, T. G. cis-Inhibition of notch by endogenous delta biases the outcome of lateral inhibition. *Curr. Biol.* **19**, 1378-1383 (2009).

11. Cordle, J. *et al.* A conserved face of the Jagged/Serrate DSL domain is involved in Notch trans-activation and cis-inhibition. *Nature Struct. Mol. Biol.* **15**, 849-857 (2008).

12. Matsuda, M. & Chitnis, A. B. Interaction with Notch determines endocytosis of specific Delta ligands in zebrafish neural tissue. *Development* **136**, 197-206 (2009).

13. Kakidani, H. & Ptashne, M. GAL4 activates gene expression in mammalian cells. *Cell* **52**, 161-167 (1988).

14. Struhl, G. & Adachi, A. Nuclear access and action of notch in vivo. *Cell* **93**, 649-660 (1998).

15. Aster, J. C. *et al.* Essential roles for ankyrin repeat and transactivation domains in induction of T-cell leukemia by Notch1. *Mol. Cell. Biol.* **20**, 7505-7515 (2000).

16. Yang, L. T. *et al.* Fringe glycosyltransferases differentially modulate Notch1 proteolysis induced by Delta1 and Jagged1. *Mol. Biol. Cell* **16**, 927-942 (2005).

17. Rothenberg, E. V., Moore, J. E. & Yui, M. A. Launching the T-cell-lineage developmental programme. *Nature Rev. Immunol.* **8**, 9-21 (2008).

18. Varnum-Finney, B. *et al.* Immobilization of Notch ligand, Delta-1, is required for induction of notch signaling. *J. Cell Sci.* **113**, 4313-4318 (2000).

19. Wang, S. *et al.* Notch receptor activation inhibits oligodendrocyte differentiation. *Neuron* **21**, 63-75 (1998).

20. Rosenfeld, N., Young, J. W., Alon, U., Swain, P. S. & Elowitz, M. B. Gene regulation at the single-cell level. *Science* **307**, 1962-1965 (2005).

21. Jacobsen, T. L., Brennan, K., Arias, A. M. & Muskavitch, M. A. Cis-interactions between Delta and Notch modulate neurogenic signalling in Drosophila. *Development* **125**, 4531-4540 (1998).

22. Shaye, D. D. &Greenwald, I. LIN-12/Notch trafficking and regulation of DSL ligand activity during vulval induction in Caenorhabditis elegans. *Development* **132**, 5081-5092 (2005).

23. de Celis, J. F. & Bray, S. J. The Abruptex domain of Notch regulates negative interactions between Notch, its ligands and Fringe. *Development* **127**, 1291-1302 (2000).

24. Collier, J. R., Monk, N. A., Maini, P. K. & Lewis, J. H. Pattern formation by lateral inhibition with feedback: a mathematical model of Delta-Notch intercellular signalling. *J. Theor. Biol.* **183**, 429-446 (1996).

25. Plahte, E. Pattern formation in discrete cell lattices. *J. Math. Biol.* **43**, 411-445 (2001).

26. Melen, G. J., Levy, S., Barkai, N. & Shilo, B. Z. Threshold responses to morphogen gradients by zero-order ultrasensitivity. *Mol. Syst. Biol.* **1**, doi:10.1038/ msb4100036 (2005).

27. Levine, E., Zhang, Z., Kuhlman, T. & Hwa, T. Quantitative characteristics of gene regulation by small RNA. *PLoS Biol.* **5**, e229 (2007).

28. Buchler, N. E. & Louis, M. Molecular titration and ultrasensitivity in regulatory networks. *J. Mol. Biol.* **384**, 1106-1119 (2008).

29. Lenz, D. H. *et al.* The small RNA chaperone Hfq and multiple small RNAs control quorum sensing in Vibrio harveyi and Vibrio cholerae. *Cell* **118**, 69-82 (2004).

Supplementary Information

Construct Name	Promoter	Gene	Mammalian Selection	Role in this work
pEV-UAS-H2B-citrine	UAS	H2B-citrine	Zeocin	Reporter for hN1-Gal4^{esn}
pEV-12xCSL-H2B-citrine	12xCSL	H2B-citrine	Zeocin	Reporter for hN1
pcDNA3-hN1-mod1	CMV	hNotch1	Neomycin	hN1 construct
pcDNA3-hN1-mcherry	CMV	hN1-mcherry	Neomycin	hN1 construct (used)
pCDNA3-hNECD – Gal4^{esn}	CMV	hNECD – Gal4^{esn}	Neomycin	hN1-Gal4^{esn} construct
pcDNA5/TO-hNICD-Gal4^{esn}	CMV-TO	hNICD-Gal4^{esn}	Hygromycin	hNICD-Gal4^{esn}
pcDNA5/TO-Delta-mcherry	CMV-TO	Delta-mcherry	Hygromycin	Inducible Delta-mCherry
pcDNA5/TO-Gal4^{esn}	CMV-TO	Gal4^{esn}	Hygromycin	Inducible Gal4^{esn}
pCS-H2B-cerulean	CMV	H2B-cerulean	-	Segmentation color
pcDNA6-UAS-H2B-citrine	UAS	H2B-citrine	Blasticidin	Reporter in dual reporter line
pEV-12xCSL-H2B-mcherry	12xCSL	H2B-mcherry	Zeocin	Reporter in dual reporter line

Supplementary Table S1: Table of plasmids/constructs

Stable Cell Line	Parental Line	Transfected Construct	Antibiotic Selection
T-REx-CHO-K1 (Invitrogen)	-	-	Blasticidin (10 ug/ml)
12xCSL-H2B-Citrine	T-REx-CHO-K1	pEV-12xCSL-H2B-Citrine	Zeocin (400 ug/ml), Blasticidin (10 ug/ml)
UAS-H2B-Citrine + CMV-H2B-Cerulean	T-REx-CHO-K1	pEV-UAS-H2B-Citrine pCS-H2B-Cerulean	Zeocin (400 ug/ml), Blasticidin (10 ug/ml)
hN1-No-Delta	12xCSL-H2B-Citrine	pcDNA3-hN1-mCherry	Zeocin (400 ug/ml), Blasticidin (10 ug/ml), Geneticin (600 ug/ml)
hN1G4^{esn}-No-Delta	UAS-H2B-Citrine + CMV-Cerulean	pcDNA3-hNECD-Gal4^{esn}	Zeocin (400 ug/ml), Blasticidin (10 ug/ml), Geneticin (600 ug/ml)
hN1	hN1-No-Delta	pcDNA5-TO-Dl-mCherry pCS-H2B-Cerulean	Zeocin (400 ug/ml), Blasticidin (10 ug/ml), Geneticin (600 ug/ml), Hygromycin (500 ug/ml)
hN1G4^{esn}	hN1G4^{esn}-No-Delta	pcDNA5-TO-Dl-mCherry	Zeocin (400 ug/ml), Blasticidin (10 ug/ml), Geneticin (600 ug/ml), Hygromycin (500 ug/ml)
TO-DMC	T-REx-CHO-K1	pcDNA5-TO-Dl-mCherry	Hygromycin (500 ug/ml), Blasticidin (10 ug/ml)
TO-DMC+hN1G4^{esn} (for fig. S9)	TO-DMC	pcDNA3-hNECD-Gal4^{esn}	Hygromycin (500 ug/ml), Blasticidin (10 ug/ml), Geneticin (600 ug/ml)
TO-Gal4^{esn}	UAS-H2B-Citrine + CMV-H2B-Cerulean	pcDNA5/TO-Gal4^{esn}	Zeocin (400 ug/ml), Blasticidin (10 ug/ml), Hygromycin (500 ug/ml)
UAS-H2B-Citrine	CHO-K1 (CCL-61)	pcDNA-UAS-H2B-Citrine	Blasticidin (10 ug/ml)
UAS-H2B-Citrine + 12xCSL-H2B-mCherry (dual reporter)	UAS-H2B-Citrine	pEV-12xCSL-H2B-Citrine	Zeocin (400 ug/ml), Blasticidin (10ug/ml)

Supplementary Table S2: Table of cell lines

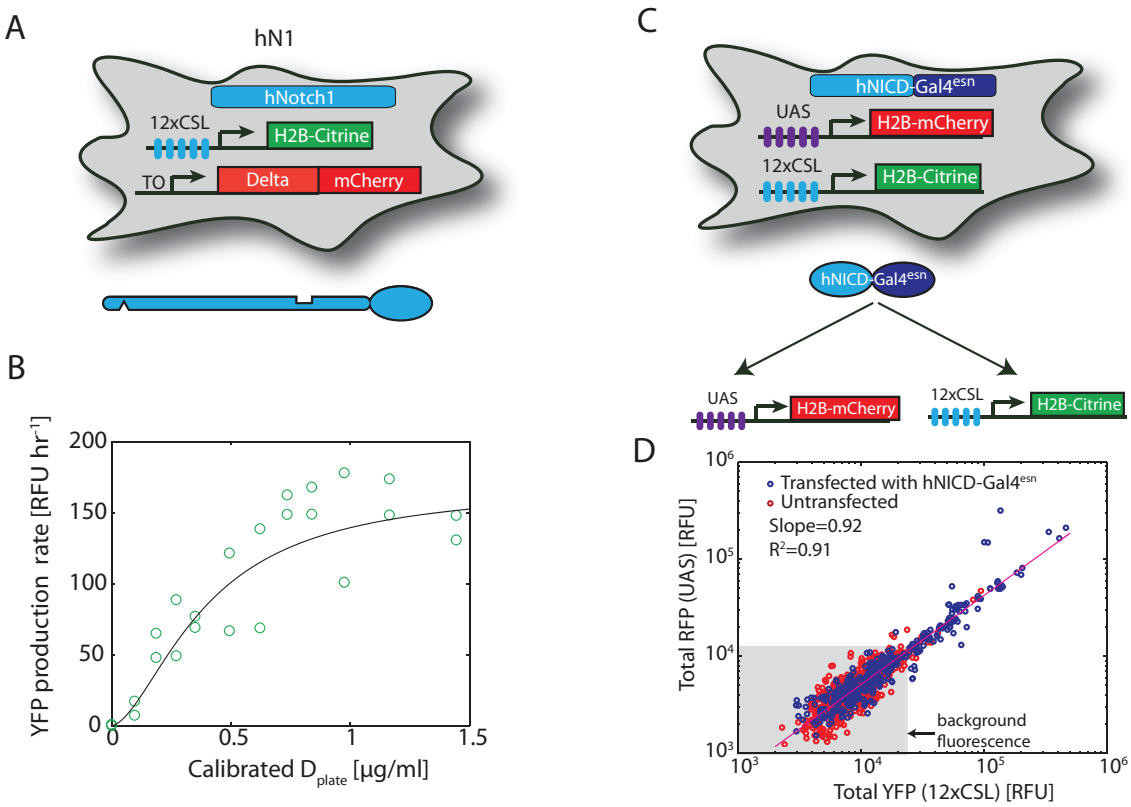

Figure S1: hN1G4^{esn} and hN1 cell lines exhibit similar response. (A) The hN1 cell line stably incorporates genes for full length hNotch1, Histone 2B (H2B)-Citrine (YFP) reporter controlled by a synthetic 12XCSL promoter[30], and a Tet-inducible Delta-mCherry fusion protein. It also constitutively express H2B-Cerulean (CFP) for image segmentation (not shown). Note that the hN1 cell line includes an mCherry domain fused to the C-terminus of hNotch1, which is not detectable experimentally and therefore omitted in the diagram. These cells exhibit no detectable endogenous Notch or Delta activities. (B) Notch response to trans-Delta in the hN1 cell line is similar to the one in hN1G4^{esn} (Fig. 2). Hill coefficient $n = 1.6$ (95% CI: 0.6-2.5). (C-D) Co-linear response of the 12xCSL and the UAS promoters. (C) A fusion protein consisting of Gal4^{esn} and the Notch Intracellular Domain (ICD) was transiently transfected into a CHO-K1 cell line containing two stably integrated reporters: 12xCSL-H2B-Citrine and UAS-H2B-mCherry. (C) Total RFP fluorescence versus total YFP fluorescence for transfected (blue circles) or untransfected (red circles) cells shows a co-linear response of the two reporters to the fusion activator (plotted on a log-log scale). A linear regression fit shows a slope of 0.92 ($R^2 = 0.91$), corresponding to a nearly linear relation between the two reporters (red line). Background fluorescence (gray area) is due to basal leakiness of reporters. Note that, due to the finite transfection efficiency of the transient transfection, only some of the cells contain the fusion activator. Data points are extracted from fluorescence images of cells, and analyzed using the techniques described in the text and methods. This result together with the non-cooperative behavior of the Gal^{esn}-UAS system shown in Fig. S2 is consistent with a non-cooperative activation of the 12xCSL promoter by Notch ICD.

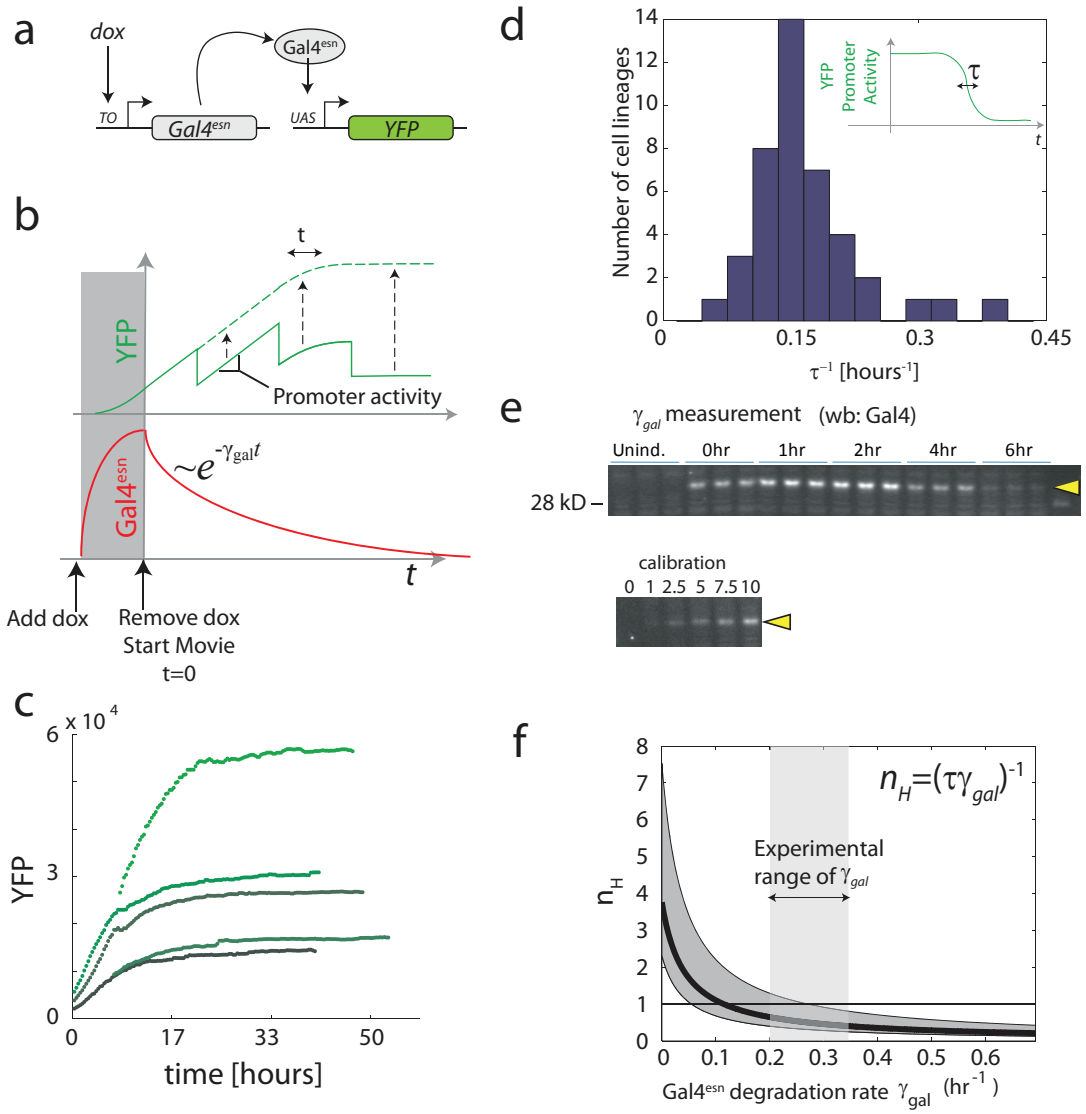

Figure S2 (caption on next page)

Figure S2 (previous page): The Gal4^{esn}-UAS transcription factor-promoter interaction shows no cooperativity. This figure describes a measurement of the relationship between Gal4^{esn} concentration and the transcriptional activity of its target UAS promoter. As in Fig. 3A and ref. 2, the approach involves allowing the transcription factor to decay and/or dilute while following the activity of its target promoter. (a) Schematic of cell line design. In this cell line, Gal4^{esn} is expressed from a *tet*-dependent promoter under the control of the doxycyline inducer. Gal4^{esn} activates expression of an H2B-YFP (Citrine) reporter gene. (b) Schematic of experimental design. Prior to the start of the movie, cells were induced with a pulse of doxycycline, which was then washed out immediately before the beginning of time-lapse movie recording. Consequently, Gal4^{esn} was expressed, and then allowed to degrade and/or dilute over time (red curve, bottom panel), while H2B-YFP fluorescence was monitored in individual cell lineages (top panel). γ_{gal} denotes the effective decay rate of Gal4^{esn}. For large enough pulses of Gal4^{esn} expression, the resulting data (shown schematically) would be expected to show constant rates of production of YFP (slopes of green line), interrupted by a 2-fold decrease in YFP levels at cell division events, due to partitioning of the YFP to daughter cells. To avoid discontinuities inherent to cell division events, the "lost" fluorescence after division is replaced (computationally) after each cell division event (dashed line and arrows). The slope of the resulting (dashed) trace is directly related to the activity of the UAS promoter, shown in the inset of (d). Here we focus on τ, the relative timescale required for the slope to fall from 73% to 23% of its initial value as Gal4^{esn} decays (cf. Fig. 3A). (c) Observed YFP accumulation in individual cell lineages. These traces have been corrected for cell division events as shown in (b). (d) Histogram of measured τ values determined from traces like those in (c) shows that, despite variability in initial levels of expression, the timescales, τ, required for turn off were relatively constant. (e) Using a time-course Western blot against Gal4^{esn}, we observed the Gal4^{esn} half-life to be between 3-5 hours (i.e. $\gamma_{\text{gal}} \sim 0.2 - 0.33$). A calibration with varying levels of cell lysate was also run to test linearity of measurement (bottom). (f) Inferring the Hill coefficient of the Gal4^{esn}-UAS interaction based on the measured values of τ and γ_{gal}, using the relationship shown in equation, inset. The black line shows how measurements of γ_{gal} constrain the possible range of underlying Hill coefficients. The dark gray region indicates the range of n_H values consistent with variability in the measurement of τ in (f). The light gray region indicates the measured range of γ_{gal}. The intersection between the two gray regions provide the range of likely for n_H values. This result shows that the effective cooperativity of the Gal4^{esn}-UAS interaction does not significantly exceed 1.

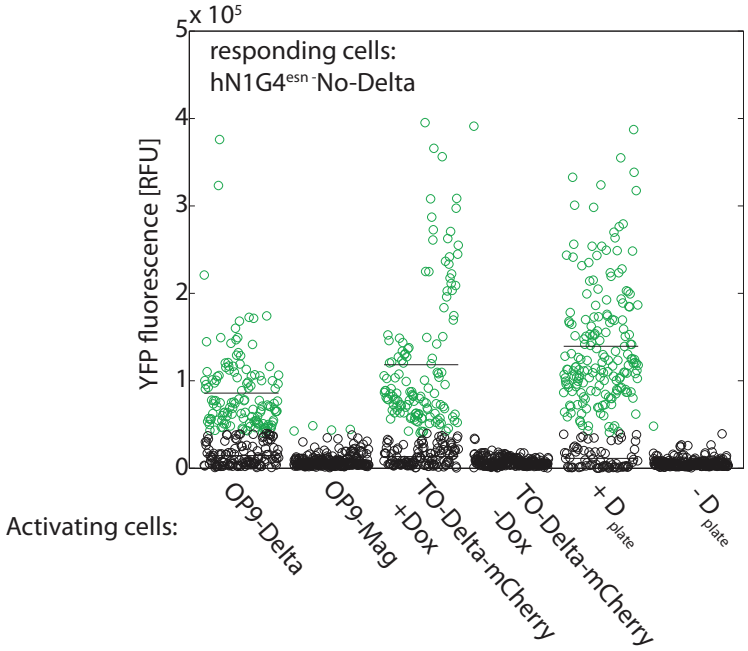

Figure S3: TO-Delta-mCherry cells trans-activate as efficiently as OP9-Delta cells. We compared the relative abilities of the TO-Delta-mCherry cell line, the OP9-Delta cell line, and D_{plate} to trans-activate Notch. Stromal OP9 cells stably expressing mDll1 (OP9-Delta) and control OP9 cells not expressing Delta[1] (both are a generous gift from Ellen Rothenberg) and inducible CHO TO-Delta-mCherry cells were co-cultured with hN1G4^{esn}-No-Delta cells (containing Notch and a reporter only-see Fig. S5). Cells were plated at a ratio of (70% Delta cells :30% Notch cells) at cell density of 1×10^5 cells/ml and incubated for 48 hours, and then imaged in an epifluorescence microscope. TO-Delta-mCherry cells were either induced with 100ng/ml Dox or not induced, as indicated. A set of controls with Notch reporter cells grown with or without plate-bound Delta (indicated by $+D_{plate}$ and $-D_{plate}$, respectively) were measured at the same time. Green and Black circles correspond to YFP fluorescence of activated and non-activated Notch cells, respectively (n=259 cells in each sample).

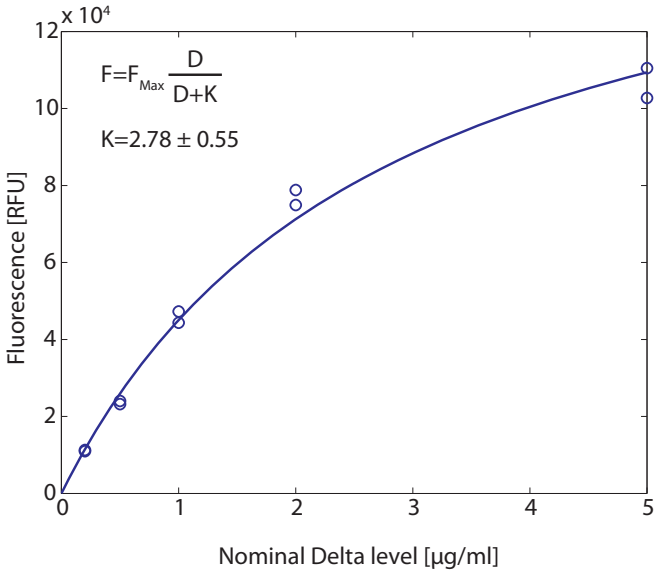

Figure S4: Calibration of plate bound Delta. Plates were incubated with different concentrations of IgG-Delta^{ext} (see methods for complete protocol). We determined the relationship between the concentration of IgG-Delta^{ext} used during incubation and the amount of IgG-Delta^{ext} actually adsorbed to the plate using a fluorescence binding assay. Right after incubation, plates were treated with anti-human-IgG conjugated to Alexa488 (Invitrogen). Fluorescence levels were measured using a plate reader (Wallac 1420, Perkin-Elmer). As seen in the figure, the binding of IgG-Delta^{ext} starts to saturate at concentrations bigger than 2ug/ml and is well-fit by the Michaelis-Menten curve $D_{plate} = \frac{D_{nominal}}{1+D_{nominal}/K}$, with $K = 2.78$ and where $D_{nominal}$ is the concentration of IgG-Delta^{ext} used in the incubation step. In addition, to assess the spatial uniformity of D_{plate}, we took snapshots of the bound antibody using a fluorescence microscope (not shown). We estimate the plate-plate variation in D_{plate} at 10-20%.

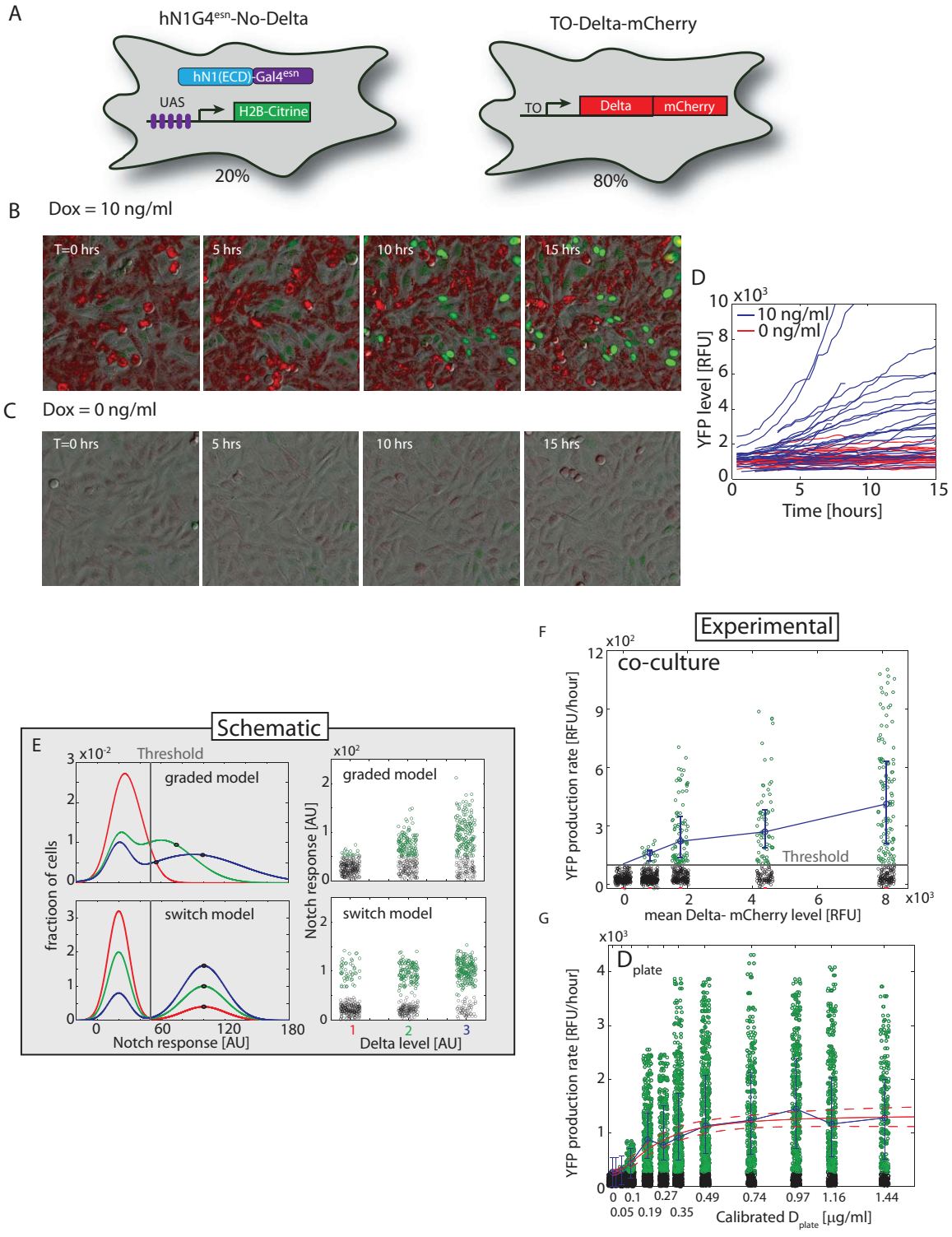

Figure S5 (caption on next page)

Figure S5 (previous page): Notch activity responds to trans-activation by cell-bound Delta in a graded fashion. (A) In order to analyze trans-activation between cells, we co-cultured two cell lines, one expressing hN1G4^{esn} and a reporter (hN1G4^{esn}-No-Delta cell line, left), and one containing only inducible Delta-mCherry (TO-DMC cell line, right). See Table S2 for strain descriptions. (B) Filmstrip of intercellular trans-activation taken from Movie S3. Here, the hN1G4^{esn}-No-Delta cell line (green nuclei) was co-cultured with TO-DMC cell line induced with 10ng/ml doxycycline to express Delta-mCherry (red cytoplasmic staining). Cell lines were co-cultured at a density ratio of 80:20 (TO-DMC: hN1G4^{esn}-No-Delta). Note the increasing Notch reporter fluorescence over time. (C) In contrast, without induction (no doxycycline), we observed much lower activation of Delta-mCherry expression and Notch activity in the reporter cell lines. Note that color (intensity) scales in (B) and (C) are the same. (D) Single cell tracks from the two movies shown in B and C. (E) Distinguishing between two possible models of activation in this experiment: graded and switch-like (schematic). Both models assume that some fraction of the cells do not respond even at maximal activation (here, we assume 20% 'non responders'). In the graded model, the responding population shows an increase of its median (black circles) response above a threshold, with higher induction levels (coefficient of variation is kept fixed). In the switch-like model, cells are in either the 'on' or 'off' states; only the fraction of cells occupying the 'on' state increases with Delta. Note that the two models predict qualitatively different responses of the mean number of activated cells with increasing Delta. (F) Experimental analysis of Notch reporter activation in individual cells (YFP production rates) at different levels of mean Delta-mCherry induction. The green circles correspond to single cell YFP production rates in the hN1G4^{esn}-No-Delta cell line above the threshold, determined by the basal expression without any Delta-mCherry induction in the TO-DMC cell line (a). The black circles correspond to cells that do not respond or that respond at levels below the threshold. The blue circles correspond to the median of activated cells. Error bars denote the 25 and 75 percentiles of the activated cells distributions. The response is consistent with a graded, rather than switch-like, model of trans-activation (e). (G) For comparison, a similar analysis was performed on the plate-bound Delta induction data shown in Fig. 2 c,d. Here, individual data points correspond to rates of YFP production. Note the graded, saturating response of the median response (blue data points and line) to D_{plate}. The red lines indicate a best fit of these median responses to a Hill function, with 95% confidence intervals bounded by the dashed red lines. The best fit Hill coefficient was 1.8 ± 0.9, in agreement with values obtained in Fig. 2D. Note that the relative fluorescence unit (RFU) scales in (F) and (G) are different due to the use of different imaging conditions. Together, these results show, first, that plate-bound and cell-expressed Delta trans-activate with similar cooperativity, and second, that the analysis based on population average response shown in Fig. 2D for plate-bound Delta produces equivalent results to the single-cell analysis of activation by cellular Delta.

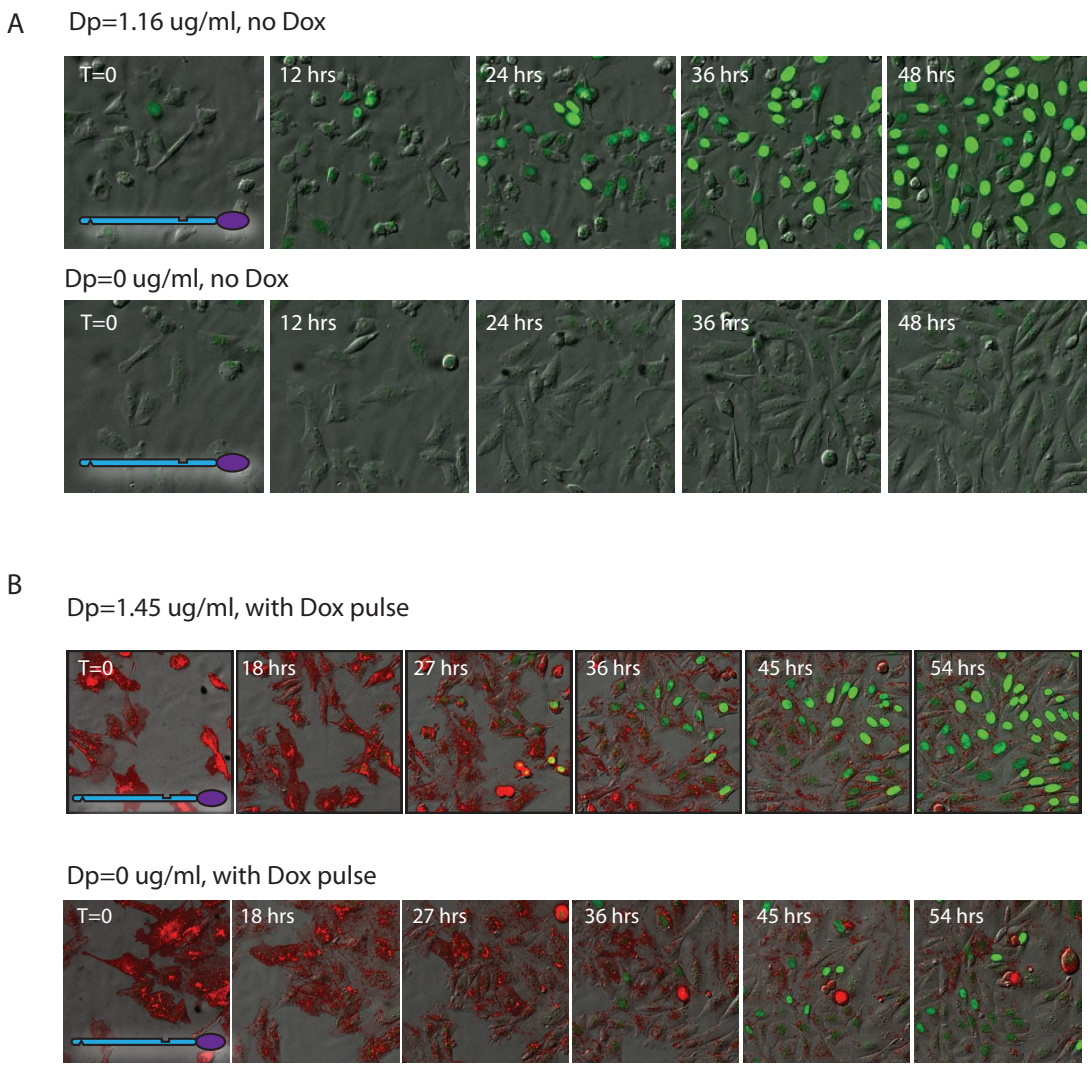

Figure S6: Induction at D_{plate}=0 is small compared to higher D_{plate} levels. (A) Filmstrips comparing activation of hN1G4^{esn} cells at D_{plate}=0 and D_{plate}=1.16 μg/ml (Fig. 2B). No induction is observed at D_{plate}=0. (B) Filmstrips comparing activation of hN1G4^{esn} cells induced with a doxycycline pulse at D_{plate}=0 and D_{plate}=1.16ug/ml (Fig. 2B). Only very few cells are induced in this case compared to higher D_{plate}. Thus, at this cell density transactivation between hN1G4^{esn} cells has only a small effect (this is also seen in the average data in Fig. 3G).

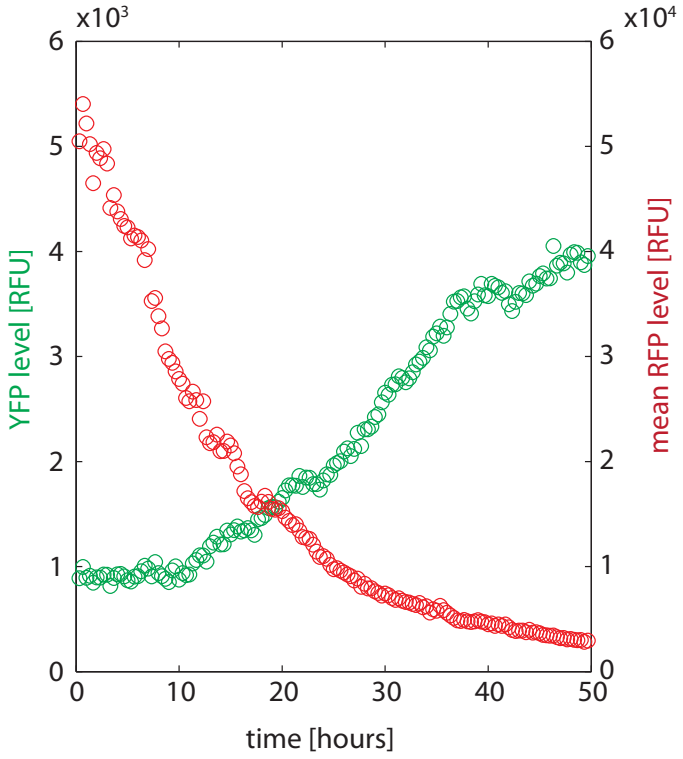

Figure S7: The hN1 cell line also shows an ultrasensitive response. hN1 cells show delayed turn-on in Notch signaling in response to slow decay of Delta-mCherry. Protocol is as described in Fig. 3A.

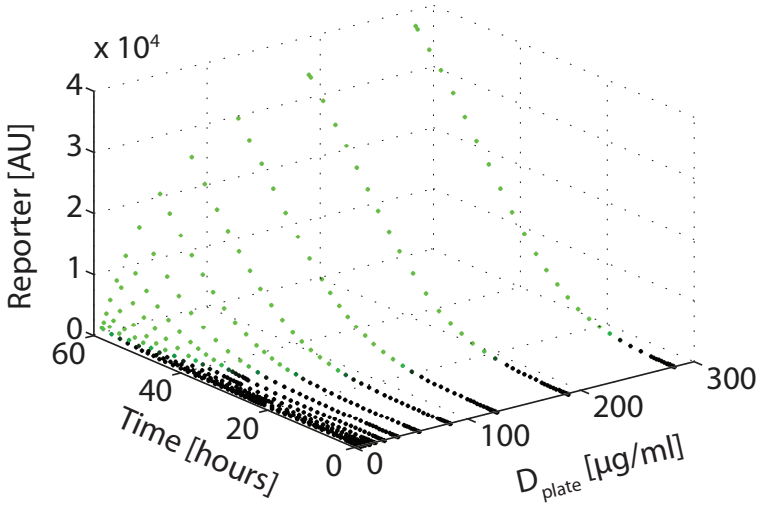

Figure S8: Delta inactivation by Notch is required for sharp responses to cis-Delta at fixed threshold. We simulated a model in which Delta inactivates Notch catalytically. In this model Delta is assumed to be recycled back after interaction with Notch (See theoretical supplementary for derivation and parameters). Note that, unlike the simulations based on the mutual inactivation model (Fig. 3H), here the turn-on curves do not exhibit sharp responses, and the threshold positions vary with D_{plate}. Note that the range of D_{plate} was scaled up to show the full response spectrum because a much higher D_{plate} is required to overcome the effect of D_{cis}.

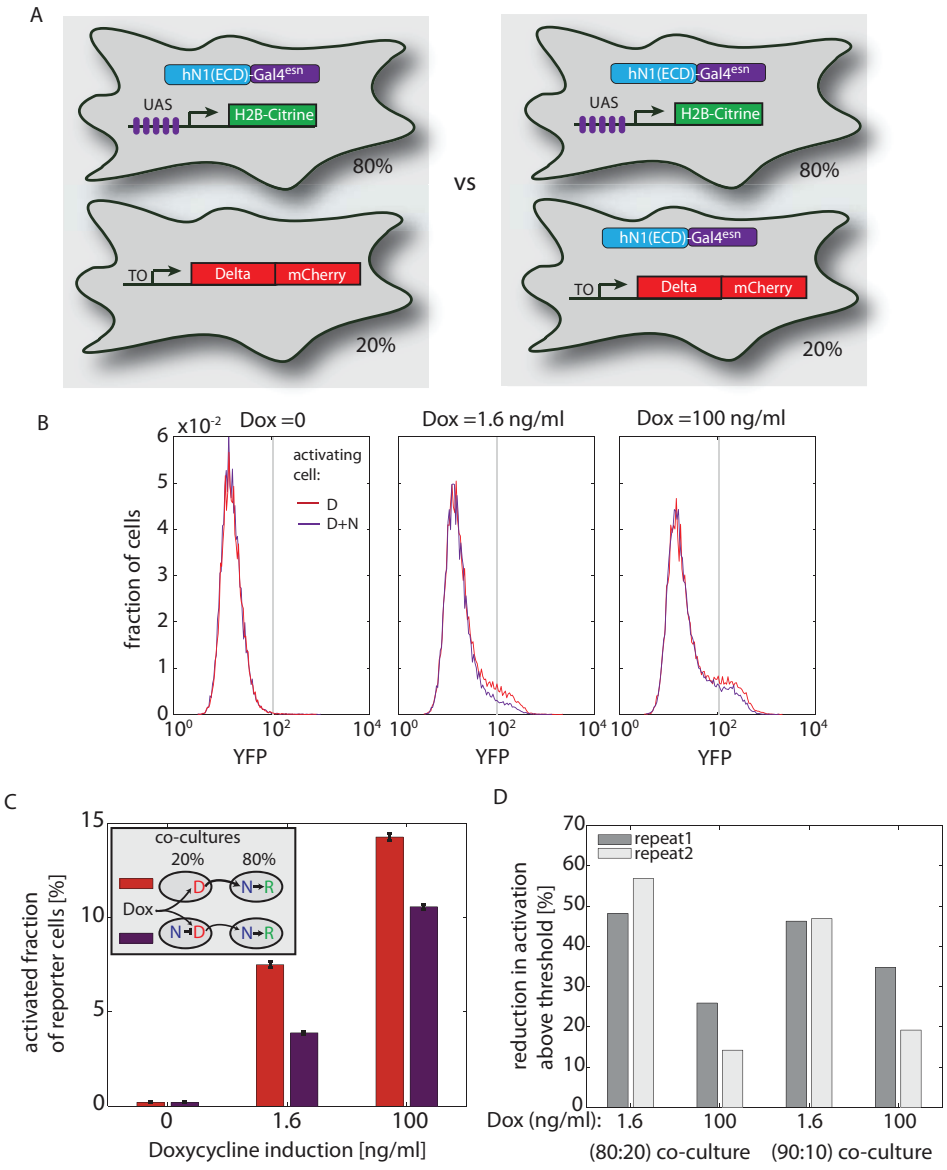

Figure S9 (caption on next page)

Figure S9 (previous page): Notch cis-inactivates Delta. (A) Cells expressing hN1G4^{esn} and a UAS-H2B-Citrine reporter (hN1G4^{esn}-No-Delta) were cocultured with cells expressing Delta (TO-DMC) or cells expressing Notch and Delta (TO-Delta-mCherry+hN1G4^{esn}). Note that TO-Delta-mCherry+hN1G4^{esn} cell line does not contain a reporter. This enables measurement of the response only from the Notch reporter cells. The level of Delta-mCherry in both of the inducing cell lines is similar across a wide dox induction range (not shown) providing evidence that Notch does not induce Delta degradation. Experimental procedure: Cells were co-cultured at the indicated ratios and plated at 1×10^5 cells/ml. Cells were subjected to a 12 hour doxycycline pulse (weak induction) with different dox levels. FACS analysis was performed 24 hours after the dox pulse using a FACSCalibur. (B) Fluorescence distributions in co-culture experiments. A total of 50,000 cells were measured for each sample. Only cells containing the Notch reporter are shown. The activation threshold (gray vertical line) is defined as a fluorescence level greater than that of 99.5% of negative control (dox=0). (C) Fraction of cells above threshold for the co-culture experiments shown in (B). Standard errors were estimated using a bootstrapping method by calculating the standard error of 20 non-overlapping subsamples. Note that the difference in the fraction of activated cells between the two samples is largest at intermediate Delta induction. This is consistent with the mutual inactivation model since the titration level of Notch should have larger effect at lower Delta expressions. (D) Qualitatively similar results were obtained in a repeat performed on a different day (dark gray vs light gray). Furthermore the relative reduction in activation of cells between the two samples remains similar even when the relative fractions of the two cell lines are changed to 10% Delta (or Delta+ Notch) cells and 90% Notch reporter cells.

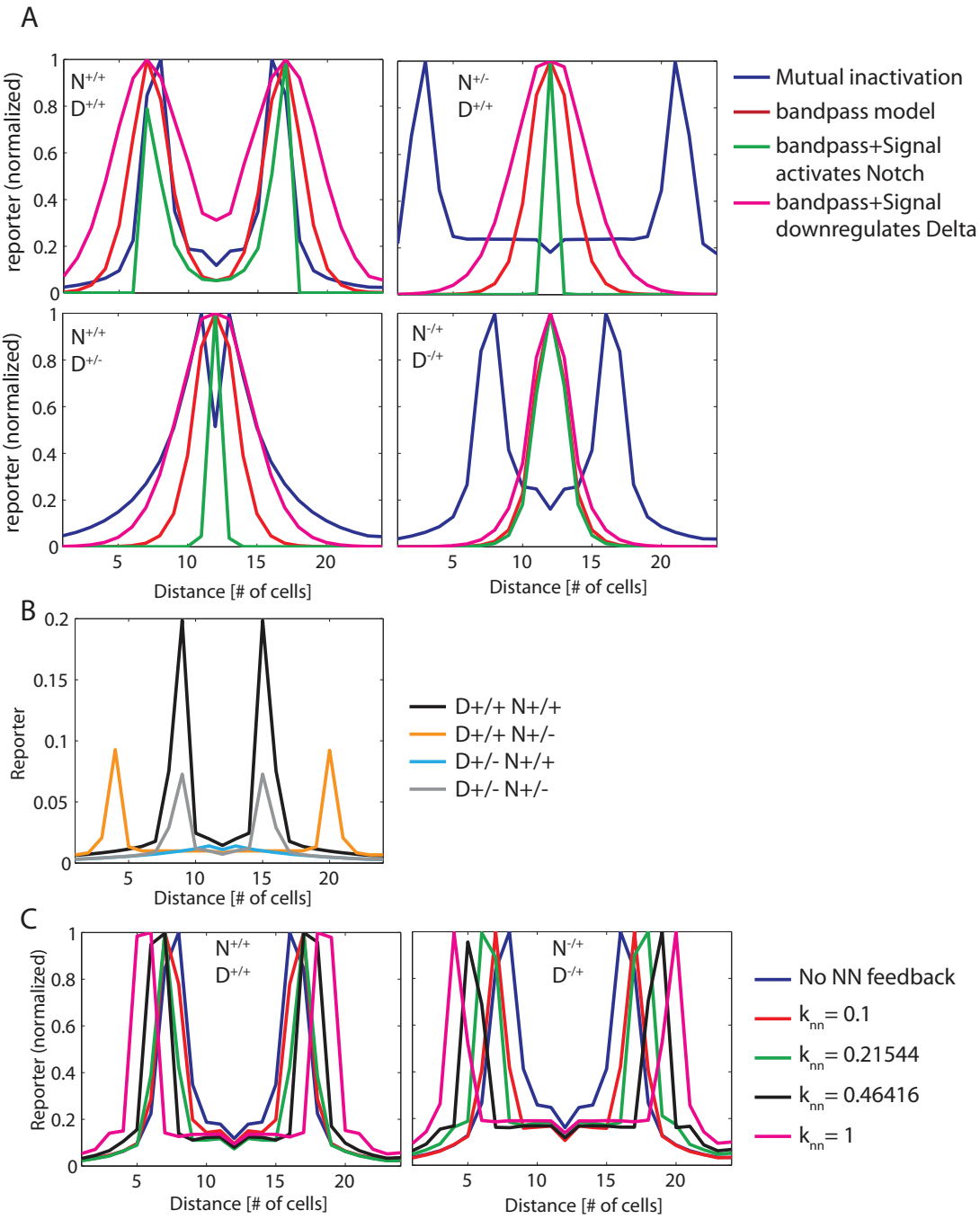

Figure S10 (caption on next page)

Figure S10 (previous page): Comparison of the mutual inactivation model to alternative models of boundary formation. (A) Three alternative models are compared to the mutual inactivation model discussed in the main text (blue). The 'band-pass' model (red) assumes that the Notch target promoter responds only to a narrow range ("band") of Notch signaling levels. This band-pass function was represented by a product of activating and repressing Hill functions, each with Hill coefficient, $n = 8$ (see section III of the supplementary modeling text). The high Hill coefficient is required to match the sharpness of the pattern generated with that obtained in the mutual inactivation model. For simplicity, no cis-inhibition was considered in this case. The second alternative model ("bandpass + signal activates Notch", green) adds an additional transcriptional feedback of Notch signaling on the production rate of Notch, so that Notch signaling activates expression of Notch. Such feedback makes the outer edge of the pattern sharper. The third alternative model (magenta, "bandpass + signal downregulates Delta") adds feedback through Delta (Notch signaling downregulates production of Delta). This lateral inhibition type feedback tends to broaden the signal response. All models are defined in the supplementary theory section. See Table S3 for parameter values. Note that the two feedback models require fine tuning of the parameters to show a qualitative effect of the feedbacks (i.e. differentiate the feedback models from the simple bandpass). The four different panels correspond to Notch signaling profiles of the different models for N+/-, D+/-, and N+/- D+/- heterozygous mutants. All profiles were normalized to their maximal level to allow comparison of the boundary positions in different heterozygous mutant combinations. Top left corresponds to the wild-type case. Top right: Only the mutual inactivation model (blue) is consistent with the observed broad but sharp wing vein phenotypes of the N+/- mutant[3]. Bottom left: The D+/- phenotype of the mutual inactivation model (blue), but not the other models, shows broadening of the signaling profile (note the extended tails at a distance of 5 cell diameters on the x-axis) and eliminates sharp side-bands (note that the central "dip" is an effect of the sharp kink in the morphogen profile at 0, and would not occur with a more realistic morphogen profile). These effects occur when the D+/- mutation makes the Delta production rate smaller than the Notch production rate. See also discussion in (B). Bottom right: In the mutual inactivation model, but not the other models, the double mutant N+/- D+/- regains the wild-type phenotype due to the ratiometric property discussed in Fig. 4D, Box 1, and in the text. This suppression is independent of the exact shape and length scale of the gradient. (B) Strong cis-inhibition selectively reduces signaling in the D+/- mutant. Here we plot the 4 un-normalized mutant profiles for the mutual inactivation model with a different parameter set (Table S3), with stronger cis-inhibition. The reporter level for the N+/+ D+/- mutant is substantially smaller than those of the wild type and all others mutants at all positions along the morphogen gradient. Such ubiquituous subthreshold activity of the reporter can be expected to resemble the null Delta phenotype of thicker and less sharply defined veins. Note that suppression in the double mutant persists for these new parameters, as shown by the invariance of the positions of the bands between wild-type and N+/- D+/-. More generally, suppression in the double mutant is maintained across a wide range of parameter values. (C) Positive feedback through Notch has a modest effect on suppression in the double mutant. Here we considered a variant of the mutual inactivation model in which Notch activity leads to increased expression of Notch. The strength of this feedback is quantified by the parameter k_{nn}, which denotes the amount of Notch signaling necessary to half-maximally induce the additional Notch production (supplementary theory section). Only intermediate values of k_{nn} change the spatial pattern (i.e. broaden it) without destroying its qualitative shape. Within this range, suppression is generally maintained except for a modest expansion ($<\sim$ 1 cell) in the double mutant compared to wild-type.

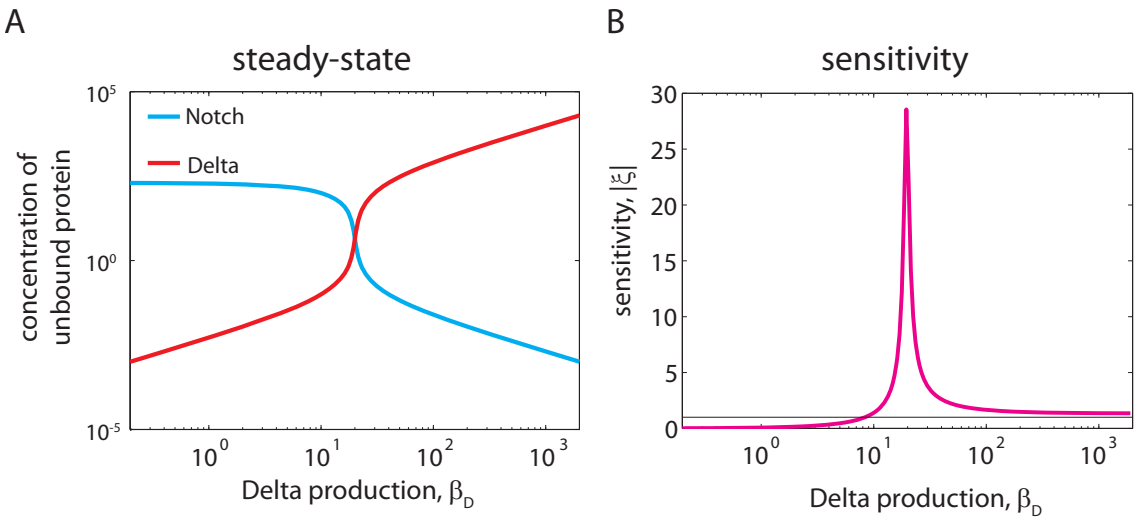

Figure S11: Steady-state sensitivity of the mutual inactivation switch. (A) The steady state levels of Notch (blue) and Delta (red) are shown with respect to the production rate of Delta, β_D, in a log-log plot, for the case presented in the Box Figure (values given in the Supplementary Table S3). This plot reveals a rapid change in Notch and Delta for a small change in the β_D near the switch location. (B) Steady-state sensitivity of the system, as defined in Box 1, for the conditions of plot A. Note that the sensitivity of the system remains larger than 1 for a very broad range of Delta production rates (to the right of the threshold).

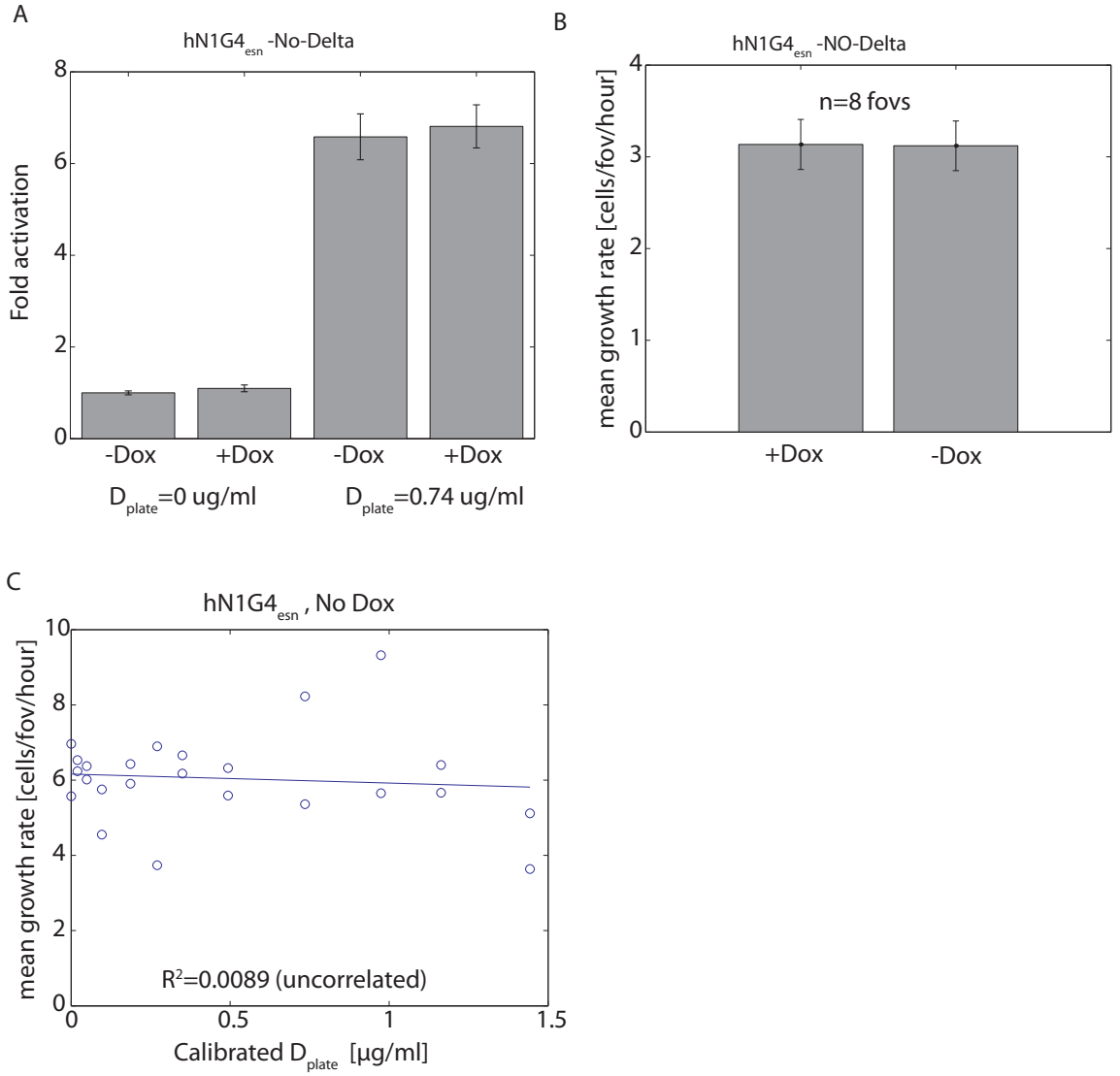

Figure S12: Negative controls show that Notch signaling is not affected by doxycycline, and growth rate is not affected by doxycycline and D_{plate}. (A) Cells expressing Notch (hN1G4^{esn} -No-Delta) were induced by D_{plate} to similar levels of Notch activity in the presence or absence of 100ng/ml doxycycline (protocol was similar to the ones used in Fig.2), showing that Notch activity is not influenced directly by doxycycine. (B) The growth rate of the Notch reporter cells was not affected by presence of doxycycline. (C) Mean growth rate of the cells shown in Fig. 2C,D,E is not affected by D_{plate}. Growth rate was defined as the rate of increase in the number of cells per field of view (fov) over time.

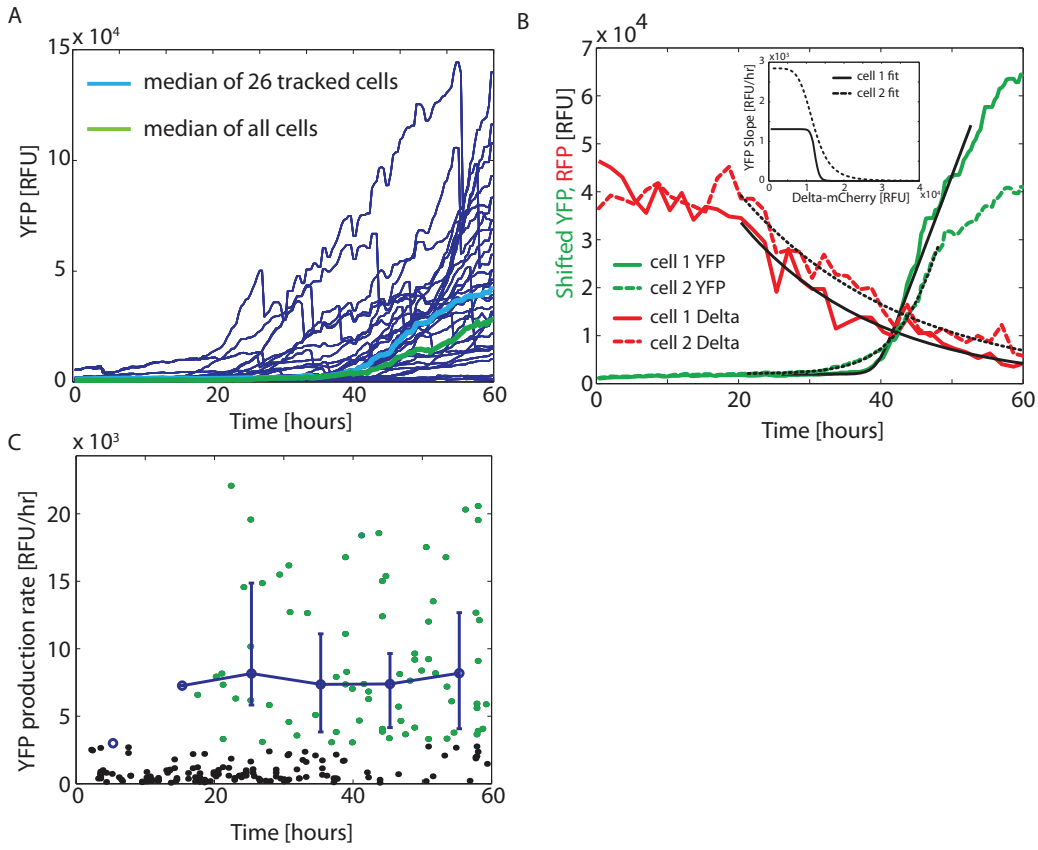

Figure S13: Relation of population average data (median over all segmented cells) and single cell data. (A) Plots of total cellular fluorescence versus time for each of 26 non-overlapping cell lineages from the movie shown in Figs. 3B, (blue lines). Sudden drops in total fluorescence are due to cell division events, as in Fig. 3D. We compare the median of these 26 responses (cyan) to the median over all cells (green). Note that this latter curve is identical to that shown in Fig. 3. For discussion see supplementary methods. (B) Analysis of sharp responses to cis-Delta in individual cells. The concentration of Delta-mCherry (red) and the shifted level of YFP (green, cf. Fig. 3e) are plotted as a function of time for two different cell lineages. Delta-mCherry concentrations were estimated from total Delta-mCherry fluorescence levels by assuming linear growth in cell volume during each cell cycle. The Delta-mCherry data were fit to exponential decays (superimposed black lines). The YFP response curves were fit to generate the turn-on function (superimposed black lines). The fit has four free parameters: a constant offset, a final slope, a turn-on time (t_{on}), and τ_{rise} (see supplementary methods). Inset: plots of resulting Hill function fits for the production rate of YFP as a function of the concentration of Delta-mCherry. These fits produced best fit Hill coefficients of $n = 22 \pm 10$ and $n = 5.5 \pm 0.8$ for cells 1 and 2, respectively. (C) Analysis of slope distributions of cis-Delta response shows a switch-like, rather than graded behavior. All 26 single cell traces were divided into short, 6 hour segments. The response on each segment was smoothed and its maximal slope was measured. Black and green points represent the values of individual slopes falling below or above a threshold, respectively. Note that the fraction of activated (green) points, but not their median value, increases over time, consistent with a switch-like model (Fig. 5e). The threshold value was determined from the early time points where cells are off. A few segments far from the switching point were filtered out, corresponding to saturating fluorescence levels or varying YFP expression at very late times (YFP curves in (b)). Similar filtering did not affect the distribution of trans-activation rates (Fig S5g). Blue circles represent the medians of the individual above-threshold (green) slopes in 30 hour bins. Error bars represent the 25th to 75th percentiles of each distribution. Comparison with trans-Delta distributions (Figs. S5e,f,g) shows that the response to cis-Delta agrees with a threshold like model.

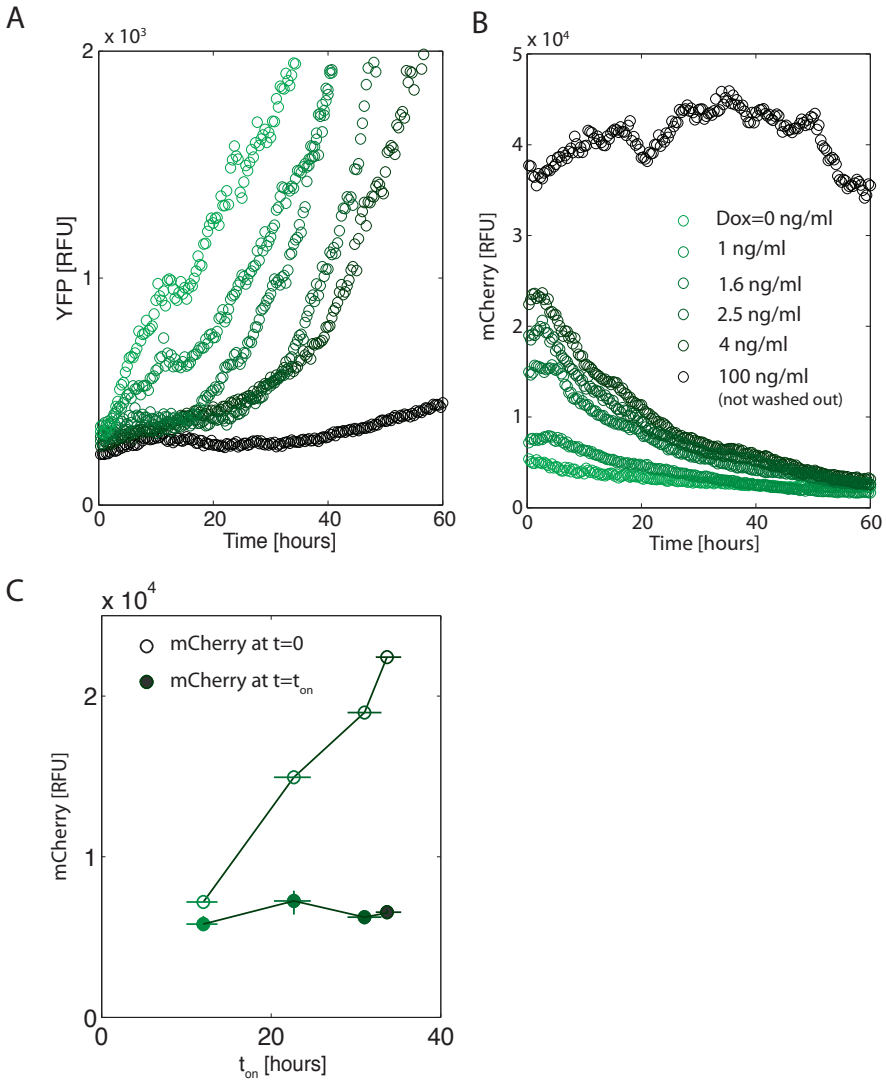

Figure S14: Initial Delta-mCherry levels correlate with turn-on time. (A) Notch signaling response was measured for varying Delta-mCherry induction levels. The experimental setup was similar to the scheme shown in Fig. 3A. Cells were grown on fixed D_{plate}=0.74 μg/ml and subjected to 12 hour pulses of varying doxycycline concentrations, as indicated in (B). Increased induction levels correspond to higher Delta-mCherry induction (B) and corresponding delays in the turn-on time (A). When doxycycline is not removed from the media (darkest green), cells show a negligible response to D_{plate}. (C) Here, t_{on} was calculated for the data in (A) and (B). For each Delta-mCherry induction level (same legend as in (B)), the Delta-mCherry fluorescence at the start of the movie (t=0) and at ton are plotted. These data show that the time of Notch activation, t_{on}, varies with the initial level of Delta-mCherry expression, but occurs at an approximately constant Delta-mCherry concentration, as expected from the experimental scheme in Fig. 3A. Note that fluorescence levels differ in this figure from those in Fig. S13 due to variations in optical parameters (e.g. lamp intensity) between the two experiments.

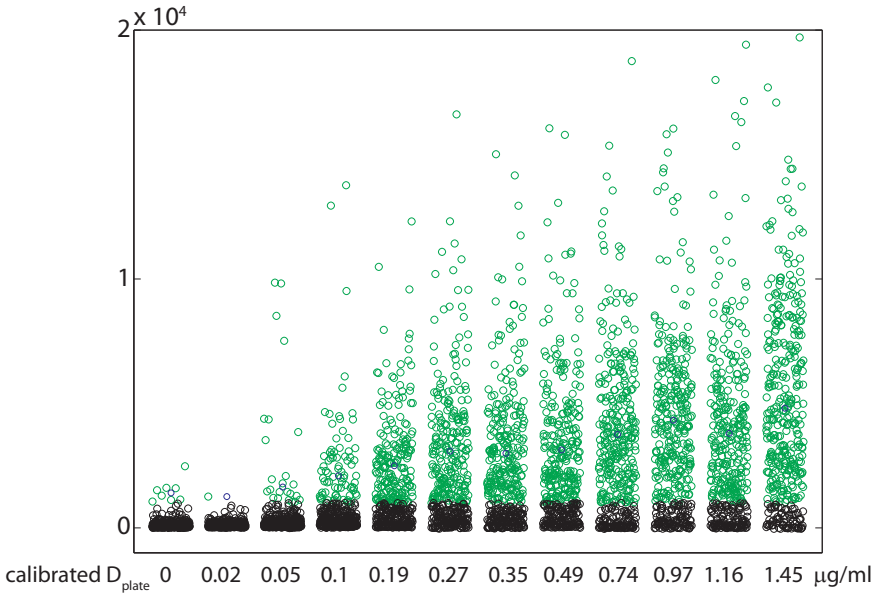

Figure S15: Distribution of activated cells at different D_{plate} shows graded response. Distributions of hN1G4^{esn} cells after onset of induction (t=50 hours) in Figure 3G. Activated cells (green circles) respond in a graded fashion to D_{plate} levels. Note that even at maximal activation there is a fraction of non-responding cells (black circles). Such variable behavior typically occurs due to silencing of viral promoters such as the CMV promoter used here. The blue circles represent the median of activated cells. Note that in figure 2C we plot the median of all cells (green and black circles). The median of all cells exhibits a similar slope to the median of activated cells at longer times, but it shows an initial lag in the response. This lag occurs since the median of all cells remains unchanged until more than 50% of the cells respond to D_{plate}. See also discussion in Fig. S5.

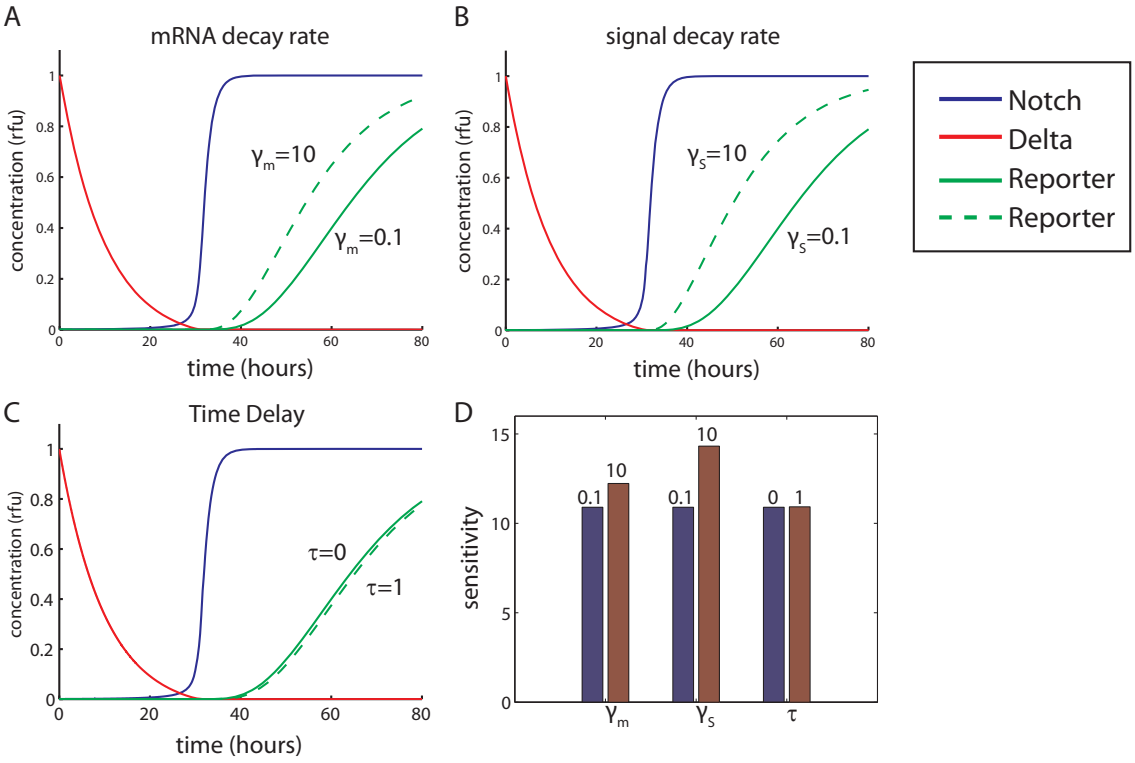

Figure S16: Effect of finite lifetimes and expression delays in the model. Time traces of Notch (blue), Delta (red), and the reporter (green) obtained from numerical simulations of the *cis*-inhibition model. Solid and dashed green lines are reporter traces for different parameter values, indicated on plot. (A) A 100x increase in the lifetime of the reporter mRNA leads to a delay of a few hours in the turn-on of reporter expression. (B) A similar effect is found for a 100x increase in the lifetime of the Signal. (C) A 1-hour delay in the expression of the reporter from the activating signal leads to a corresponding delay in reporter turn-on. (D) Despite these time shifts, the dynamic sensitivity of the system, defined as the logarithmic derivative of the Signal with respect to the total amount of Delta at any given time instant, is mostly unchanged. The sensitivity coefficient, shown in the bar plot for the different cases presented in plots A-C, increases at most 30% for the smallest lifetimes, and is effectively constant in the presence of delay in the reporter expression.

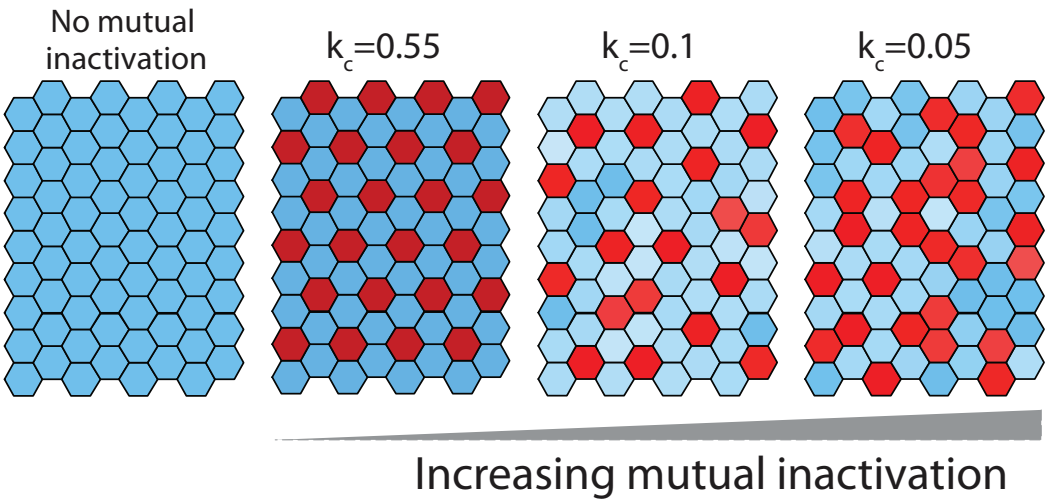

Figure S17: Lateral inhibition model with mutual inactivation (See theoretical supplementary section) facilitates broader range of patterns. Increasing the strength of mutual inactivation (reduced k_c) enables patterning (second panel), as well as the formation of alternative patterns in which cells with high Delta levels can stably co-exist next to each other (third and fourth panels). Such alternative patterns cannot be achieved using standard lateral inhibition model (even in the presence of cooperative feedback).

Supplementary Methods

Description of genetic constructs

All genetic constructs used in this paper were constructed using standard cloning and PCR techniques. All constructs were fully sequenced and the maps, sequences and construction details are available upon request. We provide below a description of the sources for vectors and DNA fragments used, as well as the main construction steps.

Reporter plasmids pEV-UAS-H2B-Citrine and pEV-12xCSL-H2B-Citrine were constructed as follows: The backbone vector pEV was constructed in the lab by amplifying pSecTagA without the secretion tag Murine Ig kappa-chain V-J2-C (Invitrogen, V900-20) and religating it with the SacII restriction site. The UAS-H2B-citrine and 12xCSL-H2B-Citrine were amplified or subcloned from earlier constructs and they contain the following DNA fragments: H2B-citrine originally obtained from pCS H2B citrine (a gift from Sean Megason and Scott Fraser[4]). UAS was obtained from ULyn-GFP (a gift from Scott Fraser[5]). 12xCSL was amplified from 12xCSL DsRedExpress (a gift from Urban Lendahl[6]).

pcDNA3-hN1-mod1 was constructed by first adding an NheI site to pcDNA3 hN1 (a gift from Jon Aster[7]). To add this NheI site we amplified the DNA fragment between the NotI to the XhoI site and included the NheI site in the reverse primer. The resulting amplicon was ligated into pcDNA3-hNI cut with the same restriction sites. This modified plasmid was then used to create pcDNA3-hN1-mCherry by inserting mCherry originally amplified from pFA6-link-mcherry-SpHis5 (a gift from Roger Tsien and Kurt Thorn[8,9]) into the NheI and XhoI sites.

pcDNA3-hNECD-Gal4^{esn} was constructed by cutting pcDNA3-hN1-mod1 with *Not*I and *Xho*I to remove hNICD. Gal4^{esn} was constructed by PCR amplification from *Saccharomyces cerevisiae* as described in Ptashne et al [10]. Gal4^{esn} amplified with *Not*I and *Sal*I restriction sites was inserted into the cut vector in the sites above. We note here that Gal4^{esn} was chosen over the more popular Gal4-VP16, since it does not use the viral activator VP16 which is extremely strong and generates high background signal.

pcDNA5/TO-hNICD-Gal4^{esn} was constructed using the pcDNA5/TO vector (Invitrogen , V1033-20) cut with *Bam*HI and *Not*I and by amplifying hNICD-Gal4^{esn} with the same restriction sites from pcDNA3-hN1-Gal4^{esn} (a construct not used here but was constructed by introducing Gal4^{esn} into pcDNA3-hN1-mod1). pcDNA5/TO-Delta-mCherry was constructed by first modifying pcDNA5/TO (Invitrogen, V1033-20) to add a *Nhe*I restriction site by cutting with *Hind*III and *Bam*HI and then ligating in 2 annealed oligos, which contained the *Nhe*I site. The vector was then digested with *Nhe*I and *Bam*HI. Delta-mCherry was cut from a previously constructed vector with the same restriction sites as pcDNA5/TO. Delta originally came from pBOS-rDelta1[11] (a gift from Gerry Weinmaster) and was fused to mCherry using fusion PCR. The overlapping sequence between the two fused proteins is: GTGTTATAGCGACTGAGGTTgtgagcaagggcgaggagga. pcDNA5/TO-Gal4^{esn} was constructed by removal of the mCherry from pcDNA5/TO-Gal4^{esn}-mCherry through BamHI and NotI digestion. A small DNA fragment (made from annealed oligos) containing a stop codon as well as the BamHI and NotI overhangs was ligated into the cut pcDNA5/TO-Gal4^{esn}-mCherry vector. The pcDNA5/TO-Gal4^{esn}-mCherry vector was originally created by first performing a fusion PCR of Gal4^{esn} and mCherry (sources for Gal4^{esn} and mCherry previously described). The PCR product was ligated into the pcDNA5/TO vector from Invitrogen. pCS-H2B-cerulean was a gift from Sean Megason and Scott Fraser[4].

pcDNA6-UAS-H2B-Citrine was constructed by subcloning UAS-H2B-citrine from pEV-UAS-H2B-Citrine into pcDNA6/ V5-HisA (Invitrogen, V220-01) using *Mfe*I and *Bst*BI restriction sites. pEV-12xCSL-H2B-mcherry was constructed by amplifying the 12xCSL promoter from 12xCSL DsRedExpress then fusing it to H2B-mCherry.The resulting amplicon was digested with *Mfe*I and *Bgl*II and inserted into pEV between *Mfe*I and *Bam*HI. H2B-mCherry was constructed by fusion PCR of H2B and mCherry fragments.

Generation of stable cell lines and cell-culture protocols

As a base cell line we used T-REx-CHO-K1 cells (Chinese Hamster Ovary cells supporting the T-REx inducible system, Invitrogen) which were grown in Alpha MEM Earle's Salts (Irvine Scientific)

supplemented with 10% Tet System Approved FBS (Clontech), 100 U/ml penicillin -100 ug/ml streptomycin - 0.292 mg/ml L-glutamine (Gibco), and 10 ug/ml Blasticidin (InvivoGen) at 37°C in the presence of 5% CO2 under a humidified atmosphere. For construction of stable cell lines, cells were plated 24 h prior to transfection in 24 well tissue culture treated plates such that 80-95% confluency would be reached by the time of transfection. Cells were transfected using Lipofectamine 2000 (Invitrogen) as per the manufacturer's instructions. The amount of total DNA used was 800 ng/well: 100 ng of DNA containing the desired cassette + 700 ng empty plasmid (pOri).

Stable cell lines containing either the 12xCSL-H2B-Citrine or UAS-H2B-Citrine reporters were created by transfection of pEV-12xCSL-H2B-Citrine or pEV-UAS-H2B-Citrine into T-REx-CHO-K1 cells. A plasmid containing H2B-Cerulean under constitutive CMV promoter (pCS-H2B-Cerulean) was co-transfected together with the pEV-UAS-H2B-Citrine. Positive cells were selected by replating transfected cells into 6 well tissue culture treated plates with media containing 400 μg/ml Zeocin (Invitrogen) and 10 μg/ml Blasticidin 24 h post-transfection. Cells transfected with DNA lacking an antibiotic resistance gene were used as a control to monitor positive cell selection. After the control cells died, and after several passages of the selecting cells, positive cell populations were either sorted by FACS (FACSAria, Beckman Dickinson) or diluted in 96 well tissue culture treated plates in order to obtain single clones to test for reporter activity. For FACS, cells were transiently transfected with pEF-GV-ICD (a plasmid containing a fusion of Gal4-VP16 and Notch ICD) 24 h prior to cell analysis and sorting. Individual cells expressing high levels of citrine were sorted into single wells in a 96 well tissue culture treated plates. Alternatively, positive cell populations were plated into 96 well tissue culture treated plates at 0.2 cells/well in order to increase the likelihood of obtaining a single cell/well. Individual cells were grown in selection media until enough cells were available to test reporter activity. Each clonal cell population was tested by transient transfection with pEF-GV-ICD, and clones with the best dynamic range of reporter induction were identified by microscopy and used for the next round of stable cell line creation. For the addition of Notch constructs into the two stable reporter cell lines constructed above, plasmids containing either hN1 fused to mCherry (pcDNA3-hN1-mCherry) or hN1G4^{esn} (pcDNA3-hNECD-Gal4^{esn}) were transfected into the 12xCSL-H2B-

Citrine or UAS-H2B-Citrine reporter cell lines, respectively. Positive cell populations were selected as previously described with selection media that contained 400 μg/ml Zeocin, 10 μg/ml Blasticidin, and 600 μg/ml Geneticin (Invitrogen). Clonal cell populations were obtained by FACS or dilution as detailed above. Positive cell populations used for FACS were plated in wells treated with 2.5 μg/ml IgG-Delta^{ext} 48 hours before sorting. Individual cells expressing high levels of citrine were sorted. Clones were tested by plating cells in wells treated with or without 2.5 μg/ml IgG-Delta^{ext} and monitoring activation of the 12xCSL-H2B-Citrine or UAS-H2B-Citrine reporter by microscopy 48-72 hours post-Delta exposure. Single hN1 and hN1G4^{esn} clones with minimal H2B-Citrine background expression and high reporter activation when exposed to Delta were selected for further use.

To create the final cell lines hN1 and hN1G4^{esn} shown schematically in Figs. 1C, S1, a plasmid expressing Dl-mCherry under an inducible promoter (pcDNA-TO-Dl-mCherry) was transfected into each of these cell lines. A plasmid containing H2B-Cerulean under constitutive CMV promoter (pCS-H2B-Cerulean) was co-transfected with the Delta-mCherry into the hN1 cell line. Cells were grown in selection media containing 400 μg/ml Zeocin, 10 μg/ml Blasticidin, 600 μg/ml Geneticin, and 500 μg/ml Hygromycin (InvivoGen) for each of the hN1 cell lines. After selection, cells were either treated with 1 μg/ml doxycyclin and subjected to FACS or diluted into 96 well tissue culture treated plates as previously described. For FACS, single cells expressing high levels of mCherry were sorted. Clonal cell populations were grown and tested for low mCherry background expression in the absence of doxycycline and good inducibility of mCherry expression when exposed to 1 μg/ml doxycycline. Optimal clones for each of the above cell lines were identified by microscopy and used in further experiments. A separate cell line containing only inducible Delta-mCherry (used in co-culture experiments), was created by transfecting T-REx-CHO-K1 cells with pcDNA-TO-Dl-mCherry. Clones were generated in a similar process as above albeit with a selection media containing only Blasticidin and Hygromycin. This cell line was used to generate the TO-DMC+hN1G4^{esn} used in Fig. S9 by stably transfecting into it the pcDNA3-hNECD-Gal4^{esn} construct (600 μg/ml Geneticin). *We note that the fusion to mCherry could in principle affect various activities of Delta. Therefore, we verified that Delta-mCherry can trans-activate Notch reporter cells efficiently (as shown in Fig. S3). This*

does not rule out the possibility that other activities or properties of Delta may be affected by the fusion.

For creation of the TO-Gal4^{esn} cell line, the UAS-H2B-Citrine + CMV-H2B-Cerulean cell line was transfected with the pcDNA5/TO-Gal4^{esn} plasmid. Cells were grown in selection media containing 400 μg/ml Zeocin, 10 μg/ml Blasticidin, and 500 μg/ml Hygromycin. After selection, cells were diluted into 96 well tissue culture treated plates to obtain single clones. Clones were tested for Gal4^{esn} inducibility by plating cells either with or without 1 μg/ml doxycycline. The clone with the lowest Citrine background expression in the absence of doxycycline and good inducible Citrine expression in the presence of doxycycline was chosen for further use in experiments.

For production of a double reporter cell line used in Figure S1, CHO-K1 cells (without T-REx, ATCC, CCL-61) were first transfected with pcDNA-UAS-H2B-Cit. A positive cell population was selected with media containing 10 μg/ml Blasticidin. After the initial selection, positive clones were obtained by FACS as previously described for the individual reporter stable cell lines. Each clone was then tested by transfection with pEF-GV-ICD, and a clone with the best reporter dynamic range was identified by microscopy and used to transfect in pEV-12xCSL-H2B-mCherry. Transfected cells were selected in media containing 10 μg/ml Blasticidin and 400 μg/ml Zeocin. A positive double reporter clone was identified by the method described above. In the clone chosen for further experiments, both reporters showed minimal background activation and high levels of Citrine and mCherry when transfected with pEF-GV-ICD.

Measurements of relative Notch expression levels in hN1G4^{esn} and hN1

To estimate the levels of ectopically expressed Notch receptors in the hN1G4^{esn} and hN1 we performed qRT-PCR on the two cell lines in which levels of Notch mRNA were compared to levels of endogenous β-actin mRNA. We found Notch levels 2.3 ± 0.15 and 4.5 ± 0.4-fold smaller than those of β-actin in the hN1G4^{esn} and hN1 cell lines , respectively. These results are within the physiological range of endogenous Notch receptors as observed in early T-cell progenitors where Notch is active[12]. See below for details of qRT-PCR analysis.

Description of experimental protocols and microscopy

Delta plating, preparation of cells for imaging, and calibration assay for IgG-Delta^{ext}. Protocol for setting up a time lapse movie: Cells were plated on a glass bottom 24 well plate (Mattek). To bind IgG-Delta^{ext} to the plate, IgG-Delta^{ext} was serially diluted to different concentrations in cold 1xPBS (Invitrogen) containing 5μg/ml hamster fibronectin (Innovative Research). 500μl of diluted IgG-Delta^{ext} was incubated at 4°C for 1 hour on a rocker. Cells were trypsinized and diluted to 2×10^4 cells/ml (1×10^5 cells/ml for coculture experiments) in growth medium containing 100ng/ml doxycycline (Sigma Aldrich). The cells were plated immediately after the incubation onto the 24 well plate containing IgG-Delta^{ext}. Prior to imaging, wells were washed twice with fresh media and media was replaced with low fluorescence imaging media αMEM without Phenol red, riboflavin, folic acid, and vitamin B12 (Invitrogen, custom made) and with 5% FBS and 1% L-glutamine+Penicilin-Streptomycin 100x mix (Invitrogen). Calibration of the IgG-Delta^{ext} bound to the plates is discussed in the captions of Fig. S4.

Microscopy details: Cells were imaged in an Olympus IX81-ZDC microscope equipped with an ASI 2000XY stage and a cooled back-thinned iKon-M CCD camera (Andor). All movies were taken with a 20x, 0.7NA objective. The microscope is also equipped with an incubator that maintains the temperature at 37C and with an environmental chamber with a humidified 5% CO2 flow (custom made). The microscopy setup is automatically controlled using commercial Metamorph (Molecular Devices) software. 48 stage positions (2 in each well) are set up manually and their coordinates are stored in the computer. In each position, the program first focuses using the Zero Drift Control module (Olympus Inc.), then takes a DIC image, and three fluorescent images (mCherry, citrine, CFP). Images are taken every 20 minutes for all positions. Typical total movie time is approximately 48 hours.

Western Blot: TO-Gal4^{esn} cells were plated in wells of a 6-well tissue culture treated plate at 5x105 cells/well. The cells were induced with 100 ng/ml of doxycycline. After 24 hr of induction, one well of cells was harvested (0 hr post-doxycycline removal) while the doxycycline was washed out

of 4 additional wells. Those cells were harvested at 1 hr, 2hr, 4 hr and 6hr post-doxycycline removal (an uninduced sample was used as a control). The harvested cells were counted, and 4x106cells were pelleted and lysed with 200μl 1.5x complete SDS loading buffer (76.7 mM Tris-HCL, pH 6.8, 1.5% (w/v) SDS, 15% (v/v) Glycerol, 0.01% (w/v) Bromophenol blue, 30 mM Dithiothreitol (DTT), 213.8 mM 2-Mercaptoethanol, 1x protease inhibitors (Roche Applied Science), 6 mM ethylenediaminetetraacetic acid (EDTA)). Cellular extracts were boiled for 5 min at 95°C, vortexed, chilled on ice and centrifuged in a Beckman TLA-100.3 ultracentrifuge rotor at 55,000 rpm for 1 h at 4°C. For each sample, 10μl of supernatant was resolved in triplicate on a NuPAGE Novex 4-12% Bis-Tris Midi Gel (Invitrogen) and transferred to a 0.2 μm nitrocellulose membrane using the iBlot from Invitrogen (a standard curve made from serial dilutions of the 0 hr post-doxycycline sample was also included on the gel). The membrane was blocked with 5% (w/v) dry milk and 2% (w/v) BSA in 1xTBST (20 mM Tris base, 137 mM sodium chloride, 0.1% (v/v) Tween 20, pH 7.6), incubated with primary antibody in blocking buffer, followed by incubation with horseradish peroxidase-labeled secondary antibody in blocking buffer. SuperSignal West Femto chemiluminescent substrate kit was used for detection (Pierce). The following primary antibody was used: rabbit anti-Gal4 DBD (sc-577, Santa Cruz Biotechnology, 1:200). The secondary antibody used was horseradish peroxidase linked anti-rabbit IgG (Amersham, 1:2000). Protein bands were visualized on a VersaDoc gel imaging system (Bio-Rad Laboratories).

qRT-PCR: Notch mRNA levels in the hN1 and hN1G4^{esn} cells were compared to endogenous Notch mRNA observed in early T-cell progenitors. RNA was isolated from hN1 and hN1G4^{esn} cells using the RNeasy kit (Qiagen). cDNA was subsequently synthesized from 1μg of RNA using the iScript cDNA Synthesis kit (Bio-Rad). From a 20μl reaction, 2μl of cDNA was used to assess Notch and β-Actin mRNA levels using real-time qRT-PCR. Primer and probe sets used were as follows:

hNotch1		
	forward	5'–ATGAGTTCCAGTGCGAGT–3'
	reverse	5'–TGTAAGTGTTGGGTCCGT–3'
	probe	5'–FAM–AGATGCCCAGTGAAGCCCGT–Blk_FQ–3'
β-actin		
	forward	5'–ACTGGGACGATATGGAGAAG–3'
	reverse	5'–GGTCATCTTTTCACGGTTGG–3'
	probe	5'–HEX–ACCACACCTTCTACAACGAGCTGC–Blk_FQ-3'

Flow cytometry: TO-DMC or TO-DMC+ hN1G4^{esn} "sending" cells were co-cultured with hN1G4^{esn} - No-Delta "receiving" cells in a transactivation assay. Co-cultures were plated at 10^5 cells/well in a 24 well plate at a ratio of 20% Delta cells to 80% Notch reporter cells. For each set of co-cultures, a 12 hr pulse of 1.6 ng/ml and 100 ng/ml doxycycline was performed (a well with no doxycycline served as a control). After doxycycline removal, the cells were washed 3x with 1xPBS (GIBCO) followed by addition of growth medium. Cells were incubated at 37°C, 5% CO_2 for an additional 24 hr before harvesting for flow cytometry analysis. Cells were trypsinized and diluted in 500μl analysis buffer (1x Hank's Balanced Salt Solution (GIBCO), 2.5 mg/ml BSA (w/v)). After filtering through a 40μm mesh, the co-cultured cells were analyzed for YFP fluorescence using a FACScalibur flow cytometer (Becton Dickinson).

Image and data analysis

Segmentation of images CFP images were used for automated segmentation of each frame of the movie. Segmentation was performed in a similar manner to previously described methods [2]. Briefly, each image was first subjected to an edge detection algorithm using Matlab. Closed edges were selected and several morphological and intensity criteria including total pixel area and mean fluorescence intensity level were used to identify the nuclei of the cells. The segmented image was used as a mask to calculate YFP and CFP fluorescence as well as centroid position for each nucleus. In some cases manual correction was applied to the segmented images. mCherry levels for the single

cell tracks in Fig. 3E were obtained by manual segmentation of the entire cell, in order to include total mCherry fluorescence.

Generating population averaged response curves To generate the YFP response curve for each movie (such as the ones in Figs. 2C and 3C), the total YFP fluorescence of each cell was calculated and background fluorescence was subtracted. Each data point on Figs. 2C and 3C represent the median of this total fluorescence per cell over all cells of one frame in the movie. The median, rather than the mean, was used for two reasons: (1) The median is less sensitive to occasional bright outliers such as dead cells and multinucleated cells which may offset the mean. (2) Median fluorescence taken in each frame roughly follows the response of the median cell lineage (see below), and thus better captures the sharp turn on feature shown in Fig. 3C-H. As shown in Fig. S13, the median curve essentially follows one of the single cell tracks for a while before switching to the next median curve. Hence, for such 'turn-on response' as in Fig. 3C, the median curve stays low until half the cells switch on. It then assumes a slope similar to that of the cells that have already responded. Thus, the rise time of the median curve provides a much better estimation of the median of the single cell lineage rise times than does the rise time of the mean curve (not shown).

The mean Delta-mCherry decay curve in Fig. 3C was calculated by taking the total mCherry level above background for each frame and dividing by the number of cells in that frame.

Single cell tracking was performed using a modified version of the Soft Assign algorithm 2,13 and was verified and corrected manually for each cell lineage tracked.

Data analysis Hill coefficients on Figs 2D, S1 were obtained by fitting the data to a Hill function of theform $y = A\frac{x^n}{K+x^n}$ where x is the $\mathrm{D_{plate}}$ value, y is the YFP production rate value, and A, K, and n are free fitting parameters. The fit was performed using a weighted non-linear least squares algorithm (Matlab). The weights vector was taken to be $\frac{1}{k+y_i}$, where y_i is the production rate value for the i^{th} data point and k is a minimal error parameter (typically 10% of $\max(y_i)$). This weighting takes into account both logarithmic errors (assuming a log-normal distribution of y_i's) and smaller fixed errors (i.e errors not proportional to y_i levels).We verified that the value obtained for the Hill

coefficients, n, was not sensitive to the exact fitting procedure and parameters. The single cell rise times for the distribution obtained in Fig. 3F were calculated by fitting the shifted YFP curves (such as the ones in Fig. 3E) to the following functional form:

$$y(t) = S(t + \frac{1}{\gamma}\ln\left(\frac{1+\exp(-\gamma(t-t_c))}{1+\exp(\gamma t_c)}\right) + c \tag{1}$$

Here, y represent the shifted YFP fluorescence level, t, represent time, t_c is the time at which the response turns on (i.e the 'knee'), γ, quantifies the sharpness of turn-on, S is the maximal slope at $> t_c$, and $c = y(0)$ is a constant. This functional form is derived in the following way: We first assume an effective Hill function response of the production rate of YFP (dy/dt) to the level of Delta-mCherry (DMC):

$$\frac{dy}{dt} = S\frac{k_d^m}{k_d^m + (DMC)^m} \tag{2}$$

Here, m and k_d represent the effective Hill coefficient and the Delta-mCherry value that gives half-maximal expression, respectively. We assume an exponential decay of Delta-mCherry (i.e. $\mathrm{D_{cis}}$): $DMC = D_0\exp(-\gamma_0 t)$ where D_0 and γ_0 are initial Delta-mCherry level and degradation rate, respectively. Hence the YFP production rate as a function of time is given by:

$$\frac{dy}{dt} = S\frac{1}{1+\exp(-\gamma(t-t_c))} \tag{3}$$

. Here, $\gamma = m\gamma_0$ and $\exp(\gamma t_c) = \left(\frac{D_0}{k_d}\right)^m$, The functional form in eq. (1) is obtained by integrating eq. (2) over time. Fitting of the data to eq. (1) was performed similarly to the Hill function fits described above. The rise time is then given by $\tau_{rise} = 2/\gamma$. We note that while eq. (1) is only an approximation to the actual response curve it fits the data well and enables estimation of rise times in simulated data.

All simulations (Figs. 3H, 4 B,C,D,G, and S5) were performed using the ode15s ordinary differential equation solver of Matlab. The following equations and parameters were used in the simulations:

Figure	Equations	Parameters	Initial conditions and remarks
3H	Eqs. 8-10,12 in theoretical supplementary	γ = 0.1, γ_S = 0.1, γ_R = 0.1, k_t = 2, k_c = .2, k_{RS} = 1500, β_N = 1, β_D = 0, β_R = 1.8X10^8, p = 2, D_p = {0.063, 0.084, 0.11, 0.15, 0.20, 0.26, 0.35, 0.46, 0.62, 0.82, 1.1, 1.4}	Dimensional units*. D_0 = 200, $N_0 = \frac{\beta_N}{\gamma+\frac{D_0}{k_c}+\frac{D_p}{k_t}}$.
Box, S11	Eqs. 8-10, 12 in theoretical supplementary	γ = 0.1, γ_S = 1.0, D_p=0, k_t = 10, k_c = 1, β_N = 20, β_D = {various from 0 to 40}	Dimensional units*. Plot displays status of cell 1 (left column of equations) with D_2 and N_2 = 0.
4B	Eqs. 21-23 in theoretical supplementary	γ = 0.1, γ_S = 1.0, k_t = 10, k_c = {0.5, 1, 10}, β_N = 20, $\beta_D^{(1)}$ = {various from 0 to 34}, $\beta_D^{(2)}$ = 1.35$\beta_D^{(1)}$	Dimensional units*.
4C	Eqs. 24-27 in theoretical supplementary	γ = 0.1, γ_S = 1.0, γ_R = 0.05, k_t = 5, k_c = .25, k_{RS} = 1500, β_N = 10, β_D^0 = 17.5, β_R = 150, p = 2, n = 1, m = 1, x_0 = 7	Dimensional units*. Use periodic boundary conditions.
4F,S17	Eqs. 50-52 in theoretical supplementary	τ =1 , κ_C ={0.55,0.1,0.05} k_{RS} = 3e5, β_N =200 , β_D = 1000, β_R =3000, m = 1, p = 1	Dimensionless, as described in theoretical supplementary. Periodic boundary conditions. $D(0), N(0), R(0)$ were randomly distributed between 0 and $\beta_D, \beta_N, \beta_R$, respectively.
S8	Eqs. 17-20 in theoretical supplementary	γ = 0.1, γ_S = 0.1, γ_R = 0.1, k_t = 2, k_c = .2, k_{RS} = 1500, β_N = 1, β_D = 0, β_R = 1.8X10^8, p = 2, D_p = {3.16, 4.76, 7.15, 10.8, 16.2, 24.3, 36.6, 55.1, 82.8}	Dimensional units*. D_0 = 200, $N_0 = \frac{\beta_N}{\gamma+\frac{D_0}{k_c}+\frac{D_p}{k_t}}$.
S10A Top Left	blue: Eqs. 24-27 in theoretical supplementary red: Eqs. 32-35 in theoretical supplementary green: Eqs. 36-39 in theoretical supplementary magenta: Eqs. 40-43 in theoretical supplementary	blue: γ = 0.1, γ_S = 1.0, γ_R = 0.05, k_t = 5, k_c = .25, k_{RS} = 1500, β_N = 10, β_D^0 = 17.5, β_R = 75, p = 2, x_0 = 7	Dimensional units*
		red: γ = 0.1, γ_S = 1.0, γ_R = 0.05, k_t = 5, k_b = 1750, β_N = 10, β_D^0 = 17.5, β_R = 75, p = 8, q = 8, x_0 = 7	
		green: : γ = 0.1, γ_S = 1.0, γ_R = 0.05, k_t = 5, k_b = 1750, k_f = 600, β_N = 0.25, β_N' = 19.75, β_D^0 = 17.5, β_R = 75, p = 8, q = 8, n = 2, x_0 = 7	
		magenta : γ = 0.1, γ_S = 1.0, γ_R = 0.05, k_t = 5, k_b = 1750, k_{f2} = 1800, β_N = 10 , β_D^0 = 35, β_R = 75, p = 8, q = 8, m = 2, x_0 = 7	
S10A Top Right	Same as top left	red: same as top left except β_N = 5	Dimensional units*
		green: same as top left except β_N = 0.125, β_N' = 9.875	
		magenta: same as top left except β_N = 5	
S10A Bottom Left	Same as top left	red: same as top left except β_D^0 = 8.75	Dimensional units*
		green: same as top left except β_D^0 = 8.75	
		magenta: same as top left except β_D^0 = 17.5	
S10A Bottom Right	Same as top left	red: same as top left except β_N = 5, β_D^0 = 8.75	Dimensional units*
		green: same as top left except β_N = 0.125, β_N' = 9.875, β_D^0 = 8.75	
		magenta: same as top left except β_N = 5, β_D^0 = 17.5	
S10B	Eqs. 24-27	black: γ = 0.1, γ_S = 1.0, γ_R = 0.05, k_t = 25, k_c = .05, k_{RS} = 1500, β_N = 10, β_D^0 = 15, β_R = 75, p = 1, x_0 = 7	Dimensional units*
		orange: same as black except β_N =5	
		light blue: same as black except β_D^0 = 7.5	
		gray: same as black except β_N =5, β_D^0 = 7.5	
S10C	Eqs. 28-31	γ = 0.1, γ_S = 1.0, γ_R = 0.05, k_t = 5, k_c = .25, k_{RS} = 1500, β_N = 5, β_N^0 = 5, β_D^0 = 17.5, β_R = 75, p = 2, x_0 = 7, nn=1, k_{nn} as indicated in legend.	Dimensional units*
S16A	Eqs: 6-10	γ = 0.1, γ_S = 0.1, γ_R = 0.1, k_t = 2, k_c = .2, k_{RS} = 1500, β_N = 1, β_D = 0, β_R = 1.8X10^8, β_m = {0.1,10}, γ_m = {0.1,10}, p = 2, D_p =1	Dimensional units*
S16B	Eqs: 6-10	γ = 0.1, γ_S = {0.1, 10}, γ_R = 0.1, k_t = 2, k_c = .2, k_{RS} = {1500,1.5}, β_N = 1, β_D = 0, β_R = 1.8X10^8, β_m = 0.1, γ_m = 0.1, p = 2, D_p =1	Dimensional units*
S16B	Eqs: 6-10	γ = 0.1, γ_S = 0.1, γ_R = 0.1, k_t = 2, k_c = .2, k_{RS} = 1500, β_N = 1, β_D = 0, β_R = 1.8X10^8, β_m = 0.1, γ_m = 0.1, p = 2, D_p =1, τ={0,1}	Dimensional units*. Delay introduced in eq. 7 for the translation step. Used dde23 in Matlab.

* Dimensional units: decay rates, γ, γ_S, γ_R are in hours^{-1}, production rates β_N, β_D, $\beta_R$in RFU/hour, affinities k_{RS}, k_b, k_f, k_{f2}in RFU, $k_c$in RFU x hours, x_0 in cell diameters, $D_p$and k_t in effective plate bound concentrations. Here Relative Fluorescent Units [RFU] replace concentrations which are unknown.

Supplementary Table S3: Simulation parameters

Supplementary Material — Theory

Cells responding to *trans*-Delta (D_{plate}) and *cis*-Delta (D_i)

Model with mutual inactivation of Delta and Notch in *cis* Let us first consider the case where cells containing Notch (N_i), Delta (D_i), and a Reporter of Notch signaling activity (R_i) are subjected to D_{plate} (D_p). The reactions we consider are the following:

$N_i + D_p \rightleftharpoons [N_i D_p] \rightarrow S_i + D_p$	*trans*–activation, with association/dissociation rates $k_D^{\pm}$ and cleavage rate k_S
$N_i + D_i \rightleftharpoons [N_i D_i] \rightarrow \varnothing$	*cis*–inhibition, with association/dissociation rates $k_C^{\pm}$ and inactivation/dilution rate γ_{ND}
$S_i \rightarrow R_i$	Signal activation of reporter

The first reaction represents the interaction of Notch with plate-bound Delta to form a complex that can then either dissociate or be cleaved to release the intracellular domain of Notch, denoted S_i. The dynamics of D_p is not relevant for the results presented below, thus we consider D_p not to be consumed in this binding reaction, so that its level is constant. The second reaction describes *cis*-inhibition with mutual inactivation of Notch and Delta. Note that in this subsubsection* we ignore the interaction between Delta in the cell and Notch in neighboring cells (*trans*-Notch), which is explicitly accounted for in the model presented in the Box. This interaction will be considered in subsubsection* II below. The third reaction represents the combined process in which the Notch intracellular domain translocates into the nucleus, binds with the CSL complex, and induces the expression of the reporter mRNA (m_R). This process is represented below phenomenologically by an increasing Hill function in the reporter production term.

These reactions are translated to the following set of ordinary differential equations:

$$\dot{N}_i = \beta_{\mathrm{N}} - \gamma_{\mathrm{N}} N_i - \left(k_{\mathrm{D}}^{+} N_i D_p - k_{\mathrm{D}}^{-} \left[N_i D_p\right]\right) - \left(k_{\mathrm{C}}^{+} N_i D_i - k_{\mathrm{C}}^{-} \left[N_i D_i\right]\right) \tag{1}$$

$$\dot{D}_i = \beta_{\mathrm{D}} - \gamma_{\mathrm{D}} D_i - \left(k_{\mathrm{C}}^{+} N_i D_i - k_{\mathrm{C}}^{-} \left[N_i D_i\right]\right) \tag{2}$$

$$\dot{[N_i D_p]} = k_{\mathrm{D}}^{+} N_i D_p - k_{\mathrm{D}}^{-} \left[N_i D_p\right] - k_{\mathrm{S}} \left[N_i D_p\right] \tag{3}$$

$$\dot{[N_i D_i]} = k_{\mathrm{C}}^{+} N_i D_i - k_{\mathrm{C}}^{-} \left[N_i D_i\right] - \gamma_{ND} \left[N_i D_i\right] \tag{4}$$

$$\dot{S}_i = k_{\mathrm{S}} \left[N_i D_p\right] - \gamma_{\mathrm{S}} S_i \tag{5}$$

$$\dot{m}_{\mathrm{R}i} = f_A \left(S_i; \beta_{\mathrm{m}}, p, k_{\mathrm{RS}}\right) - \gamma_{\mathrm{m}} m_{\mathrm{R}i} \tag{6}$$

$$\dot{R}_i = \alpha_R m_{\mathrm{R}i} - \gamma_{\mathrm{R}} R_i \tag{7}$$

The function $f_A \left(S_i; \beta_{\mathrm{m}}, p, k_{\mathrm{RS}}\right)$ is an activating Hill function of the form $\beta_{\mathrm{m}} \frac{S_i^p}{k_{\mathrm{RS}}^p + S_i^p}$. We assume fast cleavage of the Notch-D_{plate} complex, which allows us to apply the quasi-steady-state approximation to its dynamics ($\dot{[N_i D_p]} \approx 0$). Furthermore, we assume that Notch binds to *cis*-Delta irreversibly ($k_{\mathrm{C}}^{-} = 0$), and in that way the dynamics of Notch does no longer depend on the [$\mathrm{N}_i\mathrm{D}_i$] complex. Finally, we consider that the relaxation time of the receptor mRNA is much shorter than the protein relaxation times. With these approximations, the model is reduced to

$$\dot{N}_i = \beta_{\mathrm{N}} - \gamma N_i - N_i \frac{D_p}{k_t} - N_i \frac{D_i}{k_c} \tag{8}$$

$$\dot{D}_i = \beta_{\mathrm{D}} - \gamma D_i - N_i \frac{D_i}{k_c} \tag{9}$$

$$\dot{S}_i = N_i \frac{D_p}{k_t} - \gamma_{\mathrm{S}} S_i \tag{10}$$

$$\dot{R}_i = f_A \left(\frac{1}{\gamma_{\mathrm{S}}} N_i \frac{D_p}{k_t}; \beta_{\mathrm{R}}, p, k_{\mathrm{RS}}\right) - \gamma_{\mathrm{R}} R_i \tag{11}$$

where we have defined $\beta_{\mathrm{R}} = \frac{\beta_{\mathrm{m}} \alpha_R}{\gamma_{\mathrm{m}}}$, $k_t^{-1} \equiv \frac{k_{\mathrm{D}}^{+} k_{\mathrm{S}}}{k_{\mathrm{D}}^{-} + k_{\mathrm{S}}}$ and $k_c^{-1} \equiv k_{\mathrm{C}}^{+}$. We also take the simplifying assumption that $\gamma_{\mathrm{N}} = \gamma_{\mathrm{D}} \equiv \gamma$ (solving with different degradation rates is straightforward). Additionally, and based on the simplifying assumption that the promoter of the reporter R is a far from saturation (i.e., that $k_{\mathrm{RS}} \gg \frac{1}{\gamma_{\mathrm{S}}} N_i \frac{D_p}{k_t}$), we approximate its expression as

$$\dot{R}_i = \beta_{\mathrm{R}} \left(\frac{1}{\gamma_{\mathrm{S}} k_{\mathrm{RS}}} N_i \frac{D_p}{k_t}\right)^p - \gamma_{\mathrm{R}} R_i \tag{12}$$

We define the total concentration of Delta in the cell as $D_{\rm tot} = D_i + [N_i D_i]$. Using Eqs. (2) and (S1d) and assuming $\gamma = \gamma_{ND}$, we find that $D_{\rm tot}$ follows a simple linear dynamics:

$$\dot{D}_{\rm tot} = \beta_{\rm D} - \gamma D_{\rm tot} \tag{13}$$

This result holds even if the Notch-Delta binding is reversible ($k_{\rm C}^- \neq 0$), provided $\gamma = \gamma_{ND}$. The assumption of equal decay rates for both active Delta and the $[{\rm N}_i{\rm D}_i]$ complex is based on the experimental fact that adding Notch to our Delta-expressing cells does not lead to extra decrease of Delta levels beyond dilution. The trivial decay dynamics given by Eq. (13) is observed e.g. in the experiments of Fig. 3C, in which $\beta_{\rm D} = 0$. Equations (8)–(10) and (12) are the ones used in the simulations shown in Figs. 3H and Box.

Ultrasensitive response of the mutual inactivation switch Equations (8)–(9) and (12) can be readily solved in the steady state, leading to the following stationary levels of Notch and Delta:

$$N_{\rm st} = \frac{\beta_{\rm N} - \beta_{\rm D}}{2g} - \frac{\gamma k_c}{2} + \sqrt{\left(\frac{\beta_{\rm N} - \beta_{\rm D}}{2g} - \frac{\gamma k_c}{2}\right)^2 + \frac{k_c \gamma \beta_{\rm N}}{g}} \tag{14}$$

$$D_{\rm st} = \frac{\beta_{\rm D}}{\gamma + \frac{N_{\rm st}}{k_c}} \tag{15}$$

where $g = \gamma + D_p/k_t$. This solution is plotted in the Box figure of the main text, for the parameter values given in the Supplementary Table S3. For $\beta_{\rm N} > \beta_{\rm D}$ the system reaches a steady state of high Notch and low Delta, in which the cell can send, but not receive, signals. Conversely, when $\beta_{\rm D} > \beta_{\rm N}$ the steady state corresponds to high Delta and low Notch, and the cell can receive, but not send, signals. In order to quantify how sensitive the cell is in the region around the switch, we define the sensitivity parameter as the logarithmic derivative of the steady-state signal $S_{\rm st}$ with respect to a control parameter [1], which here we take to be the production rate of Delta, $\beta_{\rm D}$:

$$\xi = \frac{d \log S_{\rm st}}{d \log \beta_{\rm D}}$$

According to Eq. (10), $S_{\rm st} = D_p N_{\rm st}/\gamma_S k_t$, so that using the result given in (14) at the switch location ($\beta_{\rm D} = \beta_{\rm N}$, where the sensitivity is maximal), and in the limit of large *cis*-inhibition,

$\gamma k_c \ll \beta_{\rm N}/(\gamma + D_p/k_t)$, the sensitivity of the switch is approximately [2]

$$\xi \approx \sqrt{\frac{\beta_{\rm N}}{4k_c\gamma(\gamma + D_p/k_t)}} \tag{16}$$

For the parameters used in the Box figure, and given in the Supplementary Table S3, the switch is cleary ultrasensitive, with a sensitivity coefficient $\xi \approx 22.4$. This result does not change qualitatively when including reversibility in the binding of Notch and *cis*-Delta, since in the steady state a nonzero value of $k_{\rm C}^-$ would simply lead to a renormalization of the *cis*-inhibition parameter in the steady-state calculation, equal to $k_c = \frac{\gamma + k_{\rm C}^-}{\gamma k_{\rm C}^+}$.

The sensitivity parameter has been defined above in terms of the signal, S_i, but the experimentally accesible quantity is the reporter's promoter activity, $\dot{R}_i$. The relationship between the reporter sensitivity and the signal sensitivity is given in a straightforward way by

$$\xi_R = \frac{d\log \dot{R}_{\rm st}}{d\log \beta_{\rm D}} = \frac{d\log \dot{R}_{\rm st}}{d\log S_{\rm st}} \frac{d\log S_{\rm st}}{d\log \beta_{\rm D}} \approx p\,\xi\,,$$

where we have assumed that the reporter promoter is far from saturation, as in Eq. (12). Thus the sensitivity measured in our experiments, ξ_R, is a combination of the switch sensitivity, ξ, and the cooperativity p of the reporter promoter.

Another difference between the steady-state calculation presented above and the experimental measurements presented in Fig. 3 is the fact that in the experiments Delta production rate, $\beta_{\rm D}$, is zero, and only the decay of an initial concentration of Delta is observed, as expressed by Eq. (13). Under these conditions, in our experiments we measure the *transient* sensitivity [1] of the reporter's promoter activity as a function of the instantaneous total concentration of Delta, $D_{\rm tot}$. Extensive numerical simulations of our model show that both parameters are similar to each other within 20% in our parameter range.

Alternative model without Delta inactivation by Notch An alternative model that fails to account for several distinctive features of this system (see text) proposes that the receptor-ligand interaction is catalytic in Delta (in which case Delta is said to be rapidly recycled). The

corresponding reactions are the following:

$\mathrm{N}_i + \mathrm{D}_p \rightleftharpoons [\mathrm{N}_i\mathrm{D}_p] \rightarrow \mathrm{S}_i + \mathrm{D}_p$	*trans*–activation, with association/dissociation rates $k_D^{\pm}$ and cleavage rate k_S
$\mathrm{N}_i + \mathrm{D}_i \rightleftharpoons [\mathrm{N}_i\mathrm{D}_i] \rightarrow \mathrm{D}_i$	*cis*–inhibition, with association/dissociation rates $k_C^{\pm}$ and inactivation rate k_E
$\mathrm{S}_i \rightarrow \mathrm{R}_i$	Signal activation of reporter

The *cis*-inhibition reaction now conserves Delta, unlike the mutual-inactivation model. Using the same assumptions made in the preceding case, we obtain the following ordinary differential equations:

$$\dot{N}_i = \beta_{\mathrm{N}} - \gamma N_i - N_i \frac{D_p}{k_t} - N_i \frac{D_i}{k_c} \tag{17}$$

$$\dot{D}_i = \beta_{\mathrm{D}} - \gamma D_i \tag{18}$$

$$\dot{S}_i = N_i \frac{D_p}{k_t} - \gamma_{\mathrm{S}} S_i \tag{19}$$

$$\dot{R}_i = f_A\left(\frac{1}{\gamma_{\mathrm{S}}} N_i \frac{D_p}{k_t}; \beta_{\mathrm{R}}, p, k_{\mathrm{RS}}\right) - \gamma_{\mathrm{R}} R_i \tag{20}$$

which are the basis of the data in Fig. S8.

We note that in this case the steady-state solution of Eqs. (17)-(18) leads to the straightforward relation

$$N_{\mathrm{st}} = \frac{\gamma \beta_{\mathrm{N}}}{1 + \frac{D_p}{\gamma k_t} + \frac{\beta_{\mathrm{D}}}{k_c}} ,$$

which shows no sensitivity ($\xi = 1$) with respect to the control parameter β_{D}.

Effect of finite mRNA and signal lifetimes and reporter expression delay In the previous paragraphs we have assumed that the lifetimes of the signal, S_i, and of the reporter mRNA, $\mathrm{m}_{\mathrm{R}i}$, are very small in comparison with those of the proteins. We have also considered that the expression of the reporter is instantaneously determined by the level of signal. In order to ascertain that these approximations do not affect the qualitative behavior of our model as described above, we performed simulations of model (1)-(7), maintaining the assumptions of a fast cleavage of the Notch-D_{plate}

complex and irreversible binding between Notch and *cis*-Delta. We also added a finite delay τ in the Hill function f_A describing the transcription of the reporter mRNA, Eq. (6), which is now made to depend on the signal S_i at an earlier time τ.

Figure S16 shows the effect of these three factors, namely γ_m, γ_S, and τ, independently of each other. As expected, slower decays of the reporter mRNA and signal (plots A and B) lead to a delay in the turn-on of the reporter. A similar effect is observed in the presence of a time delay in the expression of the reporter with respect to the signal (plot C). In spite of these time shifts, the ultrasensitivity of the switch is not substantially affected, with at most a 30% change in ξ for lifetime variations in the 100× range. We also note that in these simulations the reporter expression is assumed to depend cooperatively on the signal, with a Hill coefficient $p = 2$ that is on the order of the experimentally observed value. Other parameters used in Fig. S16 are given in the Supplementary Table S3.

Two cells with varying Delta expression

In Fig. 4B of the text we show the amplification of Notch signaling in a cell with some $\beta_{\mathrm{D}}^{(1)}$ with a neighbor identical except for a higher Delta production rate $\beta_{\mathrm{D}}^{(2)}$ such that $\beta_{\mathrm{D}}^{(2)} \gtrsim \beta_{\mathrm{N}} \gtrsim \beta_{\mathrm{D}}^{(1)}$. The equations used to generate the figure are:

$$\dot{N}_1 = \beta_{\mathrm{N}} - \gamma N_1 - N_1 \tfrac{D_2}{k_t} - N_1 \tfrac{D_1}{k_c} \qquad \dot{N}_2 = \beta_{\mathrm{N}} - \gamma N_2 - N_2 \tfrac{D_1}{k_t} - N_2 \tfrac{D_2}{k_c} \tag{21}$$

$$\dot{D}_1 = \beta_{\mathrm{D}}^{(1)} - \gamma D_1 - N_2 \tfrac{D_1}{k_t} - N_1 \tfrac{D_1}{k_c} \qquad \dot{D}_2 = \beta_{\mathrm{D}}^{(2)} - \gamma D_2 - N_1 \tfrac{D_2}{k_t} - N_2 \tfrac{D_2}{k_c} \tag{22}$$

$$\dot{S}_1 = N_1 \tfrac{D_2}{k_t} - \gamma_{\mathrm{S}} S_1 \qquad \dot{S}_2 = N_2 \tfrac{D_1}{k_t} - \gamma_{\mathrm{S}} S_2 \tag{23}$$

Fig. 4B displays the numerical steady-state solution of these equations with parameter values as indicated in the Supplementary Table S3. Note that in Eq. (22) we have assumed that Delta is degraded due to its *trans* interaction with Notch. This is not, however, an essential feature of our model; ultrasensitivity is preserved even when Delta does not degrade in *trans*.

Spatially-varying Delta expression

Mutual inactivation model In Figs. 4C,D we consider a field of cells in which Delta production is given by $\beta_{\mathrm{D}}(x) = \beta_{\mathrm{D}}^{0} e^{-|x|/x_0}$ as a function of distance x from a central axis, yielding the axially-symmetric equations:

$$\dot{N}_i = \beta_{\mathrm{N}} - \gamma N_i - N_i \frac{D_i}{k_c} - N_i \frac{\langle D_j \rangle_i}{k_t} \tag{24}$$

$$\dot{D}_i = \beta_{\mathrm{D}}(x) - \gamma D_i - N_i \frac{D_i}{k_c} - \langle N_j \rangle_i \frac{D_i}{k_t} \tag{25}$$

$$\dot{S}_i = N_i \frac{\langle D_j \rangle_i}{k_t} - \gamma_{\mathrm{S}} S_i \approx 0 \quad \Longrightarrow \quad S_i \approx \frac{1}{\gamma_{\mathrm{S}}} N_i \frac{\langle D_j \rangle_i}{k_t} \tag{26}$$

$$\dot{R}_i = f_A(S_i; \beta_{\mathrm{R}}, p, k_{\mathrm{RS}}) - \gamma_{\mathrm{R}} R_i \tag{27}$$

The notation $\langle D_j \rangle_i$ refers to the average over Delta levels of all neighbors j of cell i. In particular, $\langle D_j \rangle_i \equiv \sum_j M_{ij} D_j$ where M is the connectivity matrix of a two-dimensional hexagonal lattice in which

$$M_{ij} = \begin{cases} 1/6 & \text{if } i \text{ and } j \text{ are neighbors} \\ 0 & \text{otherwise} \end{cases}$$

This assumes that Delta and Notch are uniformly distributed over the boundary of the cell. The notation $\langle N_j \rangle_i$ is defined similarly. Note that we now assume that the signal decays sufficiently faster than Notch, Delta and the reporter, which allows us to adiabatically eliminate its dynamics [Eq. (26)]. Figure S10 indicates the ratiometric character of this model by demonstrating that a common rescaling of β_{N} and β_{D} leaves the pattern unchanged.

Band–pass filter model One could alternatively conceive of a model in which Delta expression still varies as $\beta_{\mathrm{D}}(x)$ above, but instead of mutual inactivation there is a process that restricts expression of the Reporter within a narrow band of Signal values centered about some k_{b}. This

band–pass model is governed by the following equations:

$$\dot{N}_i = \beta_{\mathrm{N}} - \gamma N_i \tag{28}$$

$$\dot{D}_i = \beta_{\mathrm{D}}\left(x\right) - \gamma D_i \tag{29}$$

$$\dot{S}_i = N_i \frac{\langle D_j \rangle_i}{k_t} - \gamma_{\mathrm{S}} S_i \approx 0 \quad \Longrightarrow \quad S_i \approx \frac{1}{\gamma_{\mathrm{S}}} N_i \frac{\langle D_j \rangle_i}{k_t} \tag{30}$$

$$\dot{R}_i = \beta_{\mathrm{R}} \frac{S_i^p}{k_{\mathrm{b}}^p + S_i^p} \frac{k_{\mathrm{b}}^q}{k_{\mathrm{b}}^q + S_i^q} - \gamma_{\mathrm{R}} R_i \tag{31}$$

Figure S10 shows that this model is not ratiometric.

Band–pass filter model with Signal activating Notch Adding a proposed mechanism by which Notch signaling induces Notch expression to the band–pass filter model, we have

$$\dot{N}_i = \beta_{\mathrm{N}} + \beta'_{\mathrm{N}} \frac{S_i^n}{k_{\mathrm{f}}^n + S_i^n} - \gamma N_i \tag{32}$$

$$\dot{D}_i = \beta_{\mathrm{D}}\left(x\right) - \gamma D_i \tag{33}$$

$$\dot{S}_i = N_i \frac{\langle D_j \rangle_i}{k_t} - \gamma_{\mathrm{S}} S_i \approx 0 \quad \Longrightarrow \quad S_i \approx \frac{1}{\gamma_{\mathrm{S}}} N_i \frac{\langle D_j \rangle_i}{k_t} \tag{34}$$

$$\dot{R}_i = \beta_{\mathrm{R}} \frac{S_i^p}{k_{\mathrm{b}}^p + S_i^p} \frac{k_{\mathrm{b}}^q}{k_{\mathrm{b}}^q + S_i^q} - \gamma_{\mathrm{R}} R_i \tag{35}$$

Figure S10 shows that the addition of the Notch induction term does not generate a ratiometric response.

Band–pass filter model with Signal repressing Delta Another potential feedback which we can include in the band–pass filter model is one in which Notch signaling represses Delta expression. In this case the model reads

$$\dot{N}_i = \beta_{\mathrm{N}} - \gamma N_i \tag{36}$$

$$\dot{D}_i = \frac{\beta_{\mathrm{D}}\left(x\right)}{1 + \left(S/k_{f2}\right)^m} - \gamma D_i \tag{37}$$

$$\dot{S}_i = N_i \frac{\langle D_j \rangle_i}{k_t} - \gamma_{\mathrm{S}} S_i \approx 0 \quad \Longrightarrow \quad S_i \approx \frac{1}{\gamma_{\mathrm{S}}} N_i \frac{\langle D_j \rangle_i}{k_t} \tag{38}$$

$$\dot{R}_i = \beta_{\mathrm{R}} \frac{S_i^p}{k_{\mathrm{b}}^p + S_i^p} \frac{k_{\mathrm{b}}^q}{k_{\mathrm{b}}^q + S_i^q} - \gamma_{\mathrm{R}} R_i \tag{39}$$

Also for this feedback, Fig. S10 shows that the resulting response is not ratiometric.

Lateral inhibition patterning

In order to see the effect of Notch-Delta mutual inactivation on lateral inhibition patterning, let us first consider the classic lateral inhibition model studied by Collier *et al.* [3]:

$\mathrm{N}_i+\mathrm{D}_j \rightleftharpoons [\mathrm{N}_i\mathrm{D}_j] \rightarrow \mathrm{S}_i+\mathrm{N}_i+\mathrm{D}_j$	*trans*–activation, with association/dissociation rates $k_D^{\pm}$ and cleavage rate k_S
$\mathrm{S}_i \rightarrow \mathrm{R}_i$	Signal activation of reporter/repressor as Hill function
$\mathrm{R}_i \dashv \mathrm{D}_i$	Repression of Delta

The *trans*-activation here does not entail the degradation or inactivation of either Notch or Delta. The third reaction introduces feedback of incoming signaling on Delta expression. Applied to a two-dimensional hexagonal lattice of cells (as shown in Fig. 4F), these become the following set of ordinary differential equations:

$$\dot{N}_i = \beta_{\mathrm{N}} - \gamma N_i \tag{40}$$

$$\dot{D}_i = f_R\left(R_i; \beta_{\mathrm{D}}, m, k_{\mathrm{DR}}\right) - \gamma D_i \tag{41}$$

$$\dot{S}_i = N_i \frac{\langle D_j \rangle_i}{k_t} - \gamma_{\mathrm{S}} S_i \approx 0 \quad \Longrightarrow \quad S_i \approx \frac{1}{\gamma_{\mathrm{S}}} N_i \frac{\langle D_j \rangle_i}{k_t} \tag{42}$$

$$\dot{R}_i = f_A(S_i; \beta_{\mathrm{R}}, p, k_{\mathrm{RS}}) - \gamma_{\mathrm{R}} R_i \tag{43}$$

The function $f_R\left(R_i; \beta_{\mathrm{D}}, m, k_{\mathrm{DR}}\right)$ is a repressive Hill function of the form $\beta_{\mathrm{D}} \frac{k_{\mathrm{DR}}^m}{k_{\mathrm{DR}}^m + R_i^m}$. It is now worth switching to dimensionless units by transforming variables as $t \equiv \mathrm{t}\gamma_{\mathrm{R}}$, $N \equiv \frac{N}{N_0}$, $D \equiv \frac{D}{D_0}$, and $R \equiv \frac{R}{k_{\mathrm{DR}}}$ where $N_0 \equiv \frac{\beta_{\mathrm{N}}}{\gamma}$ and $D_0 \equiv \frac{\gamma_{\mathrm{S}} k_{RS}}{k_t} \frac{1}{N_0}$ to give

$$\tau \dot{N}_i = 1 - N_i \tag{44}$$

$$\tau \dot{D}_i = \beta_D \frac{1}{1 + R_i^m} - D_i \tag{45}$$

$$\dot{R}_i = \beta_R \frac{\left(N_i \langle D_j \rangle_i\right)^p}{1 + \left(N_i \langle D_j \rangle_i\right)^p} - R_i \tag{46}$$

where $\tau \equiv \frac{\gamma_R}{\gamma}$, $\beta_D \equiv \frac{\beta_D}{D_0\gamma}$, and $\beta_R \equiv \frac{\beta_R}{k_{DR}\gamma_R}$.

These equations can, under certain parameter ranges, generate lateral inhibition patterns as was shown by Collier *et al.* [3]. Recently, Plahte [4] has shown that the product of cooperativities $pm \equiv n$ must exceed 1 for a one-dimensional array of cells. Here we show that for a two-dimensional hexagonal lattice the condition on the product of cooperativities is more stringent, $n > 2$.

It is immediately clear that a necessary condition for patterning is the *in*stability of the homogeneous steady state (N^*, D^*, R^*) in which every cell has the same value of N_i, D_i, and R_i. Thus a linear stability analysis about the homogeneous steady state can provide necessary conditions for patterning [4]. The stability analysis requires the computation of the Jacobian at the homogeneous steady state, which is in this case complicated by the large number of variables (three times the number of cells). This is made simpler by an observation originally from Othmer and Scriven [5] that the Jacobian can be expressed as the sum of two tensor products of matrices, one for the internal dynamics and the other for interactions with neighbors: $J = I_k \otimes H + M \otimes B$. The matrix tensor product is defined as $A \otimes B = \begin{pmatrix} a_{11}B & \cdots & a_{1k}B \\ \vdots & \ddots & \vdots \\ a_{k1}B & \cdots & a_{kk}B \end{pmatrix}$. Also, here I_k is the $k \times k$ identity matrix (k is the number of cells involved in the interactions in question), $H_{ij} = \frac{\partial \dot{q}_i}{\partial q_j}$ is the change in production of species i for a change in species j in the same cell, M is the connectivity matrix as defined above, and $B_{ij} = \frac{\partial \dot{q}_i}{\partial \langle q_j \rangle}$ is the change in production of species i for a change in species j in a neighboring cell. N, D, and R correspond to species $i = 1, 2, 3$ respectively. For the model described above, the matrices are:

$$H = \begin{pmatrix} -\frac{1}{\tau} & 0 & 0 \\ 0 & -\frac{1}{\tau} & -\frac{D^*}{\tau R^*} m g_0 \\ \frac{R^*}{N^*} p f_0 & 0 & -1 \end{pmatrix} \text{ and } B = \begin{pmatrix} 0 & 0 & 0 \\ 0 & 0 & 0 \\ 0 & \frac{R^*}{D^*} p f_0 & 0 \end{pmatrix} \tag{47}$$

where $g_0 \equiv \frac{(R^*)^m}{1+(R^*)^m}$ and $f_0 \equiv \frac{1}{1+(N^* D^*)^p}$ are both ≤ 1. Othmer and Scriven [5] proved that the eigenvalues of the overall Jacobian are the eigenvalues of the various matrices $H + q_k B$ where q_k are the eigenvalues of the connectivity matrix M. Thus the eigenvalues λ of the Jacobian are set by the

characteristic equation:

$$\begin{vmatrix} -\frac{1}{\tau}-\lambda & 0 & 0 \\ 0 & -\frac{1}{\tau}-\lambda & -\frac{D^*}{\tau R^*}mg_0 \\ \frac{R^*}{N^*}pf_0 & \frac{R^*}{D^*}pf_0q_k & -1-\lambda \end{vmatrix} = 0 \tag{48}$$

which aside from $\lambda = -\frac{1}{\tau}$ happens to be quadratic in λ, meaning that for every q_k there are two eigenvalues of the Jacobian

$$\lambda_\pm = \frac{-\left(1+\frac{1}{\tau}\right) \pm \sqrt{\left(1+\frac{1}{\tau}\right)^2 - \frac{4}{\tau}\left(pmg_0f_0q_k+1\right)}}{2} \tag{49}$$

For instability we need only that a single λ have a real part that is positive, which will be so if $pmg_0f_0q_k \leq -1$. An analysis of the matrix M in [5] tells us that $q \geq -0.5$, meaning that $pmg_0f_0 > 2$ and, as $g_0, f_0 \leq 1$, $pm \equiv n > 2$ is a lower bound on the overall cooperativity of the system that must be satisfied for patterning to occur.

***cis*-Inhibition** To incorporate *cis*-inhibition we add an interaction $\mathrm{N}_i + \mathrm{D}_i \rightleftharpoons [\mathrm{N}_i\mathrm{D}_i] \rightarrow \varnothing$, and modify the *trans*-activation to annihilate Notch and Delta. Here it is more convenient to switch into a different set of dimensionless parameters in which Notch and Delta are normalized by the same quantity: $t \equiv \gamma_R \mathrm{t}$, $N \equiv \frac{N}{N_0}$, $D \equiv \frac{D}{D_0}$, and $R \equiv \frac{R}{R_0}$ where $N_0 = D_0 \equiv \gamma k_t$, and $R_0 \equiv k_{\mathrm{DR}}$. The equations are then

$$\tau\dot{N}_i = \beta_N - N_i - N_i\left\langle D_j\right\rangle_i - N_i\frac{D_i}{\kappa_c} \tag{50}$$

$$\tau\dot{D}_i = \beta_D\frac{1}{1+R_i^m} - D_i - \left\langle N_j\right\rangle_i D_i - N_i\frac{D_i}{\kappa_c} \tag{51}$$

$$\dot{R}_i = \beta_R\frac{\left(N_i\left\langle D_j\right\rangle_i\right)^p}{k_{RS}^p + \left(N_i\left\langle D_j\right\rangle_i\right)^p} - R_i \tag{52}$$

where $\tau \equiv \frac{\gamma_\mathrm{R}}{\gamma}$, $\beta_N \equiv \frac{\beta_\mathrm{N}}{\gamma N_0}$, $\beta_D \equiv \frac{\beta_\mathrm{D}}{\gamma D_0}$, $\beta_R \equiv \frac{\beta_\mathrm{R}}{\gamma_\mathrm{R} R_0}$, $\kappa_c \equiv \frac{k_c}{k_t}$, and $k_{RS} \equiv \frac{k_\mathrm{RS}\gamma_\mathrm{S}k_t}{N_0 D_0}$. These were used in Figs. 4F (right panel) and S17, which demonstrate patterning even with $pm \equiv n = 1$.

References

1. N.E. Buchler and M. Louis, *J. Mol. Biol.* **384**, 1106 (2008).

2. E. Levine, Z. Zhang, T. Kuhlman, T. Hwa, *PLOS Biol.* **5**(9), e229 (2007).

3. J.R. Collier, N.A.M. Monk, P.K. Maini, J.H. Lewis, *J. Theor. Biol.* **183**, 429 (1996).

4. E. Plahte, *J. Math. Biol.* **43**, 411 (2001).

5. H.G. Othmer, L.E. Scriven, *J. Theor. Biol.* **32**, 507 (1971).

Chapter 3

Patterning consequences of mutual *cis*-inhibition

The first section of this chapter has been published[1] in identical form, save for differences between journal and thesis formatting requirements. My contribution was as equal first author. The second section describes in additional detail properties of a Notch-mediated lateral inhibition mechanism enabled by mutual *cis*-inactivation which I conceived while work was ongoing on the contents of Chapter 1. Although it was posted to the ArXiv[2] before the preceding section was published, because we included a basic introduction to the model in the published paper the order in this chapter is chronologically inverted. The third section, describing results I have obtained by including mutual *cis*-inactivation in models of lateral induction, has not been published.

3.1 Mutual Inactivation of Notch Receptors and Ligands Facilitates Developmental Patterning

Abstract

Developmental patterning requires juxtacrine signaling in order to tightly coordinate the fates of neighboring cells. Recent work has shown that Notch and Delta, the canonical metazoan juxtacrine signaling receptor and ligand, mutually inactivate each other in the same cell. This cis-interaction generates mutually exclusive sending and receiving states in individual cells. It generally remains

[1] Sprinzak, D., Lakhanpal, A., LeBon, L., Garcia-Ojalvo, J. & Elowitz, M.B. Mutual Inactivation of Notch Receptors and Ligands Facilitates Developmental Patterning. *PLoS Comput Biol* **7**, e1002069 (2011)

[2] Lakhanpal, A., Sprinzak, D., & Elowitz, M.B. Mutual inactivation of Notch and Delta permits a simple mechanism for lateral inhibition patterning. *arXiv*:1005.4301v1 (2010).

unclear, however, how this mutual inactivation and the resulting switching behavior can impact developmental patterning circuits. Here we address this question using mathematical modeling in the context of two canonical pattern formation processes: boundary formation and lateral inhibition. For boundary formation, in a model motivated by Drosophila wing vein patterning, we find that mutual inactivation allows sharp boundary formation across a broader range of parameters than models lacking mutual inactivation. This model with mutual inactivation also exhibits robustness to correlated gene expression perturbations. For lateral inhibition, we find that mutual inactivation speeds up patterning dynamics, relieves the need for cooperative regulatory interactions, and expands the range of parameter values that permit pattern formation, compared to canonical models. Furthermore, mutual inactivation enables a simple lateral inhibition circuit architecture which requires only a single downstream regulatory step. Both model systems show how mutual inactivation can facilitate robust fine-grained patterning processes that would be difficult to implement without it, by encoding a difference-promoting feedback within the signaling system itself. Together, these results provide a framework for analysis of more complex Notch-dependent developmental systems.

Introduction

Notch signaling is the canonical metazoan juxtacrine signaling pathway. It is involved in many developmental processes in which neighboring cells adopt distinct fates. Examples of such processes include the delineation of sharp boundaries during the formation of Drosophila wing veins [1,2] and the formation of checkerboardlike patterns of differentiation, as occurs during Drosophila microchaete bristle patterning [3].

Notch signaling occurs through contact between a Notch receptor on one cell and a Delta/Serrate /LAG-2 (DSL) ligand such as Delta or Serrate (Jagged in mammalian cells) on a neighboring cell. This interaction leads to cleavage of Notch, releasing its intracellular domain, which translocates to the nucleus and serves as a co-transcription factor to activate target genes [4]. In addition to this activating trans interaction between Notch and DSL on neighboring cells, inhibitory cis interactions between Notch and DSL in the same cell suppress Notch signaling [5,6,7,8,9,10]. Recent

work indicates that this cis-interaction between Notch and DSL is symmetric: Notch inhibits its ligand, and the ligand inhibits Notch [9,11,12]. The molecular mechanism of this mutual inactivation between Notch and DSL, and whether or not it occurs at the cell surface, is still unclear [9,12,13,14].

In an individual cell, mutual inactivation of Notch and DSL results in an ultrasensitive switch between 'sending' (low Notch/ high DSL) and 'receiving' (low DSL/high Notch) cellular states (see Fig. 1) [11]. A cell with more total Notch than DSL (i.e. with a higher production rate of Notch than DSL given equal first order degradation rates) has an excess of free Notch but very little free DSL, making it a receiver (Fig. 1A, left). Conversely, a cell with more total DSL than Notch would have an excess of DSL and very little Notch, thus becoming a sender (Fig. 1A, right). In either state, both ligand-mediated inhibition of receptor and receptor-mediated inhibition of ligand contribute to the nonlinearity of the system. For a sufficiently strong cis interaction, the transition between these two states becomes very sharp, or ultrasensitive (Fig. 1A). This switch generates strongly-biased signaling if a sender cell interacts with a receiver cell (Fig. 1B, bottom), but if both interacting cells are in the same signaling state (Fig. 1B, top and middle panels) much less signal is transduced.

Given that the Notch signaling system is involved in many developmental processes, it is important to determine how this cisdependent send/receive signaling switch impacts pattern formation in developing tissues. A well-studied class of biological patterning systems is local self-activation with long-range inhibition [15]. Our model of Notch signaling-driven lateral inhibition patterning may be discussed in similar terms, with the mutual cis inhibition contributing to both the local and long-range effects. However, in this case the coupling required for "long-range" inhibition occurs via short-range nonlinear juxtracrine interaction between neighboring cells, instead of via linear diffusion of a signaling molecule across long distances [16]. Moreover, the mutual inactivation of Notch and DSL discussed above provides an improved source of intra-cellular self-activation [17] leading to the effects on pattern formation described here.

In order to understand the implications of the Notch-DSL signaling switch for developmental patterning, we analyzed mathematical models of two canonical developmental patterning processes: (1) morphogen gradient-driven boundary formation and (2) lateral inhibition. We compared models

incorporating mutual inactivation in cis to alternative models lacking this interaction. The results show how mutual inactivation provides several key advantages for patterning circuits: it can allow sharp boundary formation without intracellular feedback, maintain it across a broad range of morphogen gradient slopes, and make patterning insensitive to correlated fluctuations ('extrinsic noise') in Notch and ligand expression. In lateral inhibition circuits, mutual inactivation speeds up patterning and relaxes parametric requirements on the regulatory interactions. Finally, it permits a surprisingly simple, and counter-intuitive, lateral inhibition circuit architecture, in which Notch activates its own expression, and no additional feedback or involvement of other components is required.

Results

Mutual inactivation, even in the absence of intracellular feedback, generates sharp boundaries

Wing vein formation in the developing fly is a classic model system for studying the generation of sharp boundaries. In the *Drosophila* wing, there are four longitudinal veins that include several rows of cells that are more compact and have darker pigmentation than intervein cells. The position of the wing veins in the wing imaginal disk is initiated by EGF signaling during the early stages of larva development [18]. The final form (position and width) of the wing veins is refined by several subsequent processes. Notch signaling has been shown to specifically control the sharpening of the boundary between pro-vein (the region competent to produce vein fates) and intervein regions in the wing disc [1,2]. In this system, the Delta production rate is controlled by a gradient of veinless expression diminishing outward from the center of the pro-vein region (Fig. 2A, left). Notch signaling is observed in two sharply defined side-bands, which restrict further vein development to the region between them (Fig. 2A, right).

We analyzed two simplified models of boundary formation, with or without mutual inactivation (Figs. 2BC, Eqns. 1-6, and Supporting Information Text S1.2). In both models, we assume constant Notch production (at a rate denoted β_N) throughout the field of cells (blue line in Fig. 2D, top). We also assume that a linear gradient from the center of the vein, $x = 0$, controls the rate of ligand

production, denoted $\beta_D(x)$ (red lines in Fig. 2D, top). Alternative models with other gradient shapes lead to the same results shown below.

In the mutual inactivation (MI) model (Fig. 2C), mutually exclusive signaling states generate sharp side-bands (as observed experimentally) where 'sender' cells contact 'receiver' cells near the crossing of the Notch and DSL production rate profiles. This model does not consider any feedback of Notch signaling on either DSL or Notch itself in the same cell, and thus lateral inhibition does not arise in this case (in contrast with the lateral inhibition models below).

Alternatively, in the 'bandpass' (BP) model a similar Notch activity profile can be generated in the absence of mutual inactivation, but this requires a bandpass filter of Notch activity level which we represent phenomenologically as the product of increasing and decreasing Hill functions (Figs. 2B, S1A). Such a bandpass filter represents the effective action of diverse regulatory processes downstream of Notch signaling, which could exist in different signaling architecture alternatives to the MI mechanism. We note here that while transcriptional feedbacks on Notch and DSL have been described in vein formation [1,2], we do not explicitly consider them in these models in order to focus on the main effects of the mutual inactivation process. Our qualitative conclusions are insensitive to their inclusion. The equations representing these models are derived in the Supporting Information Text S1.2 and summarized in Eqns. 1-6.

Mutual inactivation makes boundary sharpness insensitive to morphogen gradient slope

The slope of the morphogen gradient is expected to vary in natural systems from fluctuations and/or genetic variability, and thus may be an important factor in determining boundary features. To investigate the effect of such variability on boundary formation, we systematically analyzed the responses of the two models to different morphogen gradient slopes. For both models, we maintained the position of the threshold at a constant distance from the center of the vein (Fig. 2D, top).

In the MI model, the width of the signaling bands remained nearly constant across a wide range of morphogen gradient slopes (Fig. 2D, middle). This resulted from the sharp switch from a sending to a receiving state at the $\beta_N = \beta_D(x)$ intersection. In contrast, the amplitude of the signaling bands changed systematically with the magnitude of the slope. This can be understood by considering how

much free Notch and free DSL is available at the sender-receiver interface. The concentration of free DSL or Notch in the sending or receiving cell, respectively, is approximately proportional to the difference in Notch and DSL production rates, which in turn is proportional to the slope of the gradient.

In contrast, the BP model shows substantial broadening of the bands at lower values of the gradient slope (Fig. 2D, bottom). Unlike in the MI model, here Notch signaling occurs throughout the field of cells and is simply filtered by the downstream bandpass. As a result, the width of the Notch signaling bands is approximately proportional to the width of the bandpass divided by the slope of the Notch signaling profile (Fig. S1B).

The key parameters controlling the reporter expression profiles are the strength of the *cis*-interaction, k_c^{-1} for the MI model (decreasing k_c leads to increasing *cis*-interaction strength), and cooperativity, p for the BP model. Interestingly, the BP model supports a sharp boundary only for sufficiently large p and sufficiently high slopes (Fig. 2E, bottom). In contrast, with the MI model, band sharpness is preserved across a broad range of k_c values and morphogen slopes (Fig. 2E, top). Thus, mutual inactivation enables a more robust patterning mechanism.

Wing vein mutant behavior is explained by the MI model

A striking aspect of the *Drosophila* wing vein system is observed in the heterozygous mutants of Notch and Delta (e.g. single copies of the Notch and Delta genes). While heterozygous mutants of Notch ($\text{Notch}^{+/-}$) or Delta ($\text{Delta}^{+/-}$) alone exhibit mutant phenotypes (causing thicker veins), the $\text{Notch}^{+/-}$ $\text{Delta}^{+/-}$ double mutant restores the wild-type phenotype [19,20,21]. More generally, several mutant phenotypes seem to depend on the ratio between the copy numbers of the Notch and DSL genes [19]. This ratiometric dependence of the vein width cannot be derived from the several known feedbacks operating in the *Drosophila* wing vein, but emerges automatically from the MI model. This is because the position of the Notch signaling band occurs where Notch and DSL production rates are equal. This position remains unchanged when both rates are multiplied by the same factor. By the same reasoning, the vein width (distance between side bands) increases with increasing ratios between the effective copy numbers of DSL and Notch, as shown in Figs. 3A, S2.

Interestingly, however, this picture breaks down when the maximum DSL production rate, $\beta_D^{\max} = \beta_D(x = 0)$, becomes smaller than the Notch production rate, $\beta_D^{max} < \beta_N$. What phenotype would we expect in this case? Here, since all cells are essentially 'receivers' we expect negligible levels of Notch signaling, leading to a phenotype of an unsharpened, diffusely-defined vein, that defaults to the pre-patterned vein-competent region. Indeed, the Delta$^{+/-}$ phenotype exhibits broad veins with diffuse boundaries, similar to Delta null mutant clones [19]. This result makes a quantitative prediction: the maximal DSL (Delta ligand in the case of the wing vein) production rate should be less than twice the constitutive Notch production rate in this system.

Mutual inactivation-based boundary formation is sensitive to intrinsic noise but robust to extrinsic noise

In the fly larva, the width of the vein remains quite constant over length-scales of many cells. This occurs despite the possibility of substantial fluctuations, or 'noise', in the expression of Notch, Delta, and other components [22]. In order to understand how gene expression noise affects the MI wing vein model, we considered the response of the system between two limiting cases [23]. At one extreme, noise can be completely 'intrinsic', meaning that Notch and DSL production rates fluctuate in an uncorrelated manner. At the opposite extreme, 'extrinsic' noise could dominate, generating correlated fluctuations in Notch and DSL production. As shown in Fig. 3B, intrinsic noise causes the width of the vein to become irregular (Fig. 3B, bottom), while extrinsic noise of the same magnitude has significantly less effect on width (Fig. 3B, top). To show the generality of this effect, we performed simulations of boundary formation patterning for a range of different noise amplitudes and correlations (Fig. 3C). These simulations show that the standard deviation of peak position (which is a measure of pattern robustness) decreases as the noise becomes more extrinsic.

This behavior emerges from the ratiometric sensitivity of the MI model to the levels of Notch and DSL. In the MI model, the signaling state of a cell (sending or receiving) is determined by the ratio of Notch to DSL — in 'sender' cells this ratio is smaller than one, and in 'receivers' it is greater than one. As the vein edge is defined by Notch signaling, it is restricted to the area where sender cells are in direct contact with receiver cells, at which Notch and DSL production rates are comparable (Fig.

2D). Extrinsic noise tends to maintain constant relative expression of Notch and DSL. Therefore, it does not disturb the segregation of cells into senders and receivers, and preserves the band of Notch signaling activity. This effect is maintained across a broad range of noise amplitudes and correlation levels.

Mutual inactivation speeds lateral inhibition patterning

Lateral inhibition models have been used to describe the formation of checkerboard-like patterns in which high DSL cells are surrounded by low DSL neighbors. This type of structure occurs in bristle patterning in Drosophila [3] and hair cell patterning in the vertebrate inner ear [24]. Standard lateral inhibition (LI) models assume that neighboring cells inhibit each other's differentiation through Notch signaling, which indirectly downregulates DSL expression to form an intercellular positive feedback loop (Fig. 4A, Supporting Information Text S1.3). Under the right conditions, this feedback loop can amplify small initial differences between cells and generate patterns in which neighboring cells exhibit alternating expression levels. A lateral inhibition model of this type was analyzed previously [16,25].

How does mutual inactivation affect the lateral inhibition patterning process? To address this question we systematically compared the standard LI model (Fig. 4A) to a lateral inhibition with mutual inactivation (LIMI) model (Fig. 4B, equations are summarized in Eqns. 10-12, and derived in Supporting Information Text S1.3). Because the MI interaction constitutes an additional, rapid intracellular feedback, we intuitively expected an effect on both the patterning speed and accessibility. To test this hypothesis, we performed dynamical simulations to determine patterning speed, and linear stability analysis about the system's homogeneous steady state (HSS) to determine pattern accessibility. The HSS is defined as the steady state in which all cells have identical concentrations of signaling system components [16,26].

Using dynamical simulations, we first compared how rapidly the LI and LIMI models are able to reach the patterned state from an initially non-patterned state. Fig. 4CDE shows the dynamics of DSL concentration in single cells for both models with one set of parameters (black dot in Fig. 5). The LI model initially spends a considerable time in a nearly homogeneous state (left of the

dashed line in Fig. 4D) before DSL concentrations diverge (red and blue curves, right of the dashed line). In contrast, in the LIMI model, DSL concentrations diverge much earlier (Fig. 4E). The LIMI process approaches the final patterned state more rapidly than the LI process, largely due to the difference in the rate of deviation from homogeneity. A similar difference in the patterning speed is observed over a large region in parameter space as shown in Fig. S3CDEF.

Why are the dynamics accelerated in the LIMI model? A key difference in the LIMI model is the inactivation terms, which are equivalent to effective degradation terms (e.g. $\frac{1}{k_c} N_i D_i$). Because protein degradation is assumed to be the slowest timescale in the system, increasing the degradation rate speeds up the overall response time. In principle such acceleration could be achieved in the LI model as well, just by increasing the magnitude of the constitutive degradation terms. Note, however, that in the LIMI model the additional degradation only occurs when both Notch and DSL are simultaneously present on the same cell. This causes an acceleration specifically during patterning, while avoiding unnecessary protein turnover that would result from increased constitutive degradation.

Mutual inactivation allows lateral inhibition without cooperative interactions

The potential for lateral inhibition pattern formation in a given system is strongly controlled by its dynamical behavior near the HSS. For some parameter sets, the HSS is stable and no patterning occurs. For other parameter sets, the HSS is unstable. In this case, although components' concentrations may initially approach their HSS values, in the presence of even arbitrarily small heterogeneous fluctuations they must subsequently diverge, generating the patterned state (Fig. 4C).

We next set out to systematically compare the patterning ability of the LI and LIMI models. We performed linear stability analysis of the HSS [16,26] across a broad range of parameter values, and determined the subset of parameter sets for which the system's HSS is unstable to perturbations (Fig. 5A-D). Formally, this is done by calculating the maximal escape rate from the nonpatterned HSS (Supplementary Information S4). If this rate, termed the Maximal Lyapunov Exponent (MLE), is positive, the HSS becomes unstable and patterning occurs.

In Fig. 5A-D we plot the MLE as a function of the production rates β_N and β_D for two

different effective cooperativities, for both the LI and LIMI models. At high cooperativity ($n = 3$), both models show a large region of parameter space in which the system patterns ($MLE > 0$) (Fig. 5AB), although quantitatively the LIMI MLE is generally greater than the LI MLE. In contrast, when $n = 1$, only the LIMI model supports patterning anywhere in the parameter space (Fig. 5CD). Thus, the mutual inactivation model circumvents the requirement for cooperative regulatory feedback in the standard lateral inhibition model. The qualitative behavior of Fig. 5A-D is maintained as long as the cis interaction is strong enough ($k_c \leq 1$).

Mutual inactivation permits lateral inhibition patterning with only a single level of transcriptional feedback

Mutual inactivation can have a more dramatic effect on patterning: Besides improving the performance of standard patterning circuits, it can enable an altogether different, and simpler, lateral inhibition circuit architecture. The essential requirement for lateral inhibition is that increased Notch activity in one cell reduces its ability to signal to its neighbors. In the presence of mutual inactivation, one way to achieve this is for Notch activity to directly up-regulate Notch expression (Fig. 6A). Increased levels of Notch result in more rapid removal of DSL through the mutual inactivation interaction, effectively downregulating it. Thus, a circuit in which Notch activates its own expression implements lateral inhibition with only a single level of transcriptional feedback, i.e. instead of Notch activating a repressor of DSL, there is direct downregulation of DSL through the mutual inactivation interaction. This type of autoregulation has been observed in some cases, such as the *C. elegans* AC/VU fate determination system [27]. We term this circuit architecture 'Simplest Lateral Inhibition with Mutual Inactivation' (SLIMI). Linear stability analysis of this SLIMI circuit (Fig. 6B) shows that patterning can occur across a broad range of parameter values. Moreover, as with the LIMI model, SLIMI does not require explicit cooperativity for patterning. Thus, lateral inhibition can be achieved with a startlingly simple circuit architecture.

Discussion

Even as the molecular components of patterning circuits become increasingly known, the ways in which these components interact dynamically to generate patterns often remains unclear. We and others recently reported evidence for a strong mutual inactivation interaction that occurs between Notch and DSL in the same cell [11,12]. Mutual inactivation between Notch and DSL is a relatively simple biochemical mechanism that generates an ultrasensitive, cell-autonomous, switch between "sending" and "receiving" states (Fig. 1). Other mechanisms such as cooperative binding of transcription factors and regulatory feedbacks can also generate switch-like responses, but they require a more complex regulatory setup (e.g. multiple binding sites, DNA looping, or more elaborate gene circuits) and are rarely observed to have effective cooperativity higher than 3 or 4 [28,29,30,31]. More generally, sequestration interactions are emerging as a widespread mechanism for sharp switching in diverse biological systems [32,33,34,35,36,37,38].

These and other experimental observations necessitate a revised analysis of patterning circuit mechanisms [10,11,12]. As an initial step, we have used mathematical modeling to analyze two canonical Notch-dependent patterning processes: the formation of sharp boundaries in the Drosophila wing vein [1,2] and the formation of alternating patterns of differentiation, such as that found in Drosophila SOP patterning [3,39]. The results described here show that mutual inactivation facilitates these patterning processes, and permits simpler regulatory architectures.

Boundary Formation

In the wing vein boundary, graded expression of Delta is converted to two sharply defined 'side bands' of Notch activity [1,2]. The mutual inactivation mechanism achieves this conversion without requiring additional circuit components. Furthermore, unlike a broad class of alternative models based on transcriptional cooperativity (e.g. the BP model), the MI model can generate sharp boundaries over a wide range of gradient profiles and biochemical parameters (Fig. 2DE). The MI model has a unique property that can experimentally distinguish it from other models: The pattern of expression of Notch target genes depends on the relative expression levels of Notch and DSL rather

than on their absolute concentrations (Figs. 3A, S2). This property can explain the ratiometric behavior observed in Notch and Delta heterozygous mutants [19,20] (Fig. S2). Interestingly, when DSL expression in our model is reduced below Notch expression level everywhere, very little signaling occurs (below the blue line in Fig. 3A). In this condition Notch signaling is no longer expected to restrict vein width, resulting in a broader vein with diffuse boundaries [2]. This leads to the following experimental prediction: by reducing Delta production continuously, the width of the veins should first decrease as the crossing points between Notch and Delta production rates move toward the center of the vein. However, this thinning should be followed by an abrupt switch to the unrestricted (wider) vein regime once $\beta_D^{\max} < \beta_N$ (Fig. 3A).

The same ratiometric behavior also underlies the dependence of the pattern on noise (Fig. 3BC): while the width of the boundary is sensitive to intrinsic noise (uncorrelated between Notch and DSL) it is robust to extrinsic noise (correlated between Notch and DSL). Experimental measurements of the correlations between Notch and Delta expression in wing discs (or other systems) would help to determine which noise regime is most relevant *in vivo*.

We note that transcriptional feedback of Notch signaling on Notch and Delta expression has been shown to occur in the *Drosophila* wing vein boundary [1,2]. Here we have omitted these feedbacks in order to focus specifically on the effects of mutual inactivation. However, it is important to note that these feedbacks are not sufficient to explain the experimentally observed ratiometric behavior (Fig. S10 in ref [11]). Experimental disruption of these feedbacks could help to determine what role they play in patterning, e.g. whether they function to control the pattern itself, to increase its amplitude, or to provide some other functionality in normal development.

Lateral Inhibition

Mutual inactivation facilitates lateral inhibition patterning in several ways. First, mutual inactivation accelerates patterning dynamics compared to an equivalent model without it (Fig. 4DE). The LIMI model accelerates dynamics by increasing protein turnover, but does so selectively only when both proteins are present on the same cell. Thus, once patterning is complete, there is no additional protein turnover cost. Notch has been shown to exhibit relatively fast response times

in some systems, and the lifetime of the cleaved intracellular domain of Notch is short and highly regulated [40], suggesting that the acceleration provided by mutual inactivation could be important in development. Furthermore, recent work has attributed minimization of errors in patterns of the sensory organ precursors to faster dynamics due to cis-inhibition [21].

A second advantage is that mutual inactivation removes the requirement that would otherwise exist for an explicitly cooperative step in the lateral inhibition feedback loop (Fig. 5). This requirement on the LI model was previously proven analytically both for a 1D chain [16] and a 2D [11] hexagonal lattice. In fact, mutual inactivation plays a dual role here: in addition to providing the non-linearity required for the amplification of small differences between neighboring cells, it also introduces an additional intracellular feedback reinforcing the intercellular feedback loop. When Notch signaling down-regulates DSL, this also reduces the rate of Notch inactivation, effectively freeing additional Notch receptors and leading to an additional increase in Notch signaling.

Finally, mutual inactivation allows a new, alternative circuit architecture for lateral inhibition: Instead of transcriptionally down-regulating DSL, Notch can up-regulate its own expression (Fig. 6A). This architecture is sufficient for lateral inhibition patterning across a broad range of parameters (Fig. 6B). This alternative architecture is intriguing because in some natural lateral inhibition circuits the regulatory pathway for Notchdependent down-regulation of DSL remains unclear [41,42] (we note that in other systems downregulation of DSL by Notch has been observed). At the same time, Notch up-regulation by Notch signaling has been shown in several lateral inhibition patterning examples, such as the AC/VU system in *C. elegans* [27]. This mechanism may provide the main feedback in lateral inhibition circuits, or may work in combination with the classical lateral inhibition feedback mechanisms on DSL (LIMI model). It will be interesting to determine to what extent this mechanism participates in various lateral inhibition systems.

In general, mutual inactivation of Notch and DSL in *cis* may be conceived as a direct, rapid, and sharp replacement for an additional level of intracellular feedback that would otherwise have been required to drive neighboring cells to distinct fates in a finegrained spatial pattern. In this sense we may say that an intrinsic difference-promoting logic is encoded in the signaling system itself by

the mutual inactivation phenomenon. Because of this, regulatory circuit architecture that achieves fine-grained patterns without MI can be made less complicated (i.e. with fewer regulatory levels) by including MI. Both examples analyzed here demonstrate this feature.

Together the results above provide a theoretical framework as well as testable hypotheses for the role of mutual inactivation between Notch and DSL in the generation of fine-grained developmental patterns. In the future, this analysis can be expanded to include additional circuit details such as further regulatory feedbacks, multiple Notch ligands and receptors, and modifiers of Notch signaling, and extended to additional Notchdependent patterning systems.

Materials and Methods

In summary, our model consists of three protein components - Notch (N), DSL (D), and a Reporter (R) - with two basic interactions: between Notch and DSL on different cells (in *trans*) to stimulate reporter production in the Notch-bearing cell, and between Notch and DSL on the same cell (in *cis*) to unproductively inactivate both molecules. These interactions are parametrized by the following quantities:

β_N, β_D, β_R: production rates of Notch, DSL, and Reporter target gene, respectively.

k_c^{-1}, k_t^{-1}: the strengths of the *cis*- and *trans*-interactions, respectively.

γ: degradation rate of Notch and DSL, assumed to be equal for simplicity (no loss of generality for the steady state solutions, see Supplementary).

γ_R: degradation rate of R.

k_{RS},n: affinity and Hill coefficient, respectively, of Reporter induction by Notch signaling.

$\langle D_j \rangle_i$: average concentration of DSL in all cells, indexed by j, that are neighboring cell i. Similarly, $\langle N_j \rangle_i$ denotes the average concentration of Notch in all neighbors of the i^{th} cell.

The description of the model in this section omits the dynamics of the *cis* and *trans* intermediate complexes, the Notch intracellular signaling domain, and the mRNAs corresponding to each protein. Formally, this is exact in the limit where these components' dynamics are rapid relative to that of the proteins. The former two of these conditions is reasonably expected to be valid. The Supporting

Information presents the model in full detail, and contains a demonstration that including finite mRNA lifetimes does not modify our conclusions (Fig. S4). We also note that the model considered here is insensitive to the exact mechanism for *cis*-inhibition and whether the *cis* interaction occurs at the surface or not.

MI model of boundary formation

$$\frac{dN_i}{dt} = \beta_N - \gamma N_i - \frac{N_i \langle D_j \rangle_i}{k_t} - \frac{N_i D_i}{k_c} \tag{1}$$

$$\frac{dD_i}{dt} = \beta_D(x) - \gamma D_i - \frac{D_i \langle N_j \rangle_i}{k_t} - \frac{N_i D_i}{k_c} \tag{2}$$

$$\frac{dR_i}{dt} = \beta_R \frac{\left(N_i \langle D_j \rangle_i\right)^n}{k_{RS} + \left(N_i \langle D_j \rangle_i\right)^n} - \gamma_R R_i \tag{3}$$

Bandpass (BP) model for boundary formation

$$\frac{dN_i}{dt} = \beta_N - \gamma N_i - \frac{N_i \langle D_j \rangle_i}{k_t} \tag{4}$$

$$\frac{dD_i}{dt} = \beta_D(x) - \gamma D_i - \frac{D_i \langle N_j \rangle_i}{k_t} \tag{5}$$

$$\frac{dR_i}{dt} = \beta_R \frac{\left(N_i \langle D_j \rangle_i\right)^p}{k_{RS}^p + \left(N_i \langle D_j \rangle_i\right)^p} \frac{1}{k_{RS}^p + \left(N_i \langle D_j \rangle_i\right)^p} - \gamma_R R_i \tag{6}$$

Compared to the MI model, these equations remove the *cis*-inhibition terms from the rates of change in Notch and DSL, and the production rate of the reporter R is now the product of two Hill functions, one decreasing and one increasing, with affinity k_{RS} and cooperativity p.

Lateral Inhibition (LI)

$$\frac{dN_i}{dt} = \beta_N - \gamma N_i - \frac{N_i \langle D_j \rangle_i}{k_t} \tag{7}$$

$$\frac{dD_i}{dt} = \beta_D \frac{1}{1 + R_i^m} - \gamma D_i - \frac{D_i \langle N_j \rangle_i}{k_t} \tag{8}$$

$$\frac{dR_i}{dt} = \beta_R \frac{\left(N_i \langle D_j \rangle_i\right)^n}{k_{RS} + \left(N_i \langle D_j \rangle_i\right)^n} - \gamma_R R_i \tag{9}$$

The parameters are defined consistently with the above. In these equations there is no *cis*-inhibition. The lateral inhibition is implemented by decreasing the production rate of DSL as a function of

signaling Reporter levels, by the $\frac{1}{1+R_i^m}$ factor.

Lateral Inhibition with Mutual Inactivation (LIMI)

$$\frac{dN_i}{dt} = \beta_N - \gamma N_i - \frac{N_i \langle D_j \rangle_i}{k_t} - \frac{N_i D_i}{k_c} \tag{10}$$

$$\frac{dD_i}{dt} = \beta_D \frac{1}{1+R_i^m} - \gamma D_i - \frac{D_i \langle N_j \rangle_i}{k_t} - \frac{N_i D_i}{k_c} \tag{11}$$

$$\frac{dR_i}{dt} = \beta_R \frac{\left(N_i \langle D_j \rangle_i\right)^n}{k_{RS} + \left(N_i \langle D_j \rangle_i\right)^n} - \gamma_R R_i \tag{12}$$

These differ from the LI model only by the inclusion of an additional cis-inhibition degradation term $\left(\frac{N_i D_i}{k_c}\right)$ to the dynamics of both Notch and DSL.

Simplest Lateral Inhibition by Mutual Inactivation (SLIMI)

$$\frac{dN_i}{dt} = \alpha_N + \beta_N \frac{\left(N_i \langle D_j \rangle\right)^n}{k_{NS} + \left(N_i \langle D_j \rangle\right)^n} - \gamma N_i - \frac{N_i \langle D_j \rangle_i}{k_t} - \frac{N_i D_i}{k_c} \tag{13}$$

$$\frac{dD_i}{dt} = \beta_D - \gamma D_i - \frac{D_i \langle N_j \rangle_i}{k_t} - \frac{N_i D_i}{k_c} \tag{14}$$

Numerical computations

Dynamical simulations were performed using Matlab's ode15s solver (ver. 7.6.0, The Mathworks). Figs. 2DE were generated by solving Eqs. 1-3 for the MI model and Eqns. 4-6 in the BP model. Simulations were performed on a 12x48 hexagonal cell array assuming periodic boundary conditions. The DSL production profiles used were $\beta_D = \beta_N \max\left(B\left|x\right| + 1 - 10.5, 0\right)$ for the MI model and $\beta_D(x) = \beta_N \max\left(B\left|x\right| + 0.5 - 10.5, 0\right)$ for the BP model, where B are the indicated slopes. Fig. 3A was generated using Eqns. 1-3 with DSL production rate profiles given by $\beta_D(x) = \beta_N \left(1 - \frac{f}{24}\left|x\right|\right)$, where $f = \beta_D^{\max}/\beta_N$ is as indicated in the figure. Figs. 3BC were generated using Eqns. 1-3 with multiplicative (static) noise terms for β_D and β_N. Generation of noise is described in Supporting Information Text S1.5. Figs. 4CDE were generated by solving Eqns. 7-12. These simulations were performed on a 12x12 hexagonal cell array assuming periodic boundary conditions. The MLE values in Fig. 5A-D were calculated by performing linear stability analysis on Eqns. 7-12 using previously described techniques ([16], Supporting Information Text S1.4). Parameters used throughout the

analysis are provided in Table S1.

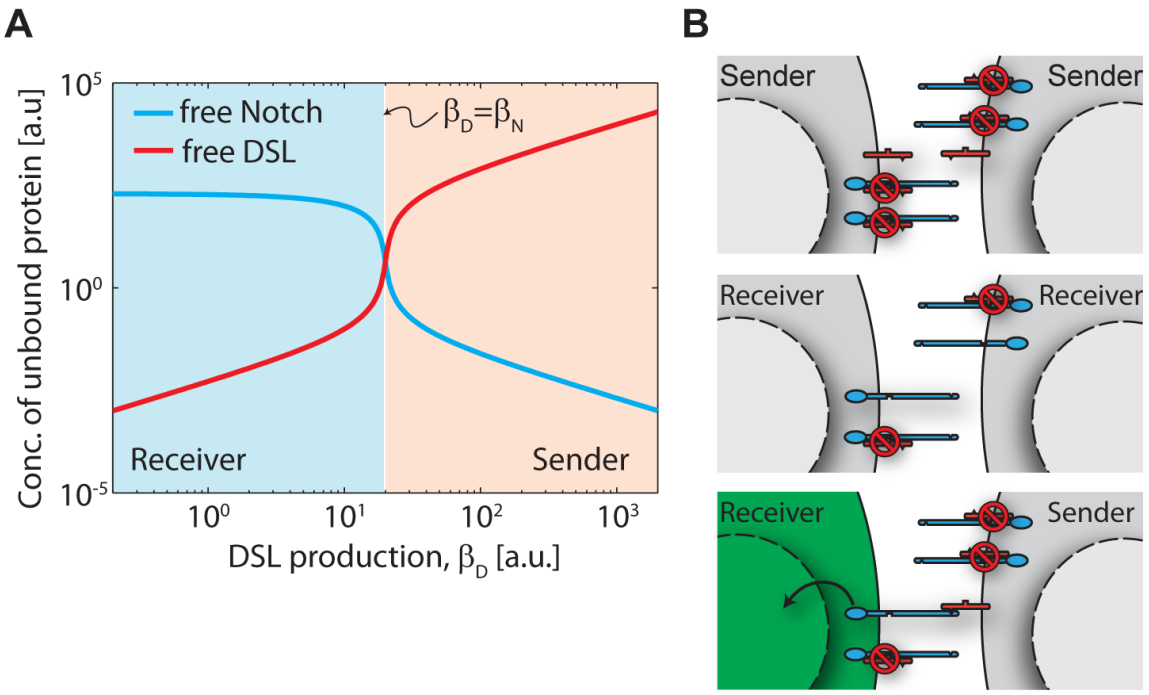

Figure 1: Ultrasensitivity due to mutual inactivation of Notch and DSL. (A) Plot of free DSL (red) and free Notch (blue) as a function of DSL production rate, β_D. A sharp switch (high logarithmic derivative) between sender and receiver states occurs when $\beta_D = \beta_N$. (B) Schematic illustration of sending and receiving states, showing that while very little signaling occurs when two neighboring cells are both senders (top) or both receivers (middle), strongly biased signaling can occur for the case of neighboring sender and receiver cells (bottom).

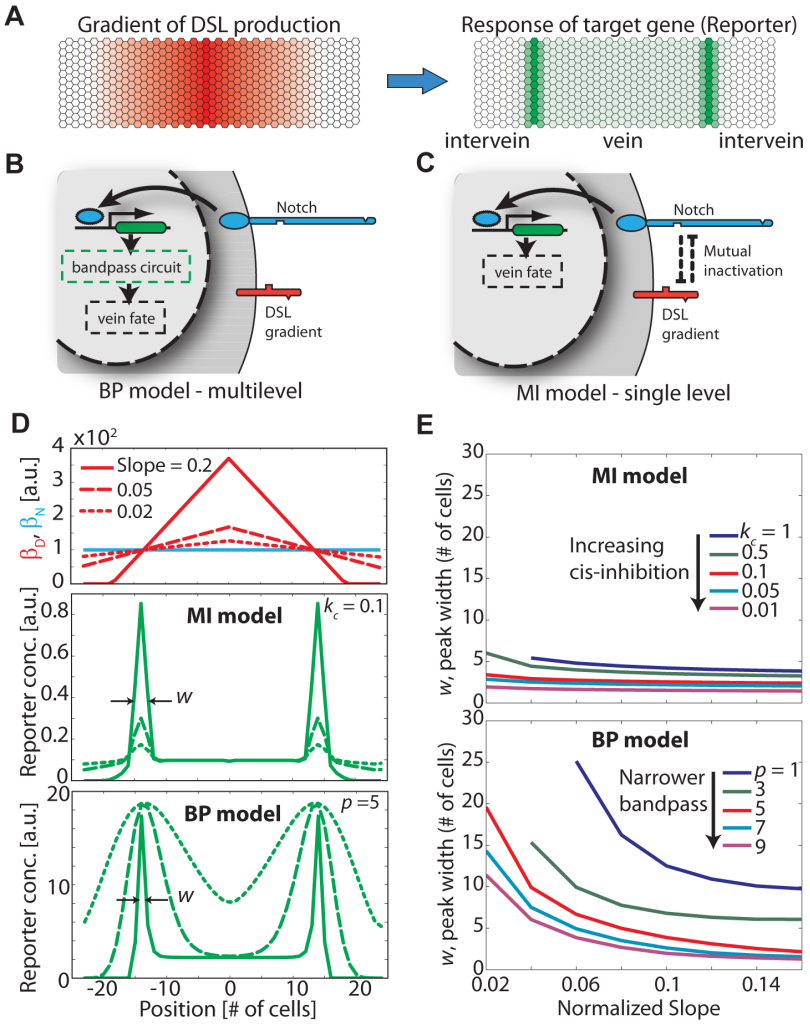

Figure 2: Mutual inactivation facilitates wing vein boundary formation. (A) Schematic of vein boundary formation. During vein formation a gradient in DSL production from the center of the vein (left, red) is converted into two sharply defined sidebands of Notch target expression (right, green). (B) Cartoon of the Bandpass regulatory mechanism, in which the boundary is determined by a transcription-level filter which determines the mapping from Notch activity to cell fate. Note that there is no feedback on the signaling system. (C) Cartoon of the Mutual Inactivation model regulatory mechanism, in which the level of Notch signaling directly determines the cell fate. Note again that there is no feedback on the signaling system. (D) Simulations of boundary formation. Top: DSL gradient profiles (three red curves) with varying slopes, chosen to generate side bands at a fixed position. Middle, bottom: Profiles of target reporter concentrations for the three slopes shown in the top panel for the MI model (middle) and the BP model (bottom). (E) Dependence of peak width on slope for the two models. In the MI model (top panel), peak width, w, remains small over a range of gradient slopes and strengths of the mutual inactivation interaction, k_c. Here, smaller k_c corresponds to stronger *cis*-inhibition (See Eqns. 12). In the BP model (bottom panel) peak width depends on the gradient slope as well as on the bandpass steepness parameter, p. Here, higher p corresponds to a steeper bandpass (see Eqn. 6 and Fig. S1). Note that for the BP model, DSL production profiles were shifted to lower levels (see Table S1) but maintained the same slopes compared to the profiles shown in (B, top). This made sure that the bandpass is in a functional regime in which Notch signaling varies linearly with position (e.g. as in Fig. S1B). See Table S1 for parameter values.

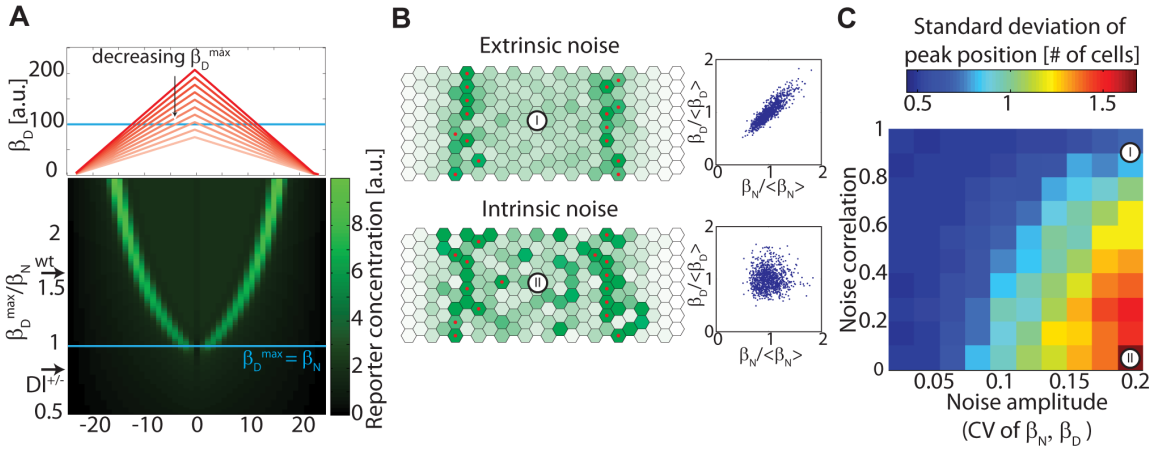

Figure 3: Boundary width is robust to correlated noise in Notch and Delta. (A) Notch reporter profiles (green heat map, bottom panel) for varying maximal production rates of DSL, $\beta_D^{\max}$ (red curves in top panel) and a fixed production rate of Notch, β_N (blueline). Spatially-uniform reduction in $\beta_D^{\max}$ levels (y-axis, lower panel) results in restriction of the vein to a progressively narrower region (lower panel). However, when the DSL production rate is lowered to the extreme when $\beta_D < \beta_N$ everywhere, all cells are in receiver states, and vein boundaries are no longer restricted by Notch signaling (see discussion in text). This is the expected behavior in the Delta$^{+/-}$ heterozygous mutant when the DSL production rate is half that of the wild-type (arrows), if in the wild type $\beta_D^{\max} < \beta_N$. (B) The Notch reporter profile is sensitive to intrinsic (uncorrelated) noise but robust to extrinsic (correlated) noise in Notch and DSL production rates. Simulations of boundary formation with static multiplicative production rate noise of similar magnitude but different degrees of correlation (blue scatter plots) show that the pattern is less sensitive to extrinsic noise (top) than intrinsic noise (bottom). (C) The effect of noise amplitude and degree of correlation on Notch reporter peak positions. Standard deviation in peak position (color bar) at each row (red dots in B) is calculated from 300 simulations of 8×24 cell arrays (such as those in B) for different noise attributes. The noise parameters used in B are marked (white circles). See Supporting Information Text S1.5 and Table S1 for parameter values and description of noise generation.

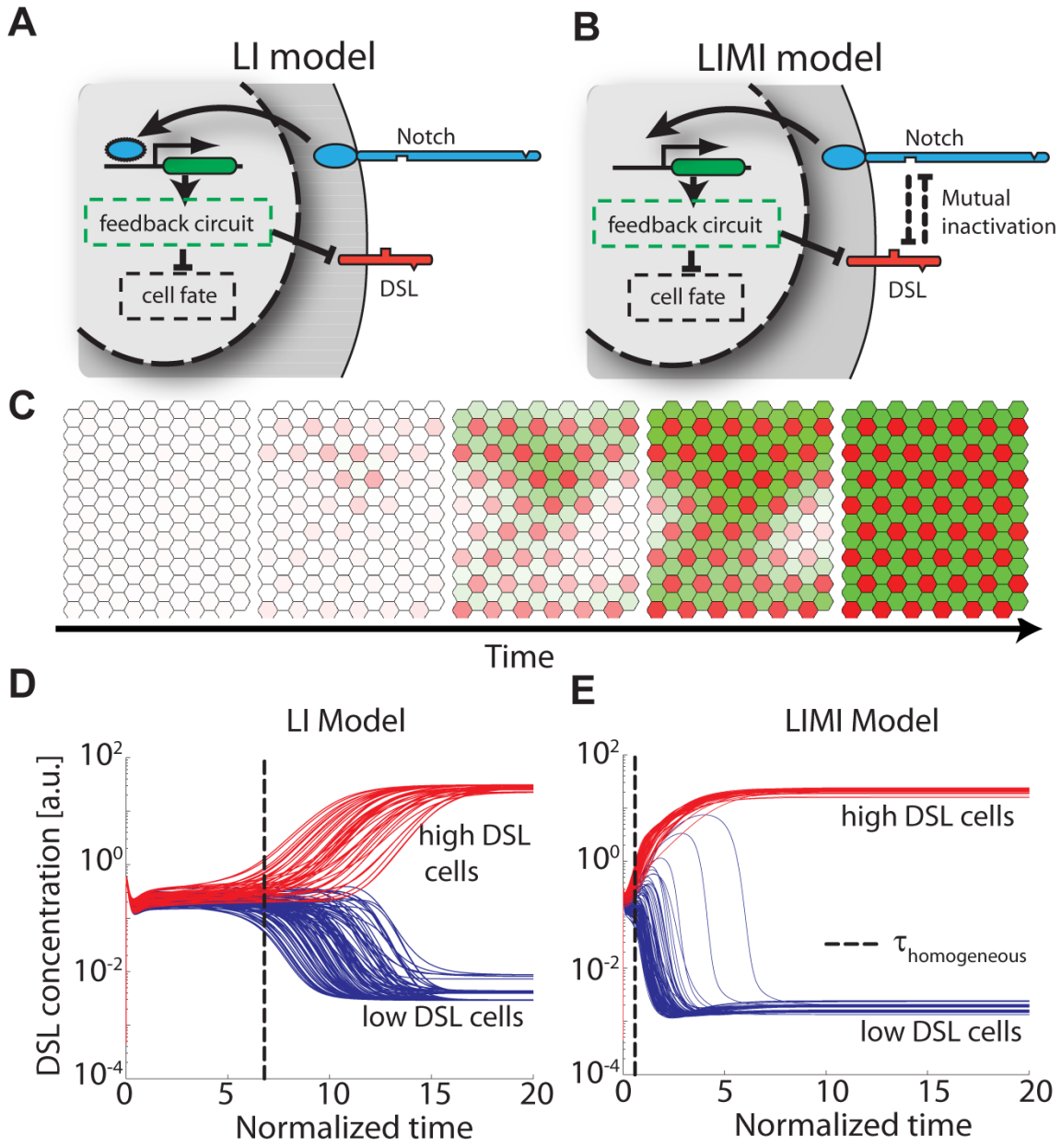

Figure 4: Mutual inactivation facilitates lateral inhibition patterning with faster dynamics. Comparison between (A) standard lateral inhibition model (LI) and (B) lateral inhibition with mutual inactivation (LIMI). (C) A typical simulation of lateral inhibition dynamics showing pattern generation from an initially homogenous steady state (HSS). (DE) Simulations reveal that the LIMI model (E) patterns faster than the LI model (D). Red and blue curves show the dynamics of DSL levels in cells with high and low final DSL levels, respectively. Vertical dashed lines indicate the homogeneous time defined as the time it takes the coefficient of variation to increase above 50% of its final value (see Fig. S3). These simulations were performed with the parameters indicated by the black dots in Fig. 5AB. Similar behavior is observed over most of the parameter space (see Fig. S3).

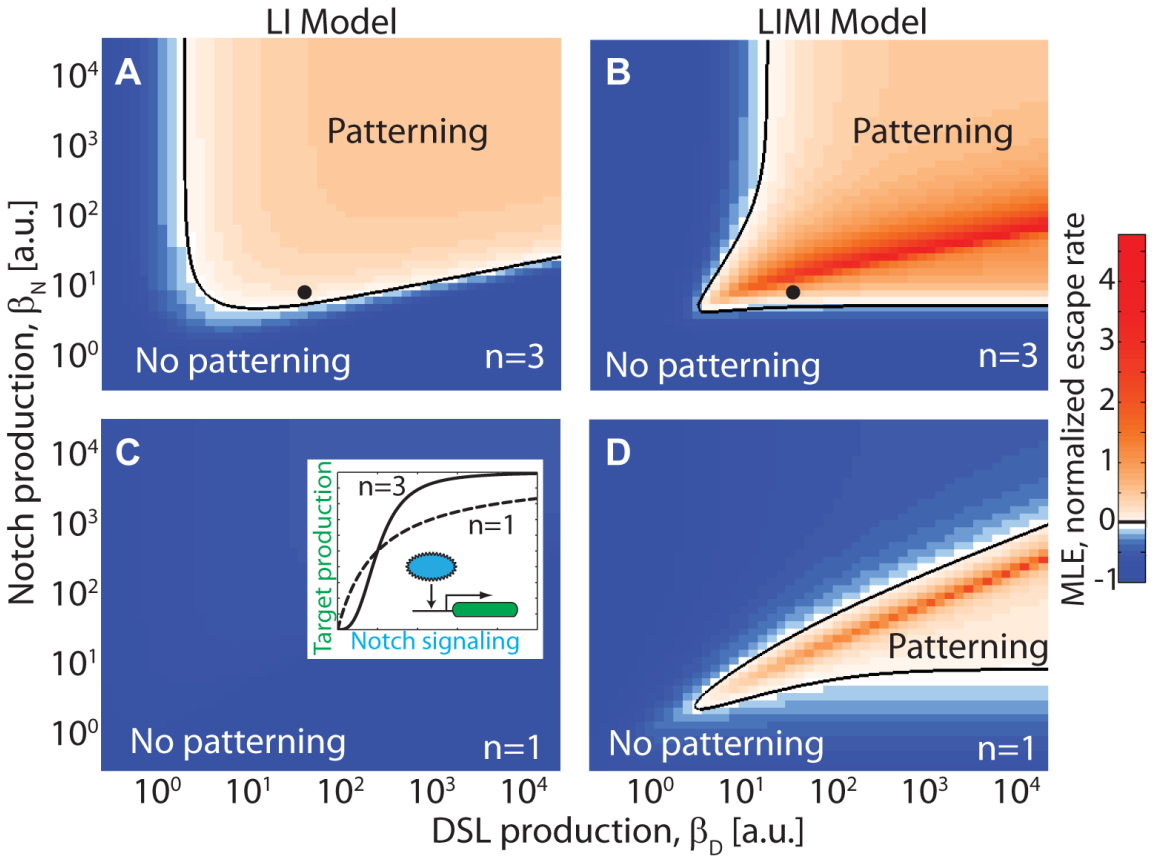

Figure 5: Mutual inactivation circumvents requirement for cooperative feedback. Escape rates from the HSS (indicated by Maximum Lyapunov Exponents, or MLE) as a function of β_D and β_N. MLE values were calculated using linear stability analysis (Supporting Information Text S1.4) for the LI (A,C) and LIMI (B,D) models. Positive MLE values (white/pink regions) support patterning, while negative MLE values (blue regions) do not. The dependence on feedback loop cooperativity (inset) can be seen by comparing (A,B) to (C,D). Black dots in A and B correspond to the parameters used to simulate Fig. 4DE.

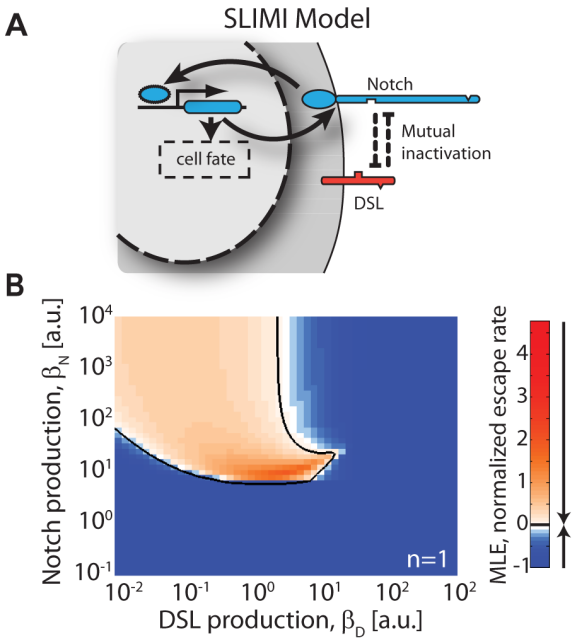

Figure 6: Simplified lateral inhibition with mutual inactivation (SLIMI). (A) Schematic of a simplified lateral inhibition circuit architecture. Here, Notch signaling activates expression of the Notch gene. Notch activation thus leads to higher Notch levels which, in turn, lead to lower levels of free DSL due to the mutual inactivation interaction between Notch and DSL proteins in *cis* (dashed arrows). (B) Calculation of the MLE for the SLIMI model. The SLIMI model can support patterning without cooperative feedback over a large region of parameter space. Color scale is the same as in Fig. 5AD. Equations and parameters are described in the Supporting Information Text S1.3 and Table S1, respectively.

References

1. Huppert SS, Jacobsen TL, Muskavitch MA (1997) Feedback regulation is central to Delta-Notch signalling required for Drosophila wing vein morphogenesis. Development 124: 3283-3291.

2. de Celis JF, Bray S, Garcia-Bellido A (1997) Notch signalling regulates veinlet expression and establishes boundaries between veins and interveins in the Drosophila wing. Development 124: 1919-1928.

3. Heitzler P, Simpson P (1991) The choice of cell fate in the epidermis of Drosophila. Cell 64: 1083-1092.

4. Bray SJ (2006) Notch signalling: a simple pathway becomes complex. Nat Rev Mol Cell Biol 7: 678-689.

5. de Celis JF, Bray S (1997) Feed-back mechanisms affecting Notch activation at the dorsoventral boundary in the Drosophila wing. Development 124: 3241-3251.

6. Micchelli CA, Rulifson EJ, Blair SS (1997) The function and regulation of cut expression on the wing margin of Drosophila: Notch, Wingless and a dominant negative role for Delta and Serrate. Development 124: 1485-1495.

7. Klein T, Brennan K, Arias AM (1997) An intrinsic dominant negative activity of serrate that is modulated during wing development in Drosophila. Dev Biol 189: 123-134.

8. Li Y, Baker NE (2004) The roles of cis-inactivation by Notch ligands and of neuralized during eye and bristle patterning in Drosophila. BMC Dev Biol 4: 5.

9. Matsuda M, Chitnis AB (2009) Interaction with Notch determines endocytosis of specific Delta ligands in zebrafish neural tissue. Development 136: 197-206.

10. Miller AC, Lyons EL, Herman TG (2009) cis-Inhibition of Notch by endogenous Delta biases the outcome of lateral inhibition. Curr Biol 19: 1378-1383.

11. Sprinzak D, Lakhanpal A, Lebon L, Santat LA, Fontes ME, et al. (2010) Cis-interactions between Notch and Delta generate mutually exclusive signalling states. Nature 465: 86-90.

12. Becam I, Fiuza UM, Arias AM, Milan M (2010) A role of receptor notch in ligand cis-inhibition in Drosophila. Curr Biol 20: 554-560.

13. Sakamoto K, Ohara O, Takagi M, Takeda S, Katsube K (2002) Intracellular cell-autonomous association of Notch and its ligands: a novel mechanism of Notch signal modification. Dev Biol 241: 313-326.

14. Glittenberg M, Pitsouli C, Garvey C, Delidakis C, Bray S (2006) Role of conserved intracellular motifs in Serrate signalling, cis-inhibition and endocytosis. EMBO J 25: 4697-4706.

15. Meinhardt H (1982) Models of biological pattern formation. London; New York: Academic Press. xi, 230 p. p.

16. Plahte E (2001) Pattern formation in discrete cell lattices. J Math Biol 43: 411-445.

17. Meinhardt H, Gierer A (1980) Generation and regeneration of sequence of structures during morphogenesis. J Theor Biol 85: 429-450.

18. Sturtevant MA, Roark M, Bier E (1993) The Drosophila rhomboid gene mediates the localized formation of wing veins and interacts genetically with components of the EGF-R signaling pathway. Genes Dev 7: 961-973.

19. de Celis JF, Bray SJ (2000) The Abruptex domain of Notch regulates negative interactions between Notch, its ligands and Fringe. Development 127: 1291-1302.

20. Vassin H, Vielmetter J, Campos-Ortega JA (1985) Genetic interactions in early neurogenesis of Drosophila melanogaster. J Neurogenet 2: 291-308.

21. Barad O, Rosin D, Hornstein E, Barkai N (2010) Error minimization in lateral inhibition circuits. Sci Signal 3: ra51.

22. Losick R, Desplan C (2008) Stochasticity and cell fate. Science 320: 65-68.

23. Elowitz MB, Levine AJ, Siggia ED, Swain PS (2002) Stochastic gene expression in a single cell. Science 297: 1183-1186.

24. Goodyear R, Richardson G (1997) Pattern formation in the basilar papilla: evidence for cell rearrangement. J Neurosci 17: 6289-6301.

25. Collier JR, Monk NA, Maini PK, Lewis JH (1996) Pattern formation by lateral inhibition with feedback: a mathematical model of delta-notch intercellular signalling. J Theor Biol 183: 429-446.

26. Othmer HG, Scriven LE (1971) Instability and dynamic pattern in cellular networks. J Theor Biol 32: 507-537.

27. Wilkinson HA, Fitzgerald K, Greenwald I (1994) Reciprocal changes in expression of the receptor lin-12 and its ligand lag-2 prior to commitment in a C. elegans cell fate decision. Cell 79: 1187-1198.

28. Ferrell JE, Xiong W (2001) Bistability in cell signaling: How to make continuous processes discontinuous, and reversible processes irreversible. Chaos 11: 227-236.

29. Saiz L, Vilar JM (2006) DNA looping: the consequences and its control. Curr Opin Struct Biol 16: 344-350.

30. Kuhlman T, Zhang Z, Saier MH Jr, Hwa T (2007) Combinatorial transcriptional control of the lactose operon of Escherichia coli. Proc Natl Acad Sci U S A 104: 6043-6048.

31. Dueber JE, Mirsky EA, Lim WA (2007) Engineering synthetic signaling proteins with ultra-sensitive input/output control. Nat Biotechnol 25: 660-662.

32. Buchler NE, Louis M (2008) Molecular titration and ultrasensitivity in regulatory networks. J Mol Biol 384: 1106-1119.

33. Levine E, Zhang Z, Kuhlman T, Hwa T (2007) Quantitative characteristics of gene regulation by small RNA. PLoS Biol 5: e229.

34. Elf J, Paulsson J, Berg OG, Ehrenberg M (2003) Near-critical phenomena in intracellular metabolite pools. Biophys J 84: 154-170.

35. Mehta P, Goyal S, Wingreen NS (2008) A quantitative comparison of sRNA-based and protein-based gene regulation. Mol Syst Biol 4: 221.

36. Lenz DH, Mok KC, Lilley BN, Kulkarni RV, Wingreen NS, et al. (2004) The small RNA chaperone Hfq and multiple small RNAs control quorum sensing in Vibrio harveyi and Vibrio cholerae. Cell 118: 69-82.

37. Buchler NE, Cross FR (2009) Protein sequestration generates a flexible ultrasensitive response in a genetic network. Mol Syst Biol 5: 272.

38. Levine E, Hwa T (2008) Small RNAs establish gene expression thresholds. Curr Opin Microbiol 11: 574-579.

39. Heitzler P (1993) Altered epidermal growth factor-like sequences provide evidence for a role of Notch as a receptor in cell fate decisions. Development 117: 1113-1123.

40. Fryer CJ, White JB, Jones KA (2004) Mastermind recruits CycC:CDK8 to phosphorylate the Notch ICD and coordinate activation with turnover. Mol Cell 16: 509-520.

41. Seugnet L, Simpson P, Haenlin M (1997) Transcriptional regulation of Notch and Delta: requirement for neuroblast segregation in Drosophila. Development 124: 2015-2025.

42. Parks AL, Shalaby NA, Muskavitch MA (2008) Notch and suppressor of Hairless regulate levels but not patterns of Delta expression in Drosophila. Genesis 46: 265-275.

Supporting Information

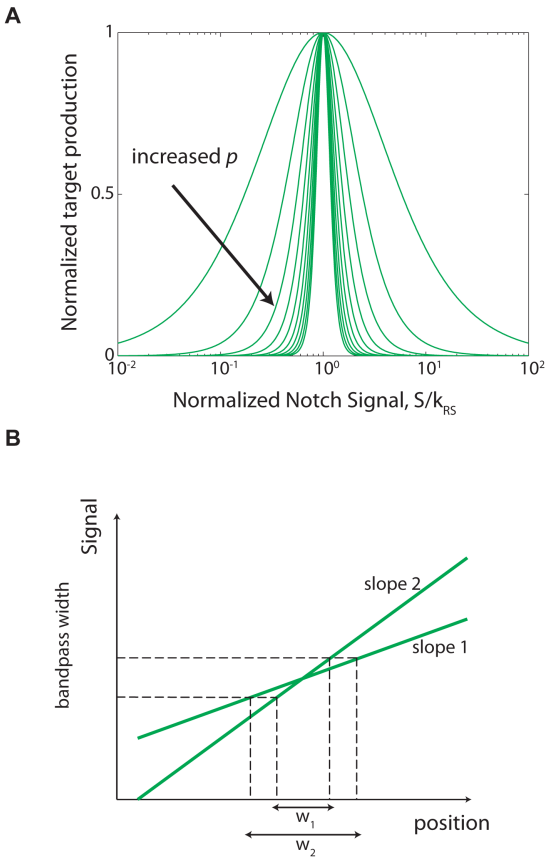

Figure S1: Properties of the bandpass function in the BP model. (A) Bandpass profiles for different cooperativities p Reporter production rate is proportional to a bandpass function given by $\beta_R \frac{\left(N_i \langle D_j \rangle_i\right)^p}{k_{RS}^p + \left(N_i \langle D_j \rangle_i\right)^p} \frac{1}{k_{RS}^p + \left(N_i \langle D_j \rangle_i\right)^p}$ (first term in the right hand side of Eqn. 6). Here, the input, $S_i = N_i \langle D_j \rangle_i$, is the concentration of cleaved Notch intracellular domain. Increased p corresponds to narrower bandpass function. (B) Width of reporter peaks in the BP model (Fig. 2D, bottom panel) is proportional to width of bandpass function and inversely proportional to slope of gradient. A schematic showing the widths of the reporter peaks (w_1,w_2) for a given bandpass width (on y-axis) and two gradient profiles (slope 1, slope 2).

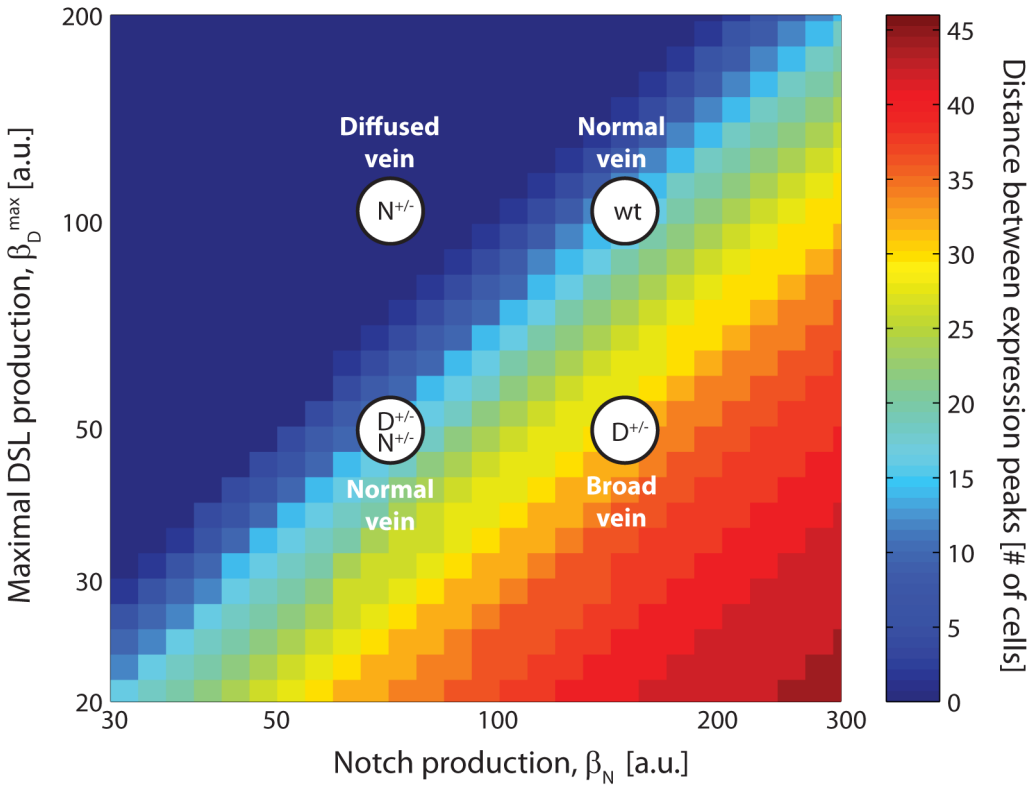

Figure S2: Ratiometric dependence of vein width on Notch and DSL production. The distance between the two reporter peaks for the MI model (shown in Figs. 2D, 3A) as a function of the production rates β_N and $\beta_D^{\max}$. Vein width is maintained when the ratio between production rates is the same. This ratiometric dependence explains why the double heterozygous mutant ($N^{+/-}D^{+/-}$) exhibits similar veins to the wildtype (wt) while the single heterozygous mutants show mutant phenotypes (four white circles). Here, the $D^{+/-}$ mutant falls in the receiving only regime (below the blue line in Fig. 3A) where very little Notch signaling is produced across the field of cells. In this case, the vein is not restricted by Notch signaling leading to a broad vein with diffused boundaries. Parameters for the presented simulations are given in Table S1.

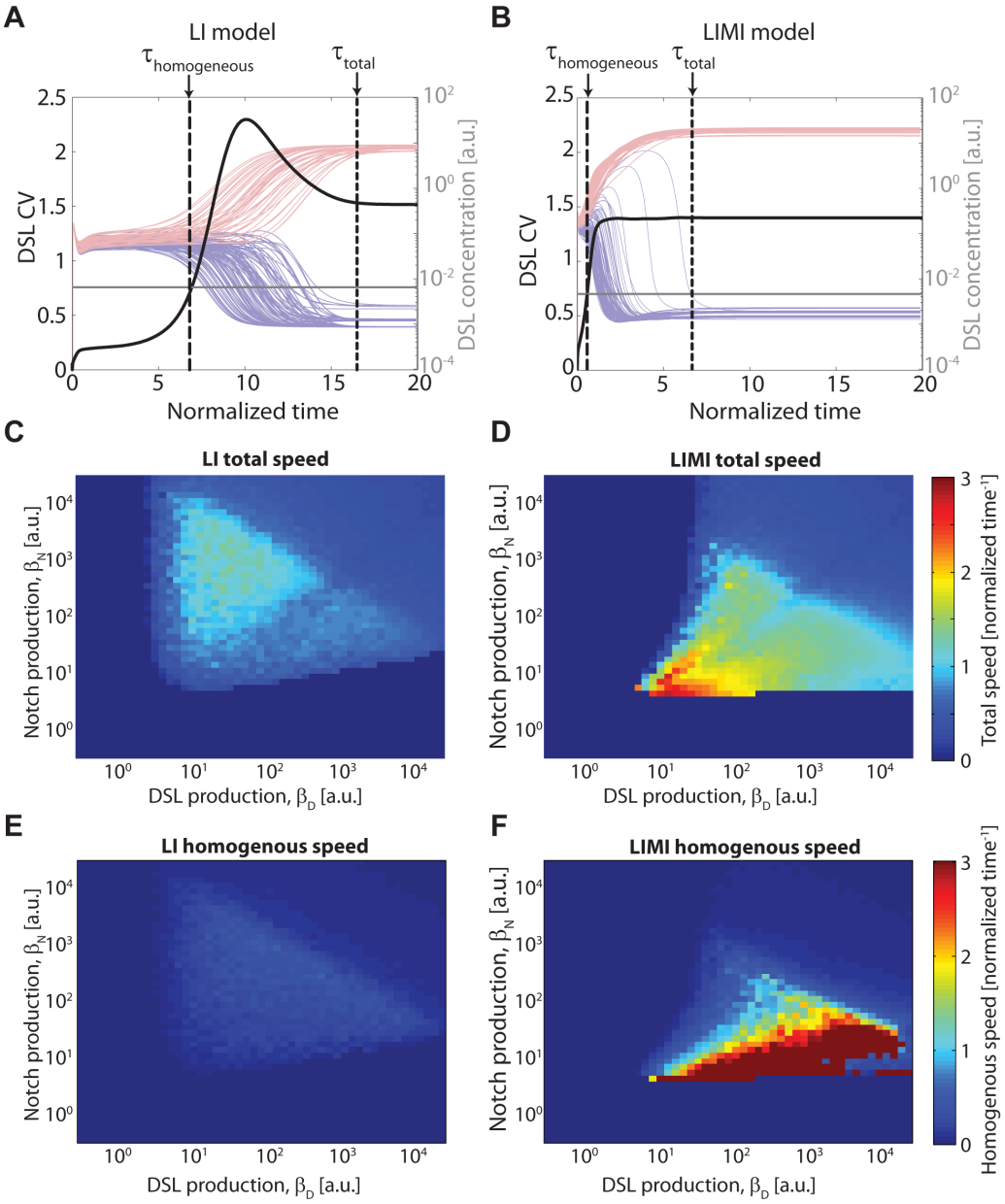

Figure S3: Faster patterning dynamics in the LIMI model. (A,B) Determination of homogeneous time and total time for patterning. Time course of the coefficient of variation (CV) of DSL concentration (black solid line) is plotted for the data shown in Fig. 4DE (faded red and blue) corresponding to the LI (S3A and 4D) and LIMI (S3B and 4E) models. Homogeneous time, $\tau_{homogeneous}$, (dashed line) is defined as the time at which the CV is 50% of its final value. The total time, τ_{total}, (dotted line) is calculated as the time it takes for the median high-DSL cell (faded red) to reach 95% of its final value. (C,D) Overall speed of patterning (defined as $1/\tau_{total}$) in the LI model (C) is lower than in the LIMI (D) model over a large range of parameters. (E,F) An even larger difference is observed for the homogeneous speed of patterning (defined as $1/\tau_{homogeneous}$) between the LI (E) and LIMI (F) models. This shows that onset of heterogeneity occurs much faster in the LIMI model and that this difference has a major contribution to the overall faster patterning dynamics.

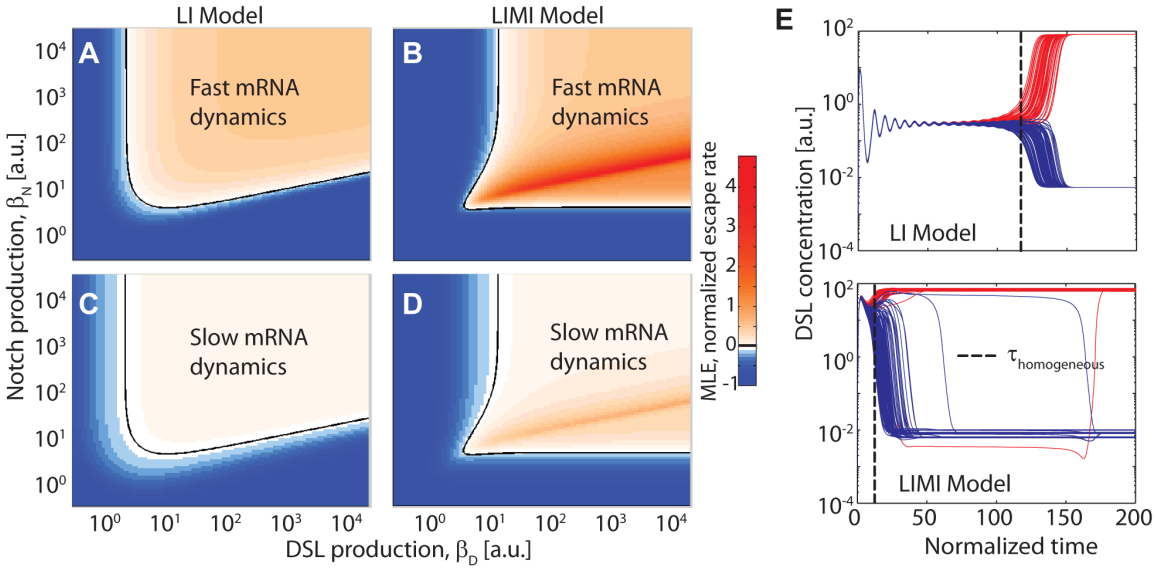

Figure S4: Effect of finite mRNA lifetimes. (A,B,C,D) The explicit inclusion of finite mRNA lifetimes in our MLE calculation does not affect the sign of the MLE, and correspondingly does not change our conclusion regarding the ability of the system to pattern. This is illustrated here for the (A,C) LI and (B,D) LIMI models with $n - 3$, with (C,D) MLE plots for mRNA dynamics comparable to the first-order protein degradation rate and (A,B) extremely fast mRNA dynamics. (E,F) We also repeated our patterning speed analysis with slow mRNA dynamics and find that our qualitative conclusion that the LIMI model (F) accelerates patterning by more rapidly departing from the homogeneous state than the LI model (E) to be unchanged from the fast mRNA case, with only a quantitative change in the overall patterning time. As in Fig. 4DE, the traces of DSL concentrations over time are colored according to the eventual fate of the cell (red for high Delta, blue for low Delta). As in Fig. 3AB, the dashed black line demarcates the homogeneous and heterogeneous phases.

Table S1: Parameter values

Figure	**Equations**	**Parameters**	**Initial conditions and comments**
1A	S1.2a,b	$\gamma = 0.1$, $\gamma_S = 1$, $k_c = 1$, $k_t = 10$, $\beta_N = 20$, $\beta_D = 0.02$-2000	
2D, middle	1–3	$\gamma = 0.1$, $\gamma_R = 1$, $k_c = 0.1$, $k_t = 5$, $k_{RS} = 1500$, $\beta_N = 100$, $\beta_D =$ see function F2Dm(x), $\beta_R = 75$, $n = 1$	
2D, lower	4–6	$\gamma = 0.1$, $\gamma_R = 1$, $k_c = 10000$, $k_t = 5$, $k_{RS} = 1500$, $\beta_N = 100$, $\beta_D =$ see function F2Dl(x), $\beta_R = 75$, $p = 5$	
2E, upper	1–3	$\gamma = 0.1$, $\gamma_R = 1$, $k_c =$ as indicated, $k_t = 5$, $k_{RS} = 1500$, $\beta_N = 100$, β_D = see function F2Eu(x), $\beta_R = 75$, n = 1	
2E, lower	4–6	$\gamma = 0.1$, $\gamma_R = 1$, $k_c = 10000$, $k_t = 5$, $k_{RS} = 1500$, $\beta_N = 100$, $\beta_D =$ see function F2El(x), $\beta_R = 75$, $p =$ as indicated	
3A	1–3	$\gamma = 0.1$, $\gamma_R = 1$, $k_c = 0.1$, $k_t = 5$, $k_{RS} = 1500$, $\beta_N = 100$, $\beta_D =$ see function F3A(x), $\beta_R = 75$, $n = 1$	
3BC	1–3, S5	$\gamma = 0.1$, $\gamma_S = 1$, $k_c = 0.1$, $k_t = 5$, $\beta_N = 100$, $\beta_D = 160$ to 40	

continued on next page...

– *continued*

Figure	**Equations**	**Parameters**	**Initial conditions and comments**
4D	S3.4	$\gamma = 1$, $\gamma_S = 1$, $\gamma_R = 1$, $k_t = 1$, $k_{DR} = 1$, $k_{RS} = 67$, $\beta_N = 0.1$ to 1e5, $\beta_D = 0.1$ to 1e5, $\beta_R = 1000000$, $m = 1$, $n = 3$	Cells initially set in a low Delta/high Notch condition with random perturbations from $D = \beta_D \cdot 10^{-5}$ and $N = \beta_N$ chosen uniformly from ±10%.
4E	S3.1	$\gamma = 1$, $\gamma_S = 1$, $\gamma_R = 1$, $k_c = 0.1$, $k_t = 1$, $k_{DR} = 1$, $k_{RS} = 67$, $\beta_N = 0.1$ to 1e5, $\beta_D = 0.1$ to 1e5, $\beta_R = 1000000$, $m = 1$, $n = 3$	Cells initially set in a low Delta/high Notch condition with random perturbations from $D = \beta_D \cdot 10^{-5}$ and $N = \beta_N$ chosen uniformly from ±10%.
5AC	S3.4	$\gamma = 1$, $\gamma_S = 1$, $\gamma_R = 1$, $k_c = 10000$, $k_t = 1$, $k_{DR} = 1$, $k_{RS} = 67$, $\beta_N = 0.1$ to 1e5, $\beta_D = 0.1$ to 1e5, $\beta_R = 1000000$, $m = 1$, $n = 3$ (A) or 1 (C)	
5BD	S3.1	$\gamma = 1$, $\gamma_S = 1$, $\gamma_R = 1$, $k_c = 0.1$, $k_t = 1$, $k_{DR} = 1$, $k_{RS} = 67$, $\beta_N = 0.1$ to 1e5, $\beta_D = 0.1$ to 1e5, $\beta_R = 1000000$, $m = 1$, $n = 3$ (B) or 1 (D)	
6	S3.2a,b	$\gamma = 1$, $\gamma_S = 1$, $k_c = 0.1$, $k_t = 1$, $k_{DR} = 1$,k_{NS} = various, $\beta_N = 0.1$ to 1e4, $\beta_D = 0.01$ to 1e3, $m = 1$, $n = 1$, $\alpha_N = 0.01 \cdot \beta_N$	
S1A	6	$p = 1$ to 10	

continued on next page...

– *continued*

Figure	**Equations**	**Parameters**	**Initial conditions and comments**
S2	1–3	$\gamma = 0.1$, $\gamma_R = 1$, $k_c = 0.1$, $k_t = 5$, $k_{RS} = 1500$, $\beta_N = 0.1$ to 3, $\beta_D =$ see function FS2(x), $\beta_R = 75$, $n = 1$	
S3ACE	S3.4	$\gamma = 1$, $\gamma_S = 1$, $\gamma_R = 1$, $k_c = 10000$, $k_t = 1$, $k_{DR} = 1$, $k_{RS} = 67$, $\beta_N =$ 0.1 to 1e5, $\beta_D = 0.1$ to 1e5, $\beta_R =$ 1000000, $m = 1$, $n = 3$	Cells initially set in a low Delta/high Notch condition with random perturbations from $D = \beta_D \cdot 10^{-5}$ and $N = \beta_N$ chosen uniformly from ±10%.
S3BDF	S3.1	$\gamma = 1$, $\gamma_S = 1$, $\gamma_R = 1$, $k_c = 0.1$, $k_t = 1$, $k_{DR} = 1$, $k_{RS} = 67$, $\beta_N =$ 0.1 to 1e5, $\beta_D = 0.1$ to 1e5, $\beta_R =$ 1000000, $m = 1$, $n = 3$	Cells initially set in a low Delta/high Notch condition with random perturbations from $D = \beta_D \cdot 10^{-5}$ and $N = \beta_N$ chosen uniformly from ±10%.

$$\text{F2Dm}(x) = \beta_N \max\left(B\,|x| + 1 - 10.5B, 0\right) \text{ where } B = \{0.02, 0.05, 0.2\}$$

$$\text{F2Dl}(x) = \beta_N \max\left(B\,|x| + 0.5 - 10.5B, 0\right) \text{ where } B = \{0.02, 0.05, 0.2\}$$

$$\text{F2Eu}(x) = \beta_N \max\left(B\,|x| + 1 - 10.5B, 0\right) \text{ where } B = \{0.02 - 0.16\}$$

$$\text{F2El}(x) = \beta_N \max\left(B\,|x| + 0.5 - 10.5B, 0\right) \text{ where } B = \{0.02 - 0.16\}$$

$$\text{F3A}(x) = \beta_N \left(1 - \frac{f}{24}\,|x|\right) \text{ where } f = \{0.5 - 2.5\}$$

$$\text{FS2}(x) = \beta_N \left(1 - \frac{f}{24}\,|x|\right) \text{ where } f = \{0.3 - 10\}$$

Derivation of equations governing Notch signaling

With inclusion of mutual inactivation (MI) Notch signaling occurs via the *trans*-interaction of Notch (N_i) on the surface of a cell i with Delta (D_j) on the surfaces of its neighbors j, which initiates a sequence of biochemical events resulting in cleavage of the Notch receptor to free its intercellular signaling domain (S_i) for translocation to the nucleus, where it may induce the expression of some Notch signaling reporter (R_i). Additionally, Notch and Delta on the same cell surface (N_i and D_i) *cis*-inhibit by forming a complex that inactivates both molecules in what we term the Mutual Inactivation (MI) mechanism [1]. Thus the reactions we consider are the following:

$\mathrm{N}_i{+}\mathrm{D}_j \rightleftharpoons [\mathrm{N}_i\mathrm{D}_j] \rightarrow \mathrm{S}_i$	*trans*–activation, with association/dissociation rates $k_D^{\pm}$ and cleavage rate k_S
$\mathrm{N}_i{+}\mathrm{D}_i \rightleftharpoons [\mathrm{N}_i\mathrm{D}_i] \rightarrow \varnothing$	*cis*–inhibition, with association/dissociation rates $k_C^{\pm}$ and inactivation/dilution rate γ_{ND}
$\mathrm{S}_i \rightarrow \mathrm{R}_i$	Signal activation of reporter

The first reaction corresponds to *trans*-activation, the second to *cis*-inhibition with mutual inactivation, and the third to Notch signaling-mediated induction of reporter expression, as described above. These reactions are described by the following kinetic equations:

$$\dot{\mathrm{N}}_i = \beta_{\mathrm{N}} - \gamma_{\mathrm{N}}\mathrm{N}_i - \left(k_{\mathrm{D}}^{+}\sum_{j=]i[}\frac{1}{l_{ij}}\mathrm{N}_i\mathrm{D}_j - k_{\mathrm{D}}^{-}\sum_{j=]i[}\frac{1}{l_{ij}}[\mathrm{N}_i\mathrm{D}_j]\right) - \left(k_{\mathrm{C}}^{+}\mathrm{N}_i\mathrm{D}_i - k_{\mathrm{C}}^{-}[\mathrm{N}_i\mathrm{D}_i]\right) \tag{S1a}$$

$$\dot{\mathrm{D}}_i = \beta_{\mathrm{D}} - \gamma_{\mathrm{D}}\mathrm{D}_i - \left(k_{\mathrm{D}}^{+}\sum_{j=]i[}\frac{1}{l_{ij}}\mathrm{N}_j\mathrm{D}_i - k_{\mathrm{D}}^{-}\sum_{j=]i[}\frac{1}{l_{ij}}[\mathrm{N}_j\mathrm{D}_i]\right) - \left(k_{\mathrm{C}}^{+}\mathrm{N}_i\mathrm{D}_i - k_{\mathrm{C}}^{-}[\mathrm{N}_i\mathrm{D}_i]\right) \tag{S1b}$$

$$[\dot{\mathrm{N}_i\mathrm{D}_j}] = k_{\mathrm{D}}^{+}\mathrm{N}_i\mathrm{D}_j - k_{\mathrm{D}}^{-}[\mathrm{N}_i\mathrm{D}_j] - k_{\mathrm{S}}[\mathrm{N}_i\mathrm{D}_j] \tag{S1c}$$

$$[\dot{\mathrm{N}_i\mathrm{D}_i}] = k_{\mathrm{C}}^{+}\mathrm{N}_i\mathrm{D}_i - k_{\mathrm{C}}^{-}[\mathrm{N}_i\mathrm{D}_i] - \gamma_{ND}[\mathrm{N}_i\mathrm{D}_i] \tag{S1d}$$

$$\dot{\mathrm{S}}_i = k_{\mathrm{S}}\sum_{j=]i[}\frac{1}{l_{ij}}[\mathrm{N}_i\mathrm{D}_j] - \gamma_{\mathrm{S}}\mathrm{S}_i \tag{S1e}$$

$$\dot{\mathrm{m}}_{\mathrm{R}i} = f_A(\mathrm{S}_i;\beta_{\mathrm{m}},n,k_{\mathrm{RS}}) - \gamma_{\mathrm{m}}\mathrm{m}_{\mathrm{R}i} \tag{S1f}$$

$$\dot{\mathrm{R}}_i = \alpha_R\mathrm{m}_{\mathrm{R}i} - \gamma_{\mathrm{R}}\mathrm{R}_i \tag{S1g}$$

The notation $j =]i[$ refers to indices j representing neighbors of cell i and l_{ij} measures the ratio of the length of the interface between cells i and j and the total perimeter of cell i, reflecting the assumption that Notch and Delta are uniformly distributed on the cell surface. The increasing Hill function $f_A\left(\mathrm{S}_i;\beta_\mathrm{m},n,k_\mathrm{RS}\right)\equiv\beta_m\frac{\mathrm{S}_i^n}{k_\mathrm{RS}^n+\mathrm{S}_i^n}$ phenomenlogically parametrizes the transcriptional promotion process. We assume that the dynamics of the *trans* intermediate $[\mathrm{N}_i\mathrm{D}_j]$, intracellular signal S_i, and the mRNA m_{R_i} are rapid relative to the Notch/Delta and Reporter protein dynamics, allowing the quasi-steady-state approximation to their dynamics ($[\dot{\mathrm{N}_i\mathrm{D}_j}]\approx\dot{\mathrm{S}}_i\approx\dot{m}_{\mathrm{R}_i}\approx 0$). Furthermore, we assume that Notch binds to *cis*-Delta irreversibly ($k_\mathrm{C}^-=0$), and thus Notch dynamics become independent of the $[\mathrm{N}_i\mathrm{D}_i]$ complex. With these approximations, the model is reduced to

$$\dot{\mathrm{N}}_i=\beta_\mathrm{N}-\gamma\mathrm{N}_i-\mathrm{N}_i\frac{\langle D_j\rangle_i}{k_t}-\mathrm{N}_i\frac{\mathrm{D}_i}{k_c} \tag{S2a}$$

$$\dot{\mathrm{D}}_i=\beta_\mathrm{D}-\gamma\mathrm{D}_i-\frac{\langle \mathrm{N}_j\rangle_i}{k_t}\mathrm{D}_i-\mathrm{N}_i\frac{\mathrm{D}_i}{k_c} \tag{S2b}$$

$$\dot{\mathrm{R}}_i=f_A\left(\frac{1}{\gamma_\mathrm{S}}\mathrm{N}_i\frac{\langle D_j\rangle_i}{k_t};\beta_\mathrm{R},n,k_\mathrm{RS}\right)-\gamma_\mathrm{R}\mathrm{R}_i \tag{S2c}$$

where we have defined $\beta_\mathrm{R}=\frac{\beta_\mathrm{m}\alpha_R}{\gamma_\mathrm{m}}$, $k_t^{-1}\equiv\frac{k_\mathrm{D}^+k_\mathrm{S}}{k_\mathrm{D}^-+k_\mathrm{S}}$ and $k_c^{-1}\equiv k_\mathrm{C}^+$, and employed the notation $\langle X_j\rangle_i\equiv\sum_{j=]i[}\frac{1}{l_{ij}}X_j$ for the average of the enclosed quantity in the neighbors j of cell i weighted by the magnitudes of the cell-cell interfaces. We have also taken the simplifying assumption that $\gamma_\mathrm{N}=\gamma_\mathrm{D}\equiv\gamma$. Solving with different degradation rates is straightforward, and is guaranteed to leave conclusions relating to the system's steady-state properties unchanged (as is clear from the freedom to rescale parameters).

Excluding *cis*–inhibition By reviewing the preceding derivation and omitting those terms relating to *cis*-inhibition, we see that the kinetic equations become

$$\dot{\mathrm{N}}_i = \beta_{\mathrm{N}} - \gamma \mathrm{N}_i - \mathrm{N}_i \frac{\langle \mathrm{D}_j \rangle_i}{k_t} \tag{S3a}$$

$$\dot{\mathrm{D}}_i = \beta_{\mathrm{D}} - \gamma \mathrm{D}_i - \frac{\langle \mathrm{N}_j \rangle_i}{k_t} \mathrm{D}_i \tag{S3b}$$

$$\dot{\mathrm{S}}_i = \mathrm{N}_i \frac{\langle \mathrm{D}_j \rangle_i}{k_t} - \gamma_{\mathrm{S}} \mathrm{S}_i \approx 0 \rightarrow \mathrm{S}_i \approx \frac{1}{\gamma_{\mathrm{S}}} \mathrm{N}_i \frac{\langle \mathrm{D}_j \rangle_i}{k_t} \tag{S3c}$$

$$\dot{\mathrm{R}}_i = f_A \left(\frac{1}{\gamma_{\mathrm{S}}} \mathrm{N}_i \frac{\langle D_j \rangle_i}{k_t}; \beta_{\mathrm{R}}, n, k_{\mathrm{RS}} \right) - \gamma_{\mathrm{R}} \mathrm{R}_i \tag{S3d}$$

Boundary formation

With mutual inactivation If the expression rate of Delta varies spatially (i.e. $\beta_{\mathrm{D}} \rightarrow \beta_{\mathrm{D}}(x)$) the dynamics of Notch signaling with MI are governed by the following equations:

$$\dot{\mathrm{N}}_i = \beta_{\mathrm{N}} - \gamma \mathrm{N}_i - \mathrm{N}_i \frac{\langle D_j \rangle_i}{k_t} - \mathrm{N}_i \frac{\mathrm{D}_i}{k_c} \tag{S4a}$$

$$\dot{\mathrm{D}}_i = \beta_{\mathrm{D}}(x) - \gamma \mathrm{D}_i - \frac{\langle \mathrm{N}_j \rangle_i}{k_t} \mathrm{D}_i - \mathrm{N}_i \frac{\mathrm{D}_i}{k_c} \tag{S4b}$$

$$\dot{\mathrm{R}}_i = f_A \left(\frac{1}{\gamma_{\mathrm{S}}} \mathrm{N}_i \frac{\langle D_j \rangle_i}{k_t}; \beta_{\mathrm{R}}, n, k_{\mathrm{RS}} \right) - \gamma_{\mathrm{R}} \mathrm{R}_i \tag{S4c}$$

These equations, labeled (1)–(3) in the main paper text, are sufficient to generate sharply-defined bands of Notch signaling at the crossing point (supposing its existence) between the Delta and Notch expression rates.

Without *cis*–inhibition — The Band–Pass Filter model In the absence of *cis*–inhibition, a mechanism that explicitly limits the report of Notch signaling to a band of signaling levels is required for the conversion of a Delta expression gradient to strips of signal Reporter activity. The band–pass model described in the main text is governed by a modification of the equations (S3a)–(S3d) to allow for spatially-varying Delta expression and restrict Reporter expression to a narrow band of Signal

induction levels, yielding the following equations:

$$\dot{\mathrm{N}}_i = \beta_{\mathrm{N}} - \gamma \mathrm{N}_i - \mathrm{N}_i \frac{\langle \mathrm{D}_j \rangle_i}{k_t} \tag{S5a}$$

$$\dot{\mathrm{D}}_i = \beta_{\mathrm{D}}\left(x\right) - \gamma \mathrm{D}_i - \frac{\langle \mathrm{N}_j \rangle_i}{k_t} \mathrm{D}_i \tag{S5b}$$

$$\dot{\mathrm{S}}_i = \mathrm{N}_i \frac{\langle \mathrm{D}_j \rangle_i}{k_t} - \gamma_{\mathrm{S}} \mathrm{S}_i \approx 0 \rightarrow \mathrm{S}_i \approx \frac{1}{\gamma_{\mathrm{S}}} \mathrm{N}_i \frac{\langle \mathrm{D}_j \rangle_i}{k_t} \tag{S5c}$$

$$\dot{\mathrm{R}}_i = \beta_{\mathrm{R}} \frac{\mathrm{S}_i^p}{k_{\mathrm{b}}^p + \mathrm{S}_i^p} \frac{k_{\mathrm{b}}^q}{k_{\mathrm{b}}^q + \mathrm{S}_i^q} - \gamma_{\mathrm{R}} \mathrm{R}_i = \beta_{\mathrm{R}} \frac{\left(\mathrm{N}_i \langle \mathrm{D}_j \rangle_i\right)^p}{k_{\mathrm{RS}}^p + \left(\mathrm{N}_i \langle \mathrm{D}_j \rangle_i\right)^p} \frac{k_{\mathrm{RS}}^p}{k_{\mathrm{RS}}^p + \left(\mathrm{N}_i \langle \mathrm{D}_j \rangle_i\right)^p} - \gamma_{\mathrm{R}} \mathrm{R}_i \tag{S5d}$$

corresponding to equations (4)–(6) in the main text.

Lateral inhibition

Transcriptional lateral inhibition with mutual inactivation (LIMI) With the condition that the production rate of Delta may be repressed by the reporter R_i, i.e. $\beta_{\mathrm{D}} \rightarrow f_R\left(\mathrm{R}_i; \beta_{\mathrm{D}}, m, k_{\mathrm{DR}}\right)$ where $f_R\left(\mathrm{R}_i; \beta_{\mathrm{D}}, m, k_{\mathrm{DR}}\right) \equiv \beta_{\mathrm{D}} \frac{k_{\mathrm{DR}}^m}{k_{\mathrm{DR}}^m + \mathrm{R}_i^m}$ is a repressive Hill function, we have the equations representing lateral inhibition by transcriptional downregulation of Delta with mutual inactivation. It is convenient to convert the equations to a set of dimensionless parameters as follows: $t \equiv \gamma_R \mathrm{t}$, $N \equiv \frac{\mathrm{N}}{N_0}$, $D \equiv \frac{\mathrm{D}}{D_0}$, and $R \equiv \frac{\mathrm{R}}{R_0}$ where $N_0 = D_0 \equiv \gamma k_t$, and $R_0 \equiv k_{\mathrm{DR}}$. The equations are then

$$\tau \dot{N}_i = \beta_N - N_i - N_i \left\langle D_j \right\rangle_i - N_i \frac{D_i}{\kappa_c} \tag{S6a}$$

$$\tau \dot{D}_i = f_R\left(R_i; \beta_D, m, 1\right) - D_i - \left\langle N_j \right\rangle_i D_i - N_i \frac{D_i}{\kappa_c} \tag{S6b}$$

$$\dot{R}_i = f_A\left(N_i \left\langle D_j \right\rangle_i; \beta_R, n, k_{RS}\right) - R_i \tag{S6c}$$

where $\tau \equiv \frac{\gamma_{\mathrm{R}}}{\gamma}$, $\beta_N \equiv \frac{\beta_{\mathrm{N}}}{\gamma N_0}$, $\beta_D \equiv \frac{\beta_{\mathrm{D}}}{\gamma D_0}$, $\beta_R \equiv \frac{\beta_{\mathrm{R}}}{\gamma_{\mathrm{R}} R_0}$, $\kappa_c \equiv \frac{k_c}{k_t}$, and $k_{RS} \equiv \frac{k_{\mathrm{RS}} \gamma_{\mathrm{S}} k_t}{N_0 D_0}$. These correspond to the equations labeled (10)–(12) in the main text.

Simplest lateral inhibition with mutual inactivation (SLIMI) The mutual inactivation mechanism permits a lateral inhibition mechanism driven by a single feedback connecting Notch

expression to Notch signaling, as follows:

$$\dot{\mathrm{N}}_i = \alpha_{\mathrm{N}} + f_A\left(\frac{1}{\gamma_{\mathrm{S}}}\mathrm{N}_i\frac{\langle \mathrm{D}_j\rangle_i}{k_t};\beta_{\mathrm{N}},n,k_{\mathrm{NS}}\right) - \gamma\mathrm{N}_i - \mathrm{N}_i\frac{\langle \mathrm{D}_j\rangle_i}{k_t} - \mathrm{N}_i\frac{\mathrm{D}_i}{k_c} \tag{S7a}$$

$$\dot{\mathrm{D}}_i = \beta_{\mathrm{D}} - \gamma\mathrm{D}_i - \frac{\langle \mathrm{N}_j\rangle_i}{k_t}\mathrm{D}_i - \mathrm{N}_i\frac{\mathrm{D}_i}{k_c} \tag{S7b}$$

where we have included a promoter "leakiness" term (α_{N}, representing imperfect repression) in the kinetic equation for the regulated component, which in this case is Notch. Here we use a set of dimensionless parameters as follows: $t \equiv \gamma \mathrm{t}$, $N \equiv \frac{\mathrm{N}}{N_0}$, and $D \equiv \frac{\mathrm{D}}{D_0}$ where $N_0 = D_0 \equiv \gamma k_t$

$$\dot{N}_i = \alpha_N + f_A\left(N_i\left\langle D_i\right\rangle_j;\beta_N,n,k_{NS}\right) - N_i - N_i\left\langle D_j\right\rangle_i - N_i\frac{D_i}{\kappa_c} \tag{S8a}$$

$$\dot{D}_i = \beta_D - D_i - \left\langle N_j\right\rangle_i D_i - N_i\frac{D_i}{\kappa_c} \tag{S8b}$$

where we have defined $\alpha_N \equiv \frac{\alpha_{\mathrm{N}}}{\gamma N_0}$, $\beta_N \equiv \frac{\beta_{\mathrm{N}}}{\gamma N_0}$, $\beta_D \equiv \frac{\beta_{\mathrm{D}}}{\gamma D_0}$, $\kappa_c \equiv \frac{k_c}{k_t}$, and $k_{NS} \equiv \frac{k_{\mathrm{NS}}\gamma_{\mathrm{S}}k_t}{N_0 D_0}$. These equations are used in Fig. 6.

Without *cis*-inhibition (LI) With the condition that the production rate of Delta may be repressed by the reporter R_i, i.e. $\beta_{\mathrm{D}} \to \beta_{\mathrm{D}}\frac{k_{\mathrm{DR}}^m}{k_{\mathrm{DR}}^m + \mathrm{R}_i^m}$, combined with equations (S3a)–(S3d), we have the equations representing "canonical" lateral inhibition by transcriptional downregulation of Delta. It is convenient to convert the equations transforming variables as $t \equiv \mathrm{t}\gamma_{\mathrm{R}}$, $N \equiv \frac{\mathrm{N}}{N_0}$, $D \equiv \frac{\mathrm{D}}{D_0}$, and $R \equiv \frac{\mathrm{R}}{k_{\mathrm{DR}}}$ where $N_0 \equiv \frac{\beta_{\mathrm{N}}}{\gamma}$ and $D_0 \equiv \frac{\gamma_{\mathrm{S}}k_{\mathrm{RS}}}{k_t}\frac{1}{N_0}$ to give

$$\tau\dot{N}_i = 1 - N_i - N_i\left\langle D_j\right\rangle_i \tag{S9a}$$

$$\tau\dot{D}_i = f_R\left(R_i;\beta_D,m,1\right) - D_i - \left\langle N_j\right\rangle_i D_i \tag{S9b}$$

$$\dot{R}_i = f_A\left(N_i\left\langle D_j\right\rangle_i;\beta_R,n,1\right) - R_i \tag{S9c}$$

where $\tau \equiv \frac{\gamma_{\mathrm{R}}}{\gamma}$, $\beta_D \equiv \frac{\beta_{\mathrm{D}}}{D_0\gamma}$, and $\beta_R \equiv \frac{\beta_{\mathrm{R}}}{k_{\mathrm{DR}}\gamma_{\mathrm{R}}}$. These correspond to the kinetic equations governing the system of which certain properties are plotted in Figs. 4D, 5AC of the main text and S3 of the Supporting Information.

Linear stability analysis of lateral inhibition equations

It is immediately clear that a necessary condition for spontaneous development of a lateral inhibition pattern from an initially near-homogeneous collection of cells is the instability of the homogeneous steady state (N^*, D^*, R^*) in which every cell has the same value of N_i, D_i, and R_i. Thus a linear stability analysis about the homogeneous steady state can provide necessary conditions for patterning [2]. The stability analysis requires the computation of the Jacobian at the homogeneous steady state, which is in this case complicated by the large number of variables (three times the number of cells). This is made simpler by an observation originally from Othmer and Scriven [3] that the Jacobian can be expressed as the sum of two tensor products of matrices, one for the internal dynamics and the other for interactions with neighbors: $J = I_k \otimes H + M \otimes B$. The matrix tensor product is defined as $A \otimes B = \begin{pmatrix} a_{11}B & \cdots & a_{1k}B \\ \vdots & \ddots & \vdots \\ a_{k1}B & \cdots & a_{kk}B \end{pmatrix}$. Also, here I_k is the $k \times k$ identity matrix (k is the number of cells involved in the interactions in question), $H_{ij} = \frac{\partial \dot{q}_i}{\partial q_j}$ is the change in production of species i for a change in species j in the same cell, $B_{ij} = \frac{\partial \dot{q}_i}{\partial \langle q_j \rangle}$ is the change in production of species i for a change in species j in a neighboring cell, and M is the connectivity matrix defined as $M_{ij} = \begin{cases} 1/6 & \text{if } i \text{ and } j \text{ are neighbors} \\ 0 & \text{otherwise} \end{cases}$. Notch, Delta, and Reporter correspond to species $i = 1, 2, 3$ respectively.

Once the Jacobian has been written in this form, Othmer and Scriven further show that its eigenvalues are the eigenvalues of the various matrices $H + q_k B$ where q_k are the eigenvalues of the connectivity matrix M. An analysis of the matrix M in [3] tells us that $q_k \geq -0.5$, meaning that we need only compute an eigenvalue for the extreme case $q_k = -0.5$ to determine if the highest eigenvalue (known as the Maximum Lyapunov Exponent — MLE) has a positive real part, simplifying the problem enormously. We can execute this process for each of the lateral inhibition models we have described above to compute their MLE profiles as a function of various parameters, as plotted in Figs. 5 and 6. The derivations of the MLEs are as follows:

Relevant partial derivatives

"Canonical" LI

$$H = \frac{1}{\tau}\begin{pmatrix} -1-\langle D_j\rangle_i & 0 & 0 \\ 0 & -1-\langle N_j\rangle_i & -\frac{m}{\beta_D R_i} f_{A1} f_{R1} \\ \tau\frac{n}{\beta_R N_i} f_{A2} f_{R2} & 0 & -\tau \end{pmatrix}$$

Where

$$f_{A1} = f_A\left(R_i;\beta_D,m,1\right),\ f_{R1} = f_R\left(R_i;\beta_D,m,1\right)$$

$$f_{A2} = f_A\left(N_i\left\langle D_j\right\rangle_i;\beta_R,n,1\right),\ f_{R2} = f_R\left(N_i\left\langle D_j\right\rangle_i;\beta_R,n,1\right)$$

$$B = \frac{1}{\tau}\begin{pmatrix} 0 & -N_i & 0 \\ -D_i & 0 & 0 \\ 0 & \frac{n\tau}{\beta_R D_j} f_A\left(S_i;\beta_R,n,1\right) f_R\left(S_i;\beta_R,n,1\right) & 0 \end{pmatrix}$$

LIMI

$$H = \frac{1}{\tau}\begin{pmatrix} -\left(1+\langle D_j\rangle_i+\frac{D_i}{\kappa_c}\right) & -\frac{N_i}{\kappa_c} & 0 \\ -\frac{D_i}{\kappa_c} & -\left(1+\langle N_j\rangle_i+\frac{N_i}{\kappa_c}\right) & -\frac{m}{\beta_D R_i} f_{A1} f_{R1} \\ \frac{n\tau}{\beta_R N_i} f_{A3} f_{R3} & 0 & -\tau \end{pmatrix}$$

Where

$$f_{A1} = f_A\left(R_i;\beta_D,m,1\right),\ f_{R1} = f_R\left(R_i;\beta_D,m,1\right)$$

$$f_{A3} = f_A\left(S_i;\beta_R,n,k_{RS}\right),\ f_{R3} = f_R\left(S_i;\beta_R,n,k_{RS}\right)$$

$$B = \frac{1}{\tau}\begin{pmatrix} 0 & -N_i & 0 \\ -D_i & 0 & 0 \\ 0 & \frac{n\tau}{\beta_R D_j} f_A\left(S_i;\beta_R,n,k_{RS}\right) f_R\left(S_i;\beta_R,n,k_{RS}\right) & 0 \end{pmatrix}$$

SLIMI

$$H = \begin{pmatrix} \frac{n}{\beta_N N_i} f_A\left(S_i;\beta_N,n,k_{NS}\right) f_R\left(S_i;\beta_N,n,k_{NS}\right) - \left(1 + \langle D_j\rangle_i + \frac{D_i}{\kappa_c}\right) & -\frac{N_i}{\kappa_c} \\ -\frac{D_i}{\kappa_c} & -\left(1 + \langle N_j\rangle_i + \frac{N_i}{\kappa_c}\right) \end{pmatrix}$$

$$B = \begin{pmatrix} 0 & \frac{n}{\beta_N D_j} f_A\left(S_i;\beta_N,n,k_{NS}\right) f_R\left(S_i;\beta_N,n,k_{NS}\right) - N_i \\ -D_i & 0 \end{pmatrix}$$

Evaluation of the homogeneous steady state In each case the homogeneous steady state of the system was found numerically by solving the systems of equations for $N_i = N$, $D_i = D$, and (if relevant) $R_i = R$.

Diagonalization of the reduced Jacobian The matrices H and B, evaluated at the values N, D, and R fixed by the homogeneous steady state, were combined as prescribed in [3] and diagonalized with $q_k = -0.5$ which is the extreme eigenvalue of the structure matrix M for a regular hexagonal lattice. The diagonalization may be written explicitly in terms of the homogeneous steady state values and q_k in each case because the characteristic equation is of order three or less, but the expressions are complicated and not very illuminating. The maximal resulting eigenvalue is the MLE.

Noise in boundary formation

As written in the main text, based on an intuitive understanding of the mutual inactivation mechanism we suspect that MI-based models might be more sensitive to intrinsic sources of noise (contributing to uncorrelated variabilities of Notch and Delta production in a given cell) than those that are extrinsic (by which the Notch and Delta production rate variabilities in a given cell are correlated). To test this we numerically simulate the boundary formation process subject to static noise in the Notch and Delta production rates with varying degrees of correlation between their variability, ranging from fully-intrinsic (correlation coefficient = 0) to fully-extrinsic (correlation coefficient = 1). In order to make the comparisons in the outcome of interest (the variability in the location of the vein boundary-defining peak) fairly we must also be able to control the total variability in the

Notch and Delta production rates *independently* of the correlation between them.

Using a model of multiplicative noise, in which the production rates of Notch in each cell are $\beta_{N,i} = \xi_N \langle \beta_N \rangle$ and the production rates of Delta are $\beta_{D,i} = \xi_D \langle \beta_D \rangle$, we thus seek to draw the random variables ξ_N and ξ_D such that:

1. Means are preserved, with $\langle \xi_N \rangle = \langle \xi_D \rangle = 1$
2. Standard deviations are equal and set to some arbitrary σ, with $\sigma_{\xi_N} = \sigma_{\xi_D} = \sigma$
3. The correlation between the variations in each production rate is some arbitrarily chosen r between zero and one, with $r_{\xi_N \xi_D} = r$
4. Unphysical negative production rates are excluded, with $\xi_N, \xi_D \geq 0$.

We have chosen a mechanism of achieving this that entails choosing two uncorrelated random variables x and y from normal distributions of mean zero and standard deviations σ_x and σ_y, respectively, rotating x and y by an angle θ and shifting the result by Λ in each direction to generate distributions u and v, and then exponentiating each to generate the final distributions ξ_{β_N} and ξ_{β_D}. The required conditions fix the free parameters σ_x, σ_y, θ, and Λ as follows:

The distributions u and v are drawn from $u = x\cos\theta - y\sin\theta + \Lambda$ and $v = x\sin\theta + y\cos\theta + \Lambda$, from which we have that $\langle u \rangle = \langle v \rangle = \Lambda$, $\sigma_u^2 = \sigma_x^2 \cos^2\theta + \sigma_y^2 \sin^2\theta$, and $\sigma_v^2 = \sigma_x^2 \sin^2\theta + \sigma_y^2 \cos^2\theta$. Then the distributions ξ_N and ξ_D drawn from $\xi_N = e^u$ and $\xi_D = e^v$ yield $\langle \xi_N \rangle = e^{\Lambda + \frac{1}{2}\sigma_u^2}$, $\langle \xi_D \rangle = e^{\Lambda + \frac{1}{2}\sigma_v^2}$, $\sigma_{\xi_N}^2 = \langle \xi_N \rangle^2 \left(e^{\sigma_u^2} - 1 \right)$, and $\sigma_{\xi_D}^2 = \langle \xi_D \rangle^2 \left(e^{\sigma_v^2} - 1 \right)$. By the first requirement that the averages of the random variables ξ must be equal to one, we have that $\sigma_u = \sigma_v \rightarrow \theta = \frac{\pi}{4}$, and that $1 = e^{\Lambda + \frac{1}{2}\sigma_u^2} \rightarrow \Lambda = -\frac{1}{2}\sigma_u^2$. The second requirement provides $\sigma^2 = e^{\sigma_u^2} - 1 \rightarrow \sigma_u^2 = \ln\left(\sigma^2 + 1\right) \rightarrow \Lambda = -\frac{1}{2}\ln\left(\sigma^2 + 1\right)$. The final condition $r_{\xi_N \xi_D} = r$ provides $\sigma^2 r + 1 = \langle \xi_N \xi_D \rangle$. By computing $\langle \xi_N \xi_D \rangle = \langle e^{u+v} \rangle = e^{2\Lambda} \left\langle e^{\sqrt{2}x} \right\rangle = e^{2\Lambda + \sigma_x^2}$ this provides $\sigma_x^2 = \ln\left(\left(\sigma^2 r + 1\right) \left(\sigma^2 + 1\right) \right)$ and correspondingly $\sigma_y^2 = \ln\left(\frac{\sigma^2 + 1}{r\sigma^2 + 1} \right)$.

Thus the following algorithm generates positive random distributions ξ_N and ξ_D such that their means are one, standard deviations are σ, and correlation coefficient is r:

1. Draw from two independent normal distributions x and y with means zero and standard deviations $\sigma_x = \sqrt{\ln\left(\left(\sigma^2 r + 1\right)\left(\sigma^2 + 1\right)\right)}$ and $\sigma_y = \sqrt{\ln\left(\frac{\sigma^2+1}{r\sigma^2+1}\right)}$

2. From these, generate two related random distributions $u = \frac{1}{\sqrt{2}}\left(x - y\right) - \frac{1}{2}\ln\left(\sigma^2 + 1\right)$ and $v = \frac{1}{\sqrt{2}}\left(x + y\right) - \frac{1}{2}\ln\left(\sigma^2 + 1\right)$

3. Let ξ_N be drawn from e^u and ξ_D be drawn from e^v

References

1. Sprinzak D et al. (2010) *Cis*-interactions between Notch and Delta generate mutually exclusive signalling states. *Nature* 465:86–90.

2. Plahte E. (2001) Pattern formation in discrete cell lattices. *J Math Biol* 43:411–445.

3. Othmer HG, Scriven LE. (1971) Instability and dynamic pattern in cellular networks. *J Theor Biol* 32:507–537.

3.2 Mutual inactivation of Notch and Delta permits a simple mechanism for lateral inhibition patterning

Abstract

Lateral inhibition patterns mediated by the Notch-Delta signaling system occur in diverse developmental contexts. These systems are based on an intercellular feedback loop in which Notch activation leads to down-regulation of Delta. However, even in relatively well-characterized systems, the pathway leading from Notch activation to Delta repression often remains elusive. Recent work has shown that *cis*-interactions between Notch and Delta lead to mutual inactivation of both proteins. Here we show that this type of *cis*-interaction enables a simpler and more direct mechanism for lateral inhibition feedback than those proposed previously. In this mechanism, Notch signaling directly up-regulates Notch expression, thereby inactivating Delta through the mutual inactivation of Notch and Delta proteins. This mechanism, which we term Simplest Lateral Inhibition by Mutual Inactivation (SLIMI), can implement patterning without requiring any additional genes or regulatory interactions. Moreover, the key interaction of Notch expression in response to Notch signaling has been observed in some systems. Stability analysis and simulation of SLIMI mathematical models show that this lateral inhibition circuit is capable of pattern formation across a broad range of parameter values. These results provide a simple and plausible explanation for lateral inhibition pattern formation during development.

Introduction

Multicellular development often involves transitions from initially near-homogeneous tissues to 'fine-grained' patterns involving sharp distinctions between neighboring cells. One such pattern is "lateral inhibition" (LI), characterized by alternating patterns of 'on' and 'off' states such as those diagrammed in Fig. 1. This phenomenon is pervasive, arising in situations as diverse as butterfly wing coloration [1], neuroectoderm specification [2], ciliated cell specification [3], and sensory organ precursors [4].

LI patterning in these and other contexts is mediated by signaling through the Notch-Delta

system. The Notch-Delta system (reviewed in [5-8]) consists of the Notch receptor family and its Delta-family ligands (blue and red molecules, respectively, in Fig. 2), along with numerous participants in the signaling mechanism. Delta interacts with Notch in two modes (Fig. 2b): activating Notch signaling in neighboring cells (*trans*-activation) while inhibiting Notch signaling in the same cell (*cis*-inhibition). LI patterning can occur when Notch signaling downregulates Delta levels. This downregulation is usually assumed to be mediated by a transcriptional repressor, although it could also be implemented through post-transcriptional mechanisms (Fig. 2c). Under certain conditions [9,10] a high level of Delta in one cell will drive all of its neighbors to low levels of Delta expression. Conversely, a cell whose neighbors are all Delta-poor will eventually express Delta at a high level. This generates the lateral inhibition pattern of Fig. 1b with high-Delta cells (red) surrounded by low-Delta cells (white).

The feedback pathway inhibiting Delta expression in response to Notch activation may be known in certain cases [11]. However, in many contexts it remains unclear what components, if any, play this role [12]. On the other hand, in some natural systems such as vein patterning [13] and lateral inhibition [14] Notch activation is known to induce Notch expression. Further, a recent quantitative study of the Notch signaling response function uncovered evidence for *mutual cis*-inhibition [15]. Not only does Delta inactivate Notch signaling in *cis* as drawn in Fig. 2b, but Notch also reciprocally inactivates Delta as drawn in Fig. 2d.

Here we report that the mutual inactivation model of *cis*-inhibition admits the possibility of a remarkably simple mechanism for achieving lateral inhibition. Notch signaling upregulation of Notch receptor expression, combined with the mutual inactivation mechanism, directly downregulates Delta levels in response to Notch signaling (Fig. 2e). Mathematical analysis of this feedback circuit shows that it can generate the LI pattern and provides some advantages compared to the canonical architecture. We describe this as the Simplest Lateral Inhibition by Mutual Inactivation (SLIMI) model.

Results

In order to analyze the SLIMI circuit, we assume an ideal two-dimensional lattice of hexagonal cells, each containing Notch (N_i) and Delta (D_i) interacting in *trans* to generate Signal (S_i) that induces Notch expression, and in *cis* with mutual inactivation. Correspondingly, we consider the following reactions:

$$\mathrm{N}_i + \mathrm{D}_j \rightleftharpoons [\mathrm{N}_i\mathrm{D}_j] \rightarrow \mathrm{S}_i \qquad \textit{trans}\text{-activation} \tag{1}$$

$$\mathrm{N}_i + \mathrm{D}_i \rightleftharpoons [\mathrm{N}_i\mathrm{D}_i] \rightarrow \varnothing \qquad \textit{cis}\text{-inactivation} \tag{2}$$

$$\mathrm{S}_i \rightarrow \mathrm{N}_i \qquad \text{Notch induction} \tag{3}$$

Reaction 1 refers to *trans*–activation in cell i by ligand on neighboring cells j, with Notch-Delta *trans* association (dissociation) rate k_D^+ (k_D^-) and signal release rate k_S. Reaction 2 refers to *cis*–inhibition, with Notch-Delta *cis* association (dissociation) rate k_C^+ (k_C^-) and mutual inactivation rate k_E. Reaction 3 refers to Signal activation of Notch expression, which we parametrize as a contribution to the rate of Notch production in the form of an increasing Hill function ($\beta_{\mathrm{SN}} \frac{\mathrm{S}_i^n}{K_{\mathrm{SN}}^n + \mathrm{S}_i^n}$). Allowing for "leakiness" in Notch production (non-zero production rate β_{N} in the absence of inducer), constant constitutive production of Delta (β_{D}), linear degradation of each component($-\gamma \mathrm{N}_i$ and $-\gamma \mathrm{D}_i$), and taking the quasi-steady-state approximation on the receptor-ligand complexes and the Signal molecule, these reactions translate to the following set of ordinary differential equations:

$$\begin{aligned} \dot{\mathrm{N}}_i = \quad & \beta_{\mathrm{N}} + \beta_{\mathrm{SN}} \frac{\mathrm{N}_i^n \langle \mathrm{D}_j \rangle_i^n}{K_{\mathrm{SN}}^n + \mathrm{N}_i^n \langle \mathrm{D}_j \rangle_i^n} - \gamma \mathrm{N}_i \\ & - \mathrm{N}_i \frac{\langle \mathrm{D}_j \rangle_i}{k_t} - \mathrm{N}_i \frac{\mathrm{D}_i}{k_c} \end{aligned} \tag{4}$$

$$\dot{\mathrm{D}}_i = \quad \beta_{\mathrm{D}} - \gamma \mathrm{D}_i - \langle \mathrm{N}_j \rangle_i \frac{\mathrm{D}_i}{k_t} - \mathrm{N}_i \frac{\mathrm{D}_i}{k_c} \tag{5}$$

Here we have employed the notation $\langle \cdot_j \rangle_i$ to denote the average of the enclosed quantity among the neighbors j of cell i. We define the parameters $k_t^{-1} \equiv \frac{k_{\mathrm{D}}^+ k_{\mathrm{S}}}{k_{\mathrm{D}}^- + k_{\mathrm{S}}}$ and $k_c^{-1} \equiv \frac{k_{\mathrm{C}}^+ k_{\mathrm{E}}}{k_{\mathrm{C}}^- + k_{\mathrm{E}}}$ to denote the strengths of the *trans* and *cis* interactions, respectively. Numerical simulation of these equations proves that they are capable of generating the LI pattern from a slightly (and randomly)

heterogeneous field of cells (Fig. 3a).

In order to more generally determine conditions under which this system of coupled, non-linear differential equations can generate the LI pattern, we performed a linear stability analysis about the system's homogeneous steady state (hss). If the hss is stable (unstable) to small perturbations, it follows that the LI pattern is inaccessible (accessible) from an initial condition near the hss. This analysis required computing and diagonalizing the Jacobian evaluated at the hss, and the system's stability there was determined by the sign of the maximal eigenvalue (known as the Maximum Lyapunov Exponent — MLE). Where the MLE is positive the hss is unstable, and the LI pattern is accessible.

Computing the MLE requires knowledge of component leves at the hss, defined as the solutions to $\dot{\mathrm{N}}_i = \dot{\mathrm{D}}_i = 0$ subject to $\mathrm{N}_i = \mathrm{N}$ and $\mathrm{D}_i = \mathrm{D}$. With $\mathrm{S} \equiv \mathrm{ND}$ and $\Lambda \equiv \frac{1}{k_c} + \frac{1}{k_t}$, this condition is

$$\beta_{\mathrm{N}} + \beta_{\mathrm{SN}} \frac{\mathrm{S}^n}{K^n + \mathrm{S}^n} + \frac{\gamma^2}{\Lambda} \frac{\mathrm{S}}{\mathrm{S} - \frac{\beta_{\mathrm{D}}}{\Lambda}} - \Lambda \mathrm{S} = 0 \tag{6}$$

We used this equation to determine the homogeneous steady state values N^* and D^*.

Directly diagonalizing the full Jacobian J, a matrix of dimension twice the total number of cells in the lattice, would be very difficult. Othmer and Scriven [16] showed that the problem can be simplified by separating cell adjacency-related intercellular contributions from the intracellular dynamics of the signaling system itself. This approach first diagonalizes the structure matrix M (in which $M_{ij} = \frac{1}{6}$ where cells i and j are neighbors and $M_{ij} = 0$ otherwise) in isolation to yield its spectrum q_k. The eigenvalues of J are then the eigenvalues of $H + q_k B$, where H and B represent the modulation of production rates due to changes in intra- and extra-cellular components, respectively. These relationships are represented by the partial derivatives $H_{uv} = \frac{\partial u_i}{v_i}$ and $B_{uv} = \frac{\partial u_i}{\partial v_{j \neq i}}$ where u and v index the chemical species involved in the interaction (here, Notch and Delta) and i,j are cell indices.

$$H = \begin{pmatrix} \beta_{\mathrm{SN}} \frac{n}{\mathrm{N}^*} f_0 g_0 - \gamma - \Lambda \mathrm{D}^* & -\frac{1}{k_c}\mathrm{N}^* \\ -\frac{1}{k_c}\mathrm{D}^* & -\gamma - \Lambda \mathrm{N}^* \end{pmatrix} \tag{7}$$

$$B = \begin{pmatrix} 0 & \beta_{\mathrm{SN}} \frac{n}{\mathrm{D}^*} f_0 g_0 - \frac{1}{k_t} \mathrm{N}^* \\ -\frac{1}{k_t} \mathrm{D}^* & 0 \end{pmatrix} \tag{8}$$

where $f_0 \equiv \frac{K_{\mathrm{SN}}^n}{K_{\mathrm{SN}}^n + (\mathrm{N}^*\mathrm{D}^*)^n}$ and $g_0 \equiv \frac{(\mathrm{N}^*\mathrm{D}^*)^n}{K_{\mathrm{SN}}^n + (\mathrm{N}^*\mathrm{D}^*)^n}$. The Othmer and Scriven method thus involves only diagonalizing one large (but sparse) matrix M representing the cell-cell adjacency of the system, and then diagonalizing a small two-by-two matrix.

The characteristic equations of the Jacobian are then

$$\begin{vmatrix} \beta_{\mathrm{SN}} \frac{n}{\mathrm{N}^*} f_0 g_0 - \gamma - \left(\frac{1}{k_t} + \frac{1}{k_c}\right) \mathrm{D}^* - \lambda & \left(-\frac{1}{k_c} - q_k \frac{1}{k_t}\right) \mathrm{N}^* + q_k \beta_{\mathrm{SN}} \frac{n}{\mathrm{D}^*} f_0 g_0 \\ \left(-\frac{1}{k_c} - q_k \frac{1}{k_t}\right) \mathrm{D}^* & -\gamma - \left(\frac{1}{k_c} + \frac{1}{k_t}\right) \mathrm{N}^* - \lambda \end{vmatrix} = 0$$

$$\begin{aligned} \rightarrow \lambda = & \frac{1}{2} \left(\frac{\Gamma}{\mathrm{N}} - 2\gamma - \Lambda(\mathrm{N} + \mathrm{D}) \right. \\ & \left. \pm \sqrt{\left(-\frac{\Gamma}{\mathrm{N}} + 2\gamma + \Lambda(\mathrm{N} + \mathrm{D})\right)^2 - 4\left(\mathrm{ND}\left(\Lambda^2 - \theta^2\right) + \Lambda\gamma\left(\mathrm{N} + \mathrm{D}\right) + \Gamma\left(q_k\theta - \Lambda\right) + \gamma^2 - \frac{\Gamma}{\mathrm{N}}\gamma\right)} \right) \end{aligned}$$

where $\Gamma \equiv \beta_{\mathrm{SN}} n f_0 g_0$, $\theta \equiv \frac{1}{k_c} + q_k \frac{1}{k_t}$, and asterisks are omitted. The sufficient criterion for homogeneous steady state instability is $\mathrm{ND}\left(\Lambda^2 - \theta^2\right) + \Lambda\gamma\left(\mathrm{N} + \mathrm{D}\right) + \Gamma\left(q_k\theta - \Lambda\right) + \gamma^2 - \frac{\Gamma}{\mathrm{N}}\gamma < 0$. For the ideal hexagonal lattice of cells with periodic boundary conditions that we consider, the minimum q_k (chosen because it corresponds to the MLE, which is the maximal eigenvalue of J) is calculated to be -0.5.

The numerical solutions for the MLE plotted in Fig. 3b for particular choices of parameters are illuminating. Even with no explicitly sharp molecular interactions ($n = 1$), there is a sizable region bounded by minimal and maximal β_D values over which the MLE is positive, and thus the system may achieve a lateral inhibition pattern as shown in Fig. 3b. A potential shortcoming of the SLIMI mechanism is its sensitivity to leakiness in Notch expression (i.e. non-negligible β_{N}). Fig. 3c plots the MLE profile for progressively greater leakiness in Notch expression indexed as a percentage of maximal Notch induction (*i.e.*, $\beta_{\mathrm{N}} = l\beta_{\mathrm{SN}}$ for l described above the appropriate plot), from which we see that the SLIMI model is fairly robust.

Discussion

The SLIMI model described here is an extraordinarily simple approach to LI patterning through the Notch-Delta signaling system, conceivable only by virtue of the previously-unappreciated inactivation of Delta by Notch in *cis*. It is appealing for a number of reasons. First, we have shown that SLIMI is a feedback architecture that supports the formation of the LI pattern across a wide range of parameters. Second, it does so even in the presence of non-ideal leakiness in the regulatory feedback. Third, and perhaps most dramatically, it does not require the action of any hypothetical intermediate factor. The sole necessary regulatory interaction has been shown to occur naturally [13,14] in at least some contexts.

Appealing though these features of SLIMI may be, it remains uncertain if natural systems in fact utilize this feedback to generate LI patterns. Results regarding Notch-Delta feedback elements operating in lateral inhibition patterning processes are varied at present, seemingly indicating a degree of context specificity [17,18] that defies efforts to postulate a universal mechanism. As mentioned earlier, there is some evidence for increased Notch expression rates induced by Notch signaling in LI-patterning systems [14], but the contribution of this relative to that of other feedbacks in driving the patterning process is unknown.

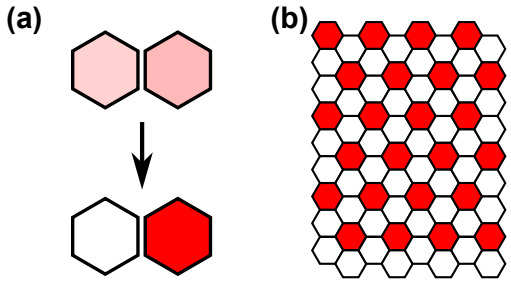

Figure 1: (a) Two initially near-equivalent cells in direct contact eventually reach very different final states, characteristic of 'fine-grained' patterning. (b) An ideal lateral inhibition pattern in a two-dimensional field of cells.

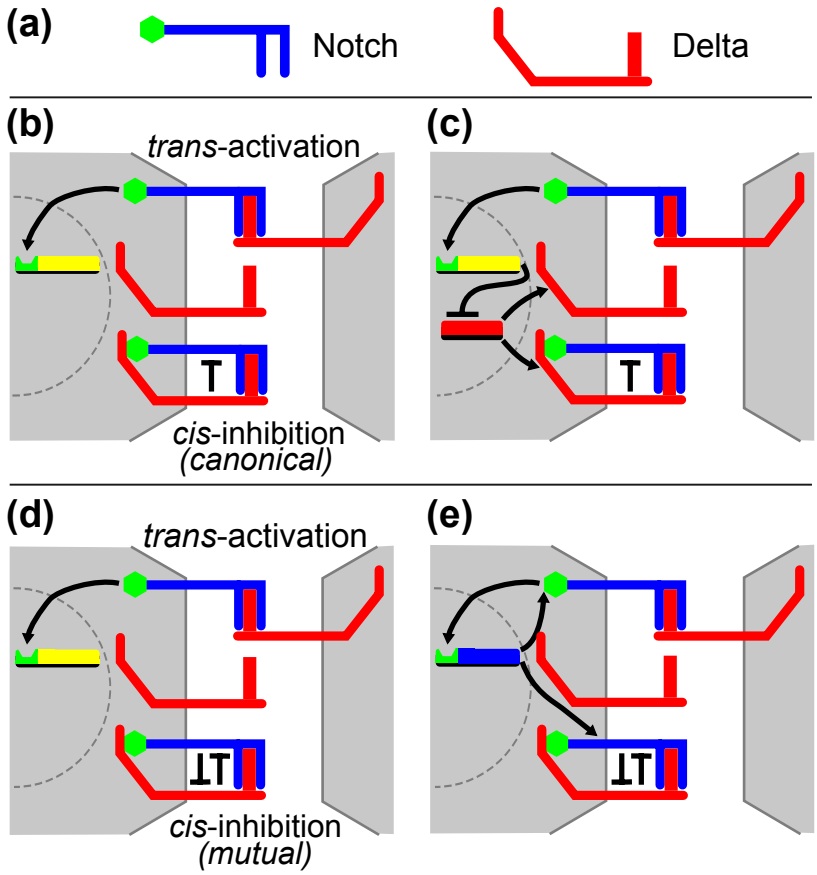

Figure 2: (a) Notch (blue) and Delta (red). (b) Notch and Delta interact in *trans* (on neighboring cell surfaces) to send the intracellular Signal domain (green) of Notch to the nucleus. Delta also inhibits Notch in *cis* (on the same cell surface). (c) A canonical lateral inhibition feedback in which Notch signaling induces expression of an intermediate (yellow) that represses Delta expression. Although not explicitly drawn in the figure, the same feedback operates in all cells. (d) The *trans* and *cis* interactions of Notch and Delta, with a *mutual* inactivation of the receptor and ligand in *cis*. (e) A surprisingly simple lateral inhibition feedback network in which Notch signaling induces Notch expression, which directly inactivates Delta by the mutual *cis*-inactivation mechanism.

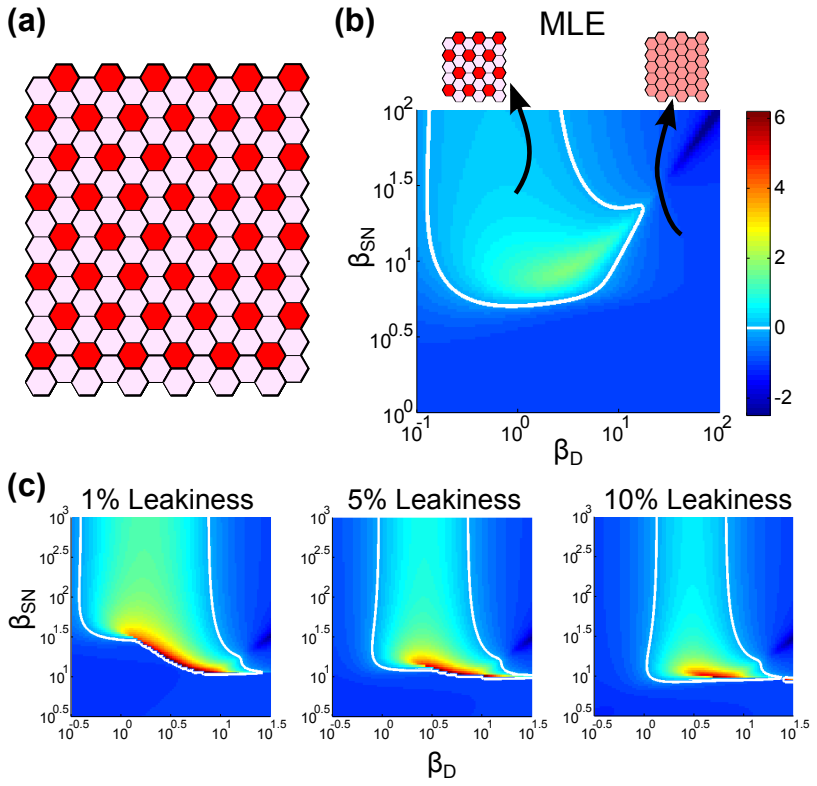

Figure 3: (a) Outcome of a numerical simulation of the SLIMI mechanism colored as in Fig. 1b. (b) Maximum Lyapunov Exponent (MLE) computed across a range of Delta production rates β_{D} and maximal Notch production rates β_{SN}, with other parameters fixed including $n = 1$. The region within the contour is above zero, indicating instability of the homogeneous steady state and thus the potential to generate the LI pattern. (c) MLE computed at $n = 2$ with increasing levels of 'leakiness' in Notch expression, leading to some shrinkage of the patterning-permissive parameter range.

References

1. R. D. Reed, Development Genes and Evolution, 214, 43 (2004).
2. M. Kunisch, M. Haenlin, and J. A. Campos-Ortega, Pro- ceedings of the National Academy of Science USA, 91, 10139 (1994).
3. G. Marnellos, G. Deblandre, E. Mjolsness, and C. Kin- ter, Pacific Symposium on Biocomputing, 5, 326 (2000).
4. P. Heitzler and P. Simpson, Cell, 64, 1083 (1991).
5. B. D'Souza, A. Miyamoto, and G. Weinmaster, Oncogene, 27, 5148 (2008).
6. G. Weinmaster and R. Kopan, Development, 133, 3277 (2006).
7. S. J. Bray, Nature Reviews Molecular Cell Biology, 7, 678 (2006).
8. S. Artavanis-Tsakonas, M. D. Rand, and R. J. Lake, Science, 284, 770 (1999).
9. J. R. Collier, N. A. Monk, P. K. Maini, and J. H. Lewis, Journal of Theoretical Biology, 183, 429 (1996).
10. E. Plahte and L. yehaug, Physica D: Nonlinear Phenomena, 226, 117 (2007).
11. M. Lecourtois and F. Schweisguth, Genes & Development, 9, 2598 (1995).
12. I. Greenwald, Genes & Development, 12, 1751 (1998).
13. S. S. Huppert, T. L. Jacobsen, and M. A. Muskavitch, Development, 124, 3283 (1997).
14. H. A. Wilkinson, K. Fitzgerald, and I. Greenwald, Cell, 79, 1187 (1994).
15. D. Sprinzak, A. Lakhanpal, L. LeBon, L. A. Santat, M. E. Fontes, G. A. Anderson, J. Garcia-Ojalvo, and M. B. Elowitz, Nature, 465, 86 (2010).
16. H. Othmer and L. Scriven, Journal of Theoretical Biology, 32, 507 (1971).
17. L. Seugnet, P. Simpson, and M. Haenlin, Development, 124, 2015 (1997).

18. A. L. Parks, N. A. Shalaby, and M. A. Muskavitch, Genesis, 46, 265 (2008).

3.3 Mutual *cis*-inactivation in the Notch-Delta signaling system affects lateral induction patterning

Introduction

The Notch signaling system is among a few canonical mechanisms by which cells transfer information [1]. In *Drosophila*, where its effects were first identified, the system consists of a single Notch receptor and two ligands, Delta and Serrate, all of which are transmembrane proteins. The system is highly conserved across metazoans to mammals, in which there are four variants of the Notch receptor, three members of the Delta family, and two of the Jagged family (the ligands are known jointly as "DSL" ligands) [2]. In spite of this additional diversity in the receptor and its ligands, much of the core interactions in the system is preserved. A signaling event is initiated by binding between a receptor on one cell with a ligand on the surface of a neighbor. The subsequent force on the receptor related to endocytosis exposes a site to proteolytic cleavage, leading to liberation of the receptor intracellular domain (its signaling domain) into the cytosol. The signaling domain is trafficked to the nucleus, where it acts on downstream targets of the system by relieving repression of their expression (Fig. 1a) [3]. In addition to this *trans*-activation of the system, more recent studies have elucidated the quantitative nature and developmental relevance of an inhibitory interaction between receptor and ligand in the same cell [4,5]. Although the precise molecular details of the interaction are not known, some features of it are. *Cis*-inhibition is a mutual inactivation of receptor and ligand that, when strong, tends to drive cells into either 'receiver' or 'sender' states, dominated by an excess of Notch or ligand on the cell surface, respectively. Experiments have established qualitative relationships between the *cis*- and *trans*- affinities of various receptor-ligand pairs, which differ substantially and are modulated by other components of the Notch system known as Fringes [6].

A wide variety of developmental patterning processes require signaling through the Notch system in order to function. The morphology of the *Drosophila* wing — in many contexts, including its DV boundary [7] and the sharpness of its vein boundaries [8] — is disrupted by Notch and Delta/Serrate mutants. In developing sensory organs including *Drosophila* bristles [9] and the mammalian inner ear

[10] Notch signaling is required for generation of an alternating "checkerboard" pattern to specify the correct number and arrangement of cells for each sensory patch. The patterning outcome in each case depends on the combination of signaling system properties and downstream feedback. A number of theoretical analyses have been performed on various types of downstream feedback, including downregulation of ligand due to Notch signaling (lateral inhibition) [11] and the opposite, upregulation of ligand by Notch signaling (lateral induction) [12]. However, these analyses have not included *cis*-inhibition in their models. We have previously reported that *cis*-inhibition in the context of lateral induction has a number of quantitative and qualitative consequences, including relaxing a requirement for explicit cooperativity in the feedback and enabling patterning with an exceptionally simple mechanism [13]. It remains unclear now *cis*-inhibition affects patterning in lateral induction feedback.

Lateral induction through the Notch signaling system has been proposed as a mechanism in a number of developmental contexts. Domains within the developing mammalian inner ear which limit the extent of prosensory patches are thought to be reinforced by lateral induction [14,15]. The differentiation of certain cells in the developing rat lens involves a lateral induction process [16]. Recent reports have established a Notch-mediated lateral induction process underlying the specification of smooth muscle cells lining a subset of the developing large arteries in mice [17]. This latter example is especially straightforward. The developing artery is initially sheathed in a layer of endothelium surrounded by undifferentiated mesenchyme. At some cue, the endothelium begins expressing Jag1. A lateral induction interaction, shown to be a direct effect of Notch signaling on Jag1 expression, propagates a high-ligand domain outward across the mesenchyme until it mysteriously terminates, at which point cells high in Jag1 differentiate into smooth muscle to line the artery.

Results

Lateral induction of ligand in a single cell is limited by *cis*-inhibition

We first analyzed the response of a single cell with the lateral induction feedback to stimulation by *trans* ligand. The cell expresses Notch receptor at a constant production rate α_N, which degrades in

a first-order linear process with rate γ. Interactions of Notch with ligand in *cis* (D) and *trans* (D_t) destroy the receptor, with interaction strengths k_c^{-1} and k_t^{-1}, respectively. The *trans* interaction generates Signal (S, the Notch intracellular domain) at the same rate as *trans* destruction of Notch, with linear first-order degradation of the Signal at a rate γ_S considerably larger than γ. Ligand is expressed at a constitutive background rate α_D, summed with a lateral induction term represented by an increasing Hill function of S. The Hill function is defined by a maximum magnitude β_{SD}, affinity k_{SD}, and sharpness n. Ligand degradation also follows a linear first-order process of rate γ, along with the *cis* destruction term of strength k_c^{-1}. The differential equations governing the signaling process are described in the Methods section below.

For a given quantity of *trans* ligand (D_t) weaker *cis*-inhibition leads smoothly to greater expression of *cis* ligand (Fig. 1c). An intuitive explanation for this feature is illustrated in Fig. 1b. The *cis* ligand generated in a lateral induction cell with strong *cis*-inhibition will compete effectively against the *trans* ligand for binding to receptor molecules, decreasing the magnitude of the response relative to a system with weaker *cis*-inhibition. Thus, the *cis* ligand participation in strong *cis*-inhibition represents a negative feedback on the Notch system, decreasing the overall signal response. Also as expected, increasing the amount of *trans* ligand increases the induced *cis* ligand. The inverse relationship between *cis*-inhibition strength and induced ligand is maintained across all levels of D_t, although it is not easily appreciated when D_t is supplied in overwhelming excess.

As D_t is varied, the maximal quantity of induced *cis* ligand is $\frac{1}{\gamma}\left(\alpha_D + \beta_{SD}\frac{\alpha_N^n}{\alpha_N^n+(k_{SD}\gamma_S)^n}\right)$, achieved when D_t is sufficiently large. The scale of D_t that constitutes "sufficiently large" itself varies with the system parameters, as $\gg \frac{\alpha_N k_t}{\gamma k_c}$. Both of these expressions are consistent with the results of numerical simulations of the system (Fig. 1d). Increasingly strong *cis*-inhibition distorts the induced response profile rightward, so that for the same amount of *trans* ligand a lower amount of *cis* ligand is generated (Fig. 1e, left). The opposite relationship occurs between the strength of the *trans* interaction and the induction of *cis* ligand (Fig. 1e, right). We also observe that the graded response of *cis* ligand to D_t stands in contrast to the sharply piecewise-linear response of *cis* ligand to variation in the constitutive *cis* ligand production rate (as observed in [13]). In other

words, *cis* ligand is not ultrasensitive to *trans* ligand in lateral induction cells in the same way that a feedback-free cell's *cis* ligand is ultrasensitive to ligand production rate.

Ligand expression gradients are highly sensitive to lateral induction system parameters

We then moved on to analyze multicellular systems, first considering the potential for Notch signaling to generate a morphogen-like spatial gradient. As illustrated in Fig. 2a (left), we simulated a regular two-dimensional hexagonal lattice of cells. Each cell is governed by the same dynamics as the single-cell case described earlier, with two exceptions: first, rather than providing the amount of *trans* ligand exogeneously as the parameter D_t, it is instead the average of the amount of ligand in each of the neighboring cells; second, we include an additional degradation term for ligand to reflect its consumption in the process of *trans* activation. In our model of gradient formation one column of cells (the leftmost, as drawn Fig. 2a) is fixed to uniformly express a high level of ligand (the signaling "source"). This boundary condition was set at the maximum possible induced *cis* ligand level to facilitate comparison between different parameter sets. For certain parameter values the system evolves to a one-dimensional gradient of *cis* ligand perpendicular to the source (Fig. 2a, right, the darkness of red corresponds to the ligand level). The example in the figure is an exceptional one in its length.

Simulation reveals a strong parameter sensitivity of the gradient length to the system parameters, portrayed for two of them (the strength of *cis*-inhibition and the affinity of the *cis* ligand induction interaction) in Fig. 2b. For several values of each parameter, we computed the gradient length scale. We choose as a measure of the gradient length scale the distance from the source cells at which the induced *cis* ligand has reached a level that is twice that of the profile minimum. The results are qualitiatively similar for a different definition of the gradient length scale given by the distance required for the *cis* Delta profile to diminish from 90% to 10% of its range. As seen in Fig. 2b, for both the *cis*-inhibition strength and induction affinity parameters the gradient length scale tends to be low except for very local spikes about specific parameter values. Thus we see that longer-range gradients by Notch lateral induction are very sensitive to system parameters. We note that the gradient requires a constant supply of ligand in the source cells, and when this is removed

the system returns to the homogeneou low-ligand state.

Spatiotemporal front propagation requires population-level bistability and a sufficiently strong initial stimulus

We next considered a dynamic spatiotemporal pattern: front propagation across a field of cells. In this process a collection of cells transitions from a low-ligand homogeneous steady state to a high-ligand homogeneous steady state. The transition is initiated by the same sort of boundary condition as in the model of gradient formation described above, a column of high-ligand source cells at one end of the strip of cells. In this case, however, instead of each subsequent column of cells expressing less ligand than the one before it, the increase in ligand is sustained from cell to cell. As a result there appears to be a high-ligand front progressing away from the source cells. Because multiple steady states are required for this behavior, we probe the structure of homogeneous steady states of the system. With respect to the receptor production rate, for instance, we plot the intersection (or intersections) of nullclines representing steady state levels of receptor and ligand as a function of varying α_N in Fig. 3a. Below a critical value of the receptor production rate there is only one stable steady state (black line, against a light blue background), while above there are three (light red background). Of those three, only the high-ligand (red line) and low-ligand (black line) steady states are stable. The middle steady state (blue line) is unstable. At a given value of the receptor production rate, the level of Delta corresponding to the middle steady state is the threshold above which all of the cells in the system must be raised in order to uniformly transition the system from the low- to the high-ligand state. This is related, although not simply, to the amount of ligand required in a high-ligand source to 'kick off' the front across the lattice of cells (Fig. 4). Because the new state is stable, after a minimal time related to the intracellular dynamics the front will continue to propagate through the lattice even if the source is turned off. We can compute the number of steady states for various parameter values, such as for the *trans* and *cis* receptor-ligand interaction strengths (Fig. 3b). In this case we see that at strong *cis* and *trans* strengths an approximately linear relationship between the parameters is required to support front propagation (lower left corner of Fig. 3b). At weaker strengths (elsewhere in Fig. 3b), the ability to sustain front propagation with

respect to *cis* interaction has only a cutoff at high strength, while with respect to *trans* strength must be bounded between two values. One strict requirement is that the feedback cannot be totally graded (i.e., its cooperativity n must be greater than 1), but the amount of sharpness in the lateral induction term can be arbitrarily small if other parameters are chosen appropriately.

Lateral induction effectively converts a slow variation in parameters to a sharp boundary between cell types

Neither of the two patterns analyzed above, gradient formation or front propagation, are reported to arise from Notch signaling-mediated lateral induction processes in natural systems. Instead, each case involves an approximately homogeneous expression of a high level of ligand across a restricted spatial domain. For instance, the layers of smooth muscle surrounding certain large arteries in the mouse are known to be specified by high levels of ligand initiated and maintained by a lateral induction feedback [17,18]. The outer layer of endothelium surrounding the developing artery begins to express Jag1, which signals to the surrounding mesenchyme. The mesenchyme responds by beginning to adopt the smooth muscle fate and upregulating its own Jag1 expression, which transmits a Notch signal to the next layer of mesenchymal cells. This process iterates through a specific number of layers until, for reasons currently unknown, it terminates [17].

We have previously reported that the Notch signaling system can convert shallow gradients of ligand expression rates to sharply-delineated bands of signaling activity [13]. Motivated by this, and noting that the accessibility of a high-ligand homogeneous steady state is sensitive to system parameters that are known to be modulated in natural systems, we asked if lateral induction in the background of a shallow gradient in one or more of the system parameters could solve the termination problem (Fig. 5). To achieve this we once again simulated a hexagonal lattice of cells with a boundary condition enforcing high-ligand source cells at one end. We modified the parameter values in each cell to reflect the desired gradient – for instance, k_c^{-1} for a gradient in *cis*-interaction strength (Fig. 5a), or α_N for a gradient in Notch expression (Fig. 5b). In both cases the gradients were constructed to begin in a region of parameter space that supports homogeneous bistability and end in a region that does not. As indicated in Fig. 5, both gradients generate relatively

homogeneous ligand expression within a limited domain. The lengthscale of the termination of the ligand profile in each case is appreciably shorter than the lengthscale of the gradient underlying it, to a greater degree for the gradient of *cis*-inhibition strength than that of Notch expression. We thus show that lateral induction can convert a show variation in parameters to a sharp boundary between high- and low-ligand cells. This gradient interpretation could conceivably also be achieved directly by a response to the gradient molecule that is very sharp. In this sense, we can say that for defining a near-homogeneous, limited spatial domain of cells, lateral induction substitutes for explicit cooperativity in the feedback circuit. This observation also suggests experiments to probe the spatial distribution of known modulators of Notch signaling, for example the Fringes which modulate Notch-ligand affinities or expression of Notch receptors themselves, especially in contexts such as arterial wall formation where there are known to be gradients of other signaling factors with as-yet undefined effect.

Lateral induction with strong *cis*-inhibition and delayed feedback allows pulse propagation

We have shown that the *cis*-inhibition interaction provides an intrinsic negative feedback on the lateral induction interaction. This negative autoregulation is half of what we would expect to be required for the generation of a soliton-like pulse that propagates across a field of cells, along with a time delay in the lateral induction feedback circuit. We assessed whether this delay could be provided by rendering the Notch signaling intermediate (S, the receptor's intracellular domain) persistent. Once again modeling on a hexagonal lattice of cells with a high-ligand boundary source at the initial time, we find that a single pulse can be triggered by a transient source (Fig. 6a). The pulse propagation is unchanged if the boundary source is allowed to persist throughout the process, as the parameters do not allow multistability and thus the effect of the boundary is restricted to a short-range gradient of the type discussed earlier. We simulated this process for a variety of parameters. The plots in Fig. 6 indicate whether a given parameter set supported pulse propagation (red for high-magnitude pulses, white for marginal pulses, blue for no pulses). The shape of the pulse-permissive patches allows us to refine our intuition for the system. We observe that pulsing is

restricted to a patch of sufficiently strong *cis*-inhibition and sufficiently long-lived S. The patch is also bounded when *cis*-inhibition becomes too strong because under those conditions an insufficient quantity of S is generated to maintain the feedback delay at the necessary strength. The upper bound on S lifetime reflects a threshold beyond which the persistence of signal is so great it overcomes the negative *cis*-inhibition at any strength. We also studied pulse dependence on the maximal ligand production rate and the lateral induction affinity. The linear relationship between the two along the area allowing pulsing arises because the increased lateral induction output of a higher-affinity interaction is compensated by decreasing the scale of ligand, allowing the system to behave qualitatively similarly along the line in this parameter space. Pulses of this sort are not known to occur in any natural context, but in a cell culture system using existing techniques to increase the lifetime of the Notch intracellular signaling domain it may be possible to achieve synthetically.

Discussion

We find that Notch signaling coupled with downstream lateral induction to generate long-range morphogen-like gradients is not an effective mechanism, because it is not robust to parameter fluctuations. The evidence provided by our simulations above supports this claim. Furthermore, an intuitive line of reasoning suggests why any juxtacrine signaling-mediated gradient is likely to be very sensitive to variation in its parameters. The basic feature of signal response is the input-output relationship, in this case the connection between the amount of ligand used to stimulate the cell (input) and the amount generated by the cell as as result (output), which defines a "signal response curve" on a ligand input-output plane. In a regular lattice of cells in contact with one another the value (or values) of ligand at which the output is equal to the input correspond to the homogeneous steady states of the system, which are thus identified by the intersection(s) of the signal response curve and the diagonal line on the ligand input-output plane. A perturbation provided by a boundary cell fixed to generate a high level of ligand induces excess signaling in its neighbors, driving them to ligand levels above the homogenous steady state. In order for the gradient to be long-range, the response of the neighbors should be close to the amount by which they were stimulated. This

implies that the signal response curve should be very close to the diagonal. If it deviates significantly there is a twofold penalty against the gradient length: first in the direct sense that each subsequent neighbor produces less ligand, shortening the gradient; and second in the indirect sense that the amount of input ligand to each cell becomes much less than the amount provided by the greater neighbor if the gradient becomes shorter. However, even if we suppose that the signaling system permits a response that is nearly linear over a large range of ligand input, it would be a response that sits on a 'knife edge', just below the diagonal line, where a slight perturbation upward would send the system into a higher homogeneous state and a slight perturbation downward would dramatically shorten the gradient. This intuition is not exact, but it motivates the observed behavior. Returning to the particular situation we consider here, the specific signal response curves accessible by Notch signaling can be made nearly linear over long distances (corresponding to the high points in the gradient length plots above) but small parameter variations dramatically shorten the resulting gradient.

On the other hand, when the lattice of cells is bistable in ligand expression Notch-mediated lateral induction effectively allows propagation of a signal front across the lattice to transition it from the low to the high state. Even though the population-level bistability is a global property, a local pertubation to one side of the lattice (or even in one cell, if it is suitably strong) is sufficient to induce a switch in the entire collection of cells. This provides a means of coordinating a change in cell state across a large number of cells that can be induced by an initiating factor that is initially localized to a small spatial area. Such a procedure, however, does not by itself provide for a mechanism by which the front propagation can be terminated. This is a very relevant shortcoming in light of the spatial restriction of the Notch-mediated lateral induction processes that have been reported in the literature [17,18]. Motivated by the knowledge that known modulators of the Notch system affect its signaling parameters, and observing that changes in those parameters can take a system from a state that supports bistability to one that does not, we have found that slowly-varying gradients of system parameters lead to a sharp termination of front propagation. This is related to a previous finding we reported in [13], in which the Notch system converts a shallow gradient of

ligand expression rate into sharly-defined peaks of Notch signaling. The Notch system with a lateral induction feedback again provides a mechanism for converting a graded input into a sharp output without requiring a corresponding level of explicit cooperativity in the regulation.

Finally, the intrinsic negative feedback on the Notch system provided by *cis* inhibition decreases the number of modifications that would be needed for propagation of a pulse across a field of cells. Such a pulse requires a negative feedback on the signaling response along with a delay in the positive feedback reponse to signaling. *Cis* inhibition provides the former, while increasing the lifetime of the signaling intermediate provides the latter. With knowledge of factors regulating the rate of protein degradation [19], and techniques for modulating decay timescales [20,21], the intracellular domain of Notch could be replaced with a subunit of much longer lifetime. Tuning the intracellular domain degradation rate and observing the outcome is a potentially accessible experiment.

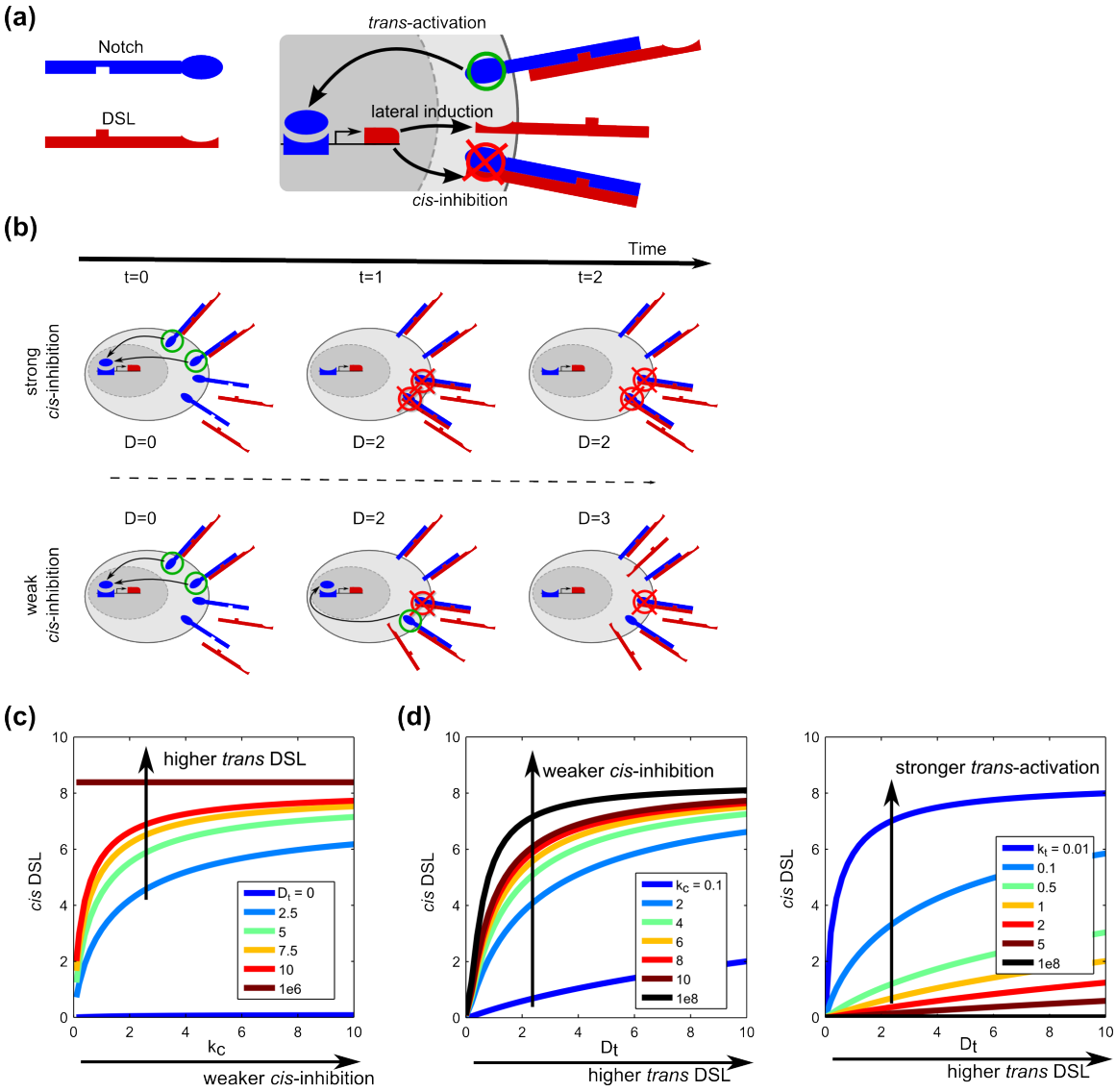

Figure 1: Notch signaling-mediated lateral induction is negatively regulated by *cis*-inhibition. (a) The Notch signaling system consists of Notch receptors and DSL ligands, which interact on neighboring surfaces to *trans*-activate the system (green circle) and on the same surface to *cis*-inhibit it (red cross-circle). Lateral induction refers to upregulation of ligand expression in response to Notch signaling (right). (b) Stronger *cis*-inhibition should lead to a diminished Notch signaling response to an idential *trans* ligand stimulus. In the cell with stronger *cis*-inhibition, a greater part of the ligand expressed due to lateral induction will successfully compete away the *trans* ligand, leading to less signaling. (c) Plots of induced *cis* Delta as a function of *cis*-inhibition strength indicate that as *cis*-inhibition becomes weaker (as the x axis increases), the response of a cell to *trans* ligand becomes stronger. At any value of *cis*-inhibition strength, the response of the cell is increasing in *trans* ligand. (d) The single-cell response to *trans* ligand is influenced by both *cis*-inhibition and *trans*-activation strength. As the *cis*(*trans*) interaction becomes stronger, the induced ligand profile moves lower(higher).

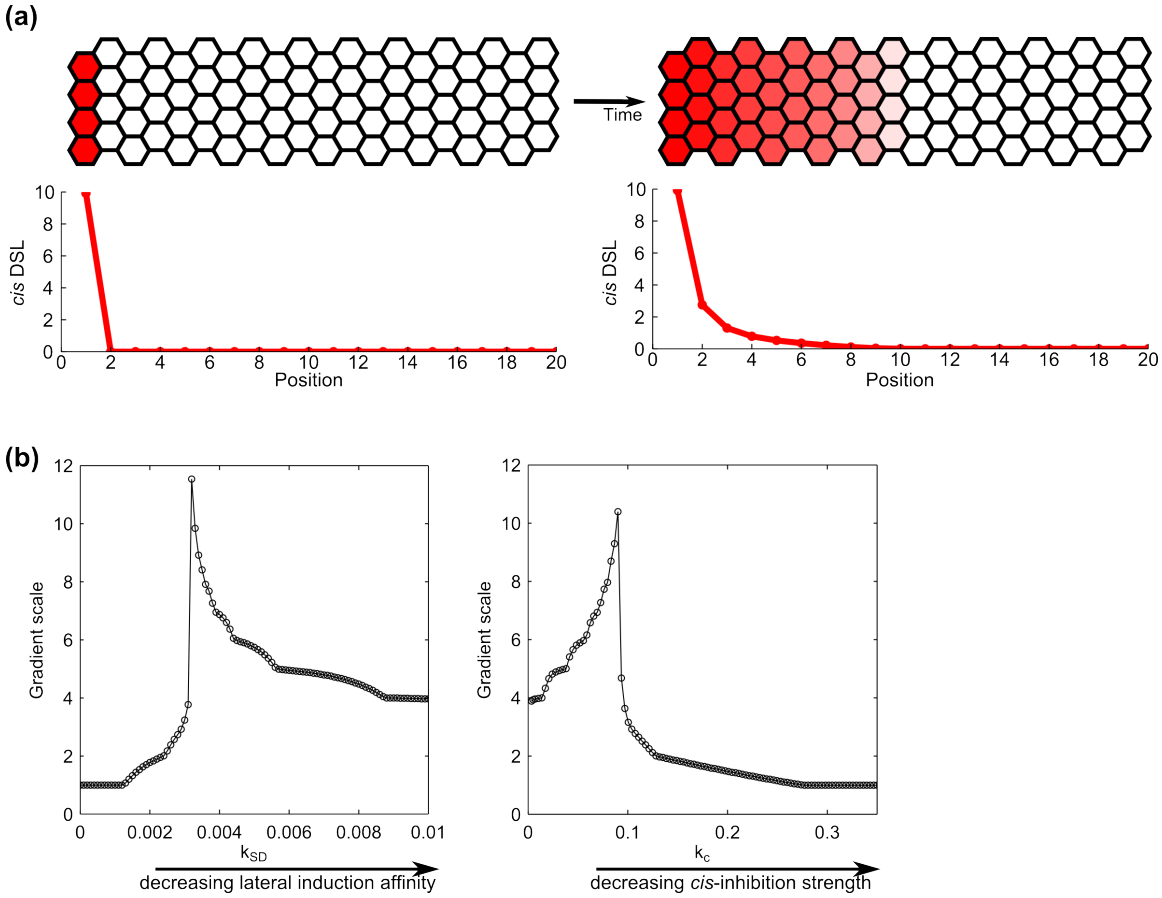

Figure 2: Gradient formation by Notch-mediated lateral induction. (a) A regular hexagonal lattice of cells containing the lateral induction feedback is stimulated by a column of high-ligand source cells from the left. Under these circumstances, if the source is maintained at its high level a gradient of *cis* ligand forms (darker red corresponds to more *cis* ligand). (b) Plots of the *cis* ligand gradient lengthscale as a function of *cis* interaction strength and lateral induction affinity show that the lengthscale is typically quite short, but for very small parameter ranges can be reasonably large.

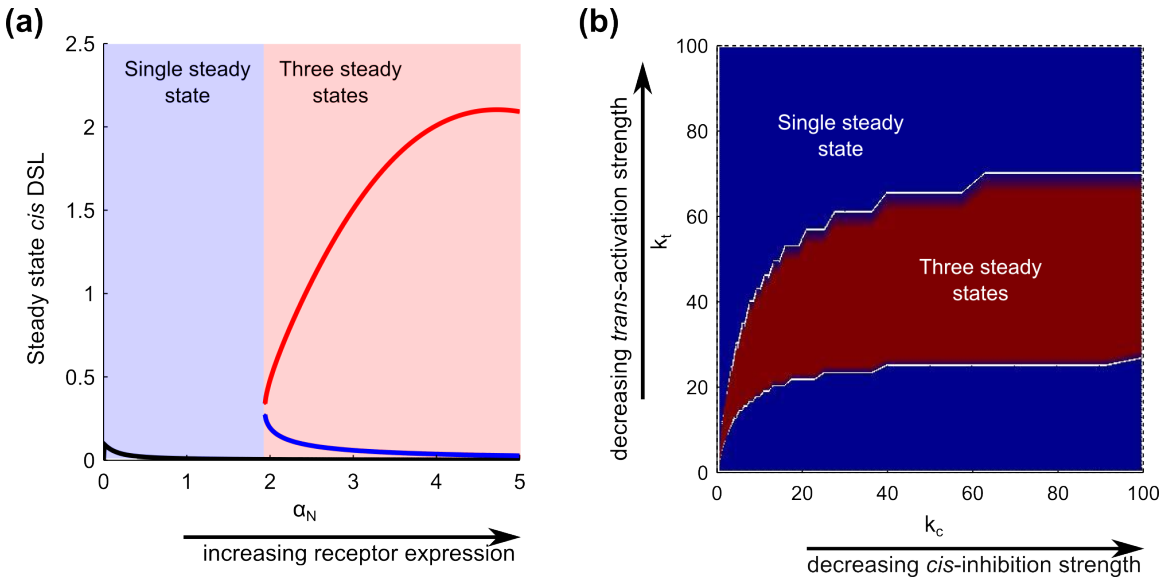

Figure 3: Lateral induction through Notch signaling can admit multiple population homogeneous steady states. (a) Solving the homogeneous steady state condition for varying Notch production rates yields a single low-ligand steady state at low receptor production, but above a threshold the system bifurcates into three (red, black, blue) steady states of which the former two are stable. (b) Parameter scans indicate regions of population-level bistability (red) and monostability (blue).

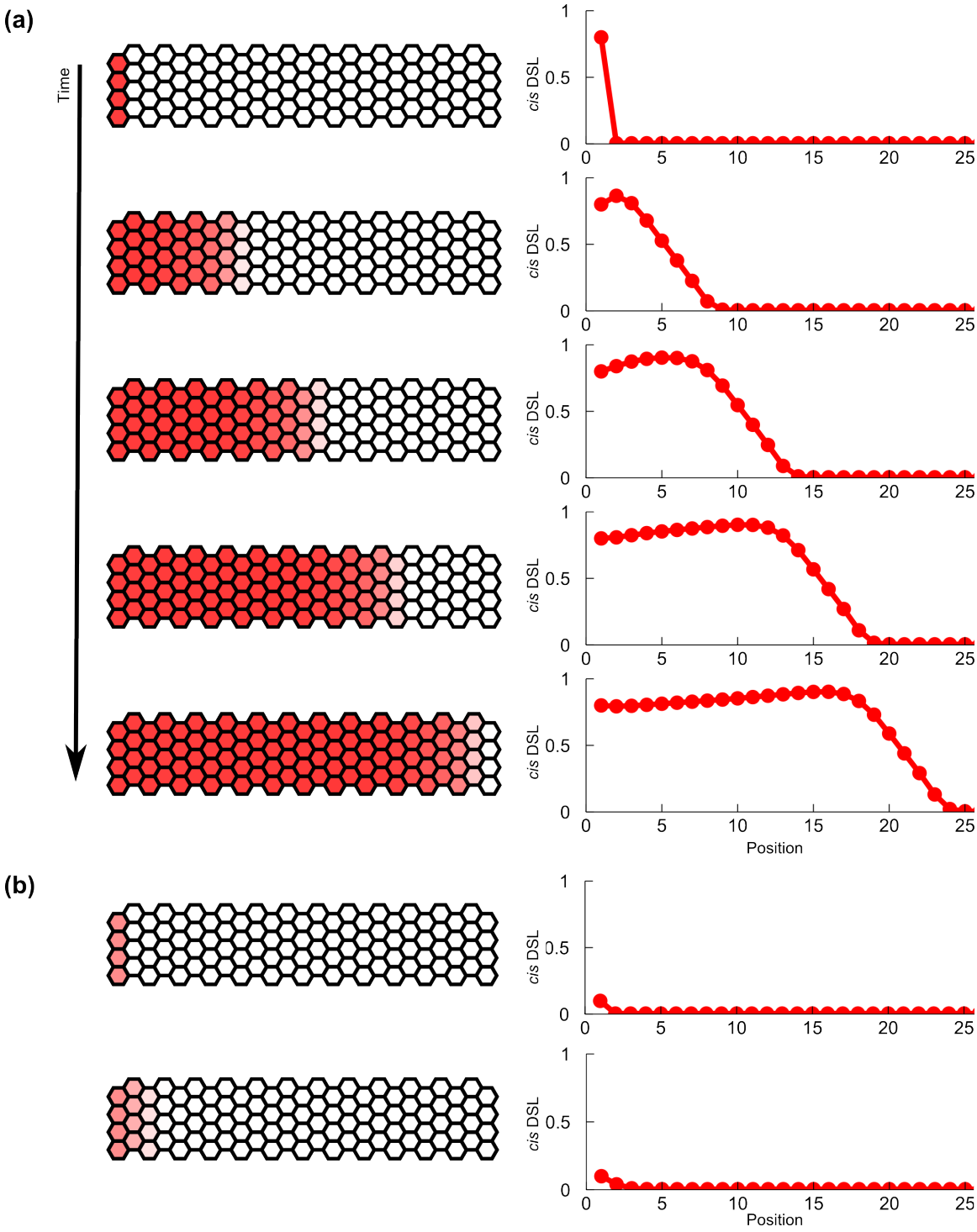

Figure 4: Front propagation occurs in a bistable population. (a) A lattice of lateral induction cells with parameters allowing bistability is stimulated on its left by a high-ligand source, which sets off a front that transitions the collection of cells to the high-ligand state. Time proceeds downward, and brighter red indicates greater ligand. (b) Initiation of front propagation requires that the source stimulus be above some threshold, or as this plot indicates local gradient formation results.

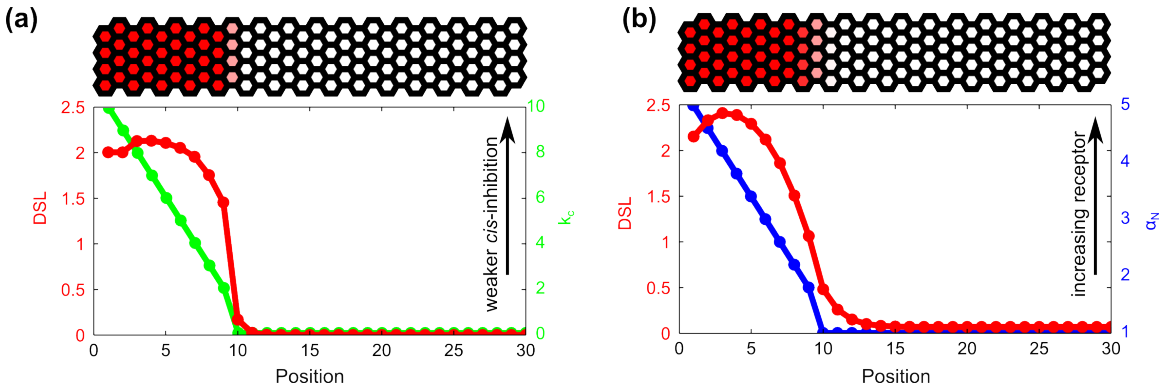

Figure 5: Bistable lateral induction can convert a gentle gradient in the system parameters to a sharp delineation between populations of high- and low-ligand cells. (a) A linear gradient of *cis*-inhibition strength is converted to a ligand profile that drops off much more steeply. (b) A similar phenomenon is observed with a gradient in the Notch expression rate, but the effect is less pronounced and the uniformity of high-ligand cells is far less than the case in Fig. 5a.

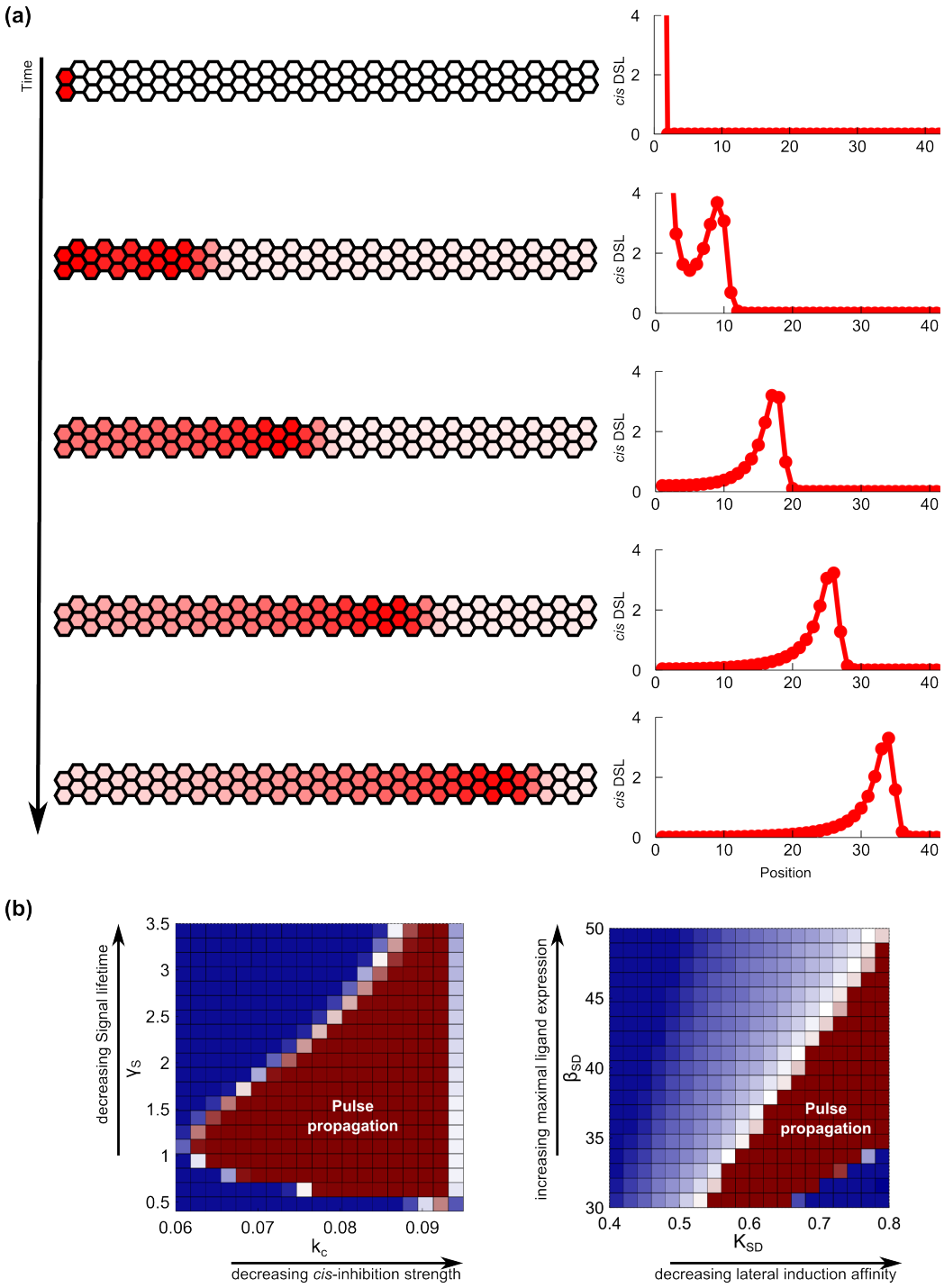

Figure 6: The signaling turnoff effect of *cis*-inhibition combined with a persistent signaling intermediate to introduce a time delay in the lateral induction feedback permits a moving pulse pattern. (a) In a setup identical to that of the front propagation, giving the Notch intracellular signaling domain slow dynamics (i.e., a long lifetime) allows pulse propagation across the lattice of cells. (b) Pulse propagation is limited to certain parameters. The left plot shows that strong *cis*-inhibition and long-lived Notch intracelllar signaling domain are required for pulse propagation, and the right plot shows that the lateral induction affinity and maximum ligand production rate must be chosen to lie along a diagonal strip.

Methods

Our model incorporates the concentrations of three species in each cell: Notch receptor (N), DSL ligand (D), and cleaved intracellular Notch signaling domain (S). N interacts with *trans* D on neighboring cell surfaces by second-order kinetics with rate k_t^{-1} (a function of the receptor-ligand binding, unbinding, and cleavage rates) to generate S in a process that destroys both N and D at the same rate of S production. N and D in the same cell also interact in *cis*, leading to their mutual inactivation by second-order kinetics with rate k_c^{-1}. S induces expression of D. N, D, and S all also undergo first-order degradation. The parameters governing the system are:

α_N,α_D	Constitutive production rates of N and D
γ	First-order degradation rate of N and D
γ_S	First-order degradation rate of S
k_t, k_c	Strength of *trans*- and *cis*-interactions between N and D, respectively
β_{SD}, k_{SD}, n	Maximum magnitude, affinity, and cooperativity of the increasing Hill function of S that contributes to D expression
$\langle D_j \rangle_i$	Denotes the average of D in the cells j that are neighbors of cell i
$\langle N_j \rangle_i$	Denotes the average of N in the cells j that are neighbors of cell i

Every simulation in this paper is governed by the following equations:

$$\begin{aligned}
\frac{dN_i}{dt} &= \alpha_N - \gamma N_i - \frac{1}{k_c} N_i D_i - \frac{1}{k_t} N_i \langle D_j \rangle_i \\
\frac{dD_i}{dt} &= \alpha_D + \beta_{SD} \frac{S^n}{k_{SD}^n + S^n} - \gamma D_i - \frac{1}{k_c} N_i D_i - \frac{1}{k_t} \langle N_j \rangle_i D_i \\
\frac{dS_i}{dt} &= \frac{1}{k_t} N_i \langle D_j \rangle_i - \gamma_S S_i
\end{aligned}$$

In the study of single-cell response to *trans* ligand D_t, we set $\langle D_j \rangle_i = D_t$ and $\langle N_j \rangle_i = 0$.

The simulations of gradient formation, front propagation, and pulse propagation all used these same equations with different parameters and boundary conditions. Computation of the homogeneous steady states was achieved by obtaining the intersection of the system's nullclines.

All computations were coded and executed in Matlab 2010a (The Mathworks) using the ode15s solver for differential equations.

References

1. Gazave, E. et al. Origin and evolution of the Notch signalling pathway: an overview from eukaryotic genomes. *BMC Evol Biol* **9**, 249-249 (2009)

2. Radtke, F., Schweisguth, F. & Pear, W. The Notch 'gospel'. *EMBO Rep* **6**, 1120-1125 (2005).

3. Lai, E.C. Notch signaling: control of cell communication and cell fate. *Development* **131**, 965-973 (2004).

4. Becam, I., Fiuza, U.-M., Arias, A.M. & Miln, M. A Role of Receptor Notch in Ligand cis-Inhibition in Drosophila. *Current Biology* **20**, 554-560 (2010).

5. Sprinzak, D. et al. Cis-interactions between Notch and Delta generate mutually exclusive signalling states. *Nature* **465**, 86-90 (2010).

6. Hicks, C. et al. Fringe differentially modulates Jagged1 and Delta1 signalling through Notch1 and Notch2. *Nat Cell Biol* **2**, 515-520 (2000).

7. de Celis, J.F. & Bray, S. Feed-back mechanisms affecting Notch activation at the dorsoventral boundary in the Drosophila wing. *Development* **124**, 3241 -3251 (1997).

8. Huppert, S.S., Jacobsen, T.L. & Muskavitch, M.A. Feedback regulation is central to Delta-Notch signalling required for Drosophila wing vein morphogenesis. *Development* **124**, 3283 -3291 (1997).

9. Barad, O., Rosin, D., Hornstein, E. & Barkai, N. Error Minimization in Lateral Inhibition Circuits. *Sci. Signal.* **3**, ra51 (2010).

10. Kiernan, A.E. Notch signaling during cell fate determination in the inner ear. *Seminars in Cell & Developmental Biology* **24**, 470-479 (2013).

11. Collier, J.R., Monk, N.A.M., Maini, P.K. & Lewis, J.H. Pattern Formation by Lateral Inhibition with Feedback: a Mathematical Model of Delta-Notch Intercellular Signalling. *Journal of Theoretical Biology* **183**, 429-446 (1996).

12. Owen, M.R. & Sherratt, J.A. Mathematical modelling of juxtacrine cell signalling. *Mathematical Biosciences* **153**, 125-150 (1998).

13. Sprinzak, D., Lakhanpal, A., LeBon, L., Garcia-Ojalvo, J. & Elowitz, M.B. Mutual Inactivation of Notch Receptors and Ligands Facilitates Developmental Patterning. *PLoS Comput Biol* **7**, e1002069 (2011).

14. Neves, J., Parada, C., Chamizo, M. & Giraldez, F. Jagged 1 regulates the restriction of Sox2 expression in the developing chicken inner ear: a mechanism for sensory organ specification. *Development* **138**, 735-744 (2011).

15. Daudet, N., Ariza-McNaughton, L. & Lewis, J. Notch signalling is needed to maintain, but not to initiate, the formation of prosensory patches in the chick inner ear. *Development* **134**, 2369 -2378 (2007).

16. Saravanamuthu, S.S., Gao, C.Y. & Zelenka, P.S. Notch signaling is required for lateral induction of Jagged1 during FGF-induced lens fiber differentiation. *Developmental Biology* **332**, 166-176 (2009).

17. Manderfield, L.J. et al. Notch activation of Jagged1 contributes to the assembly of the arterial wall. *Circulation* **125**, 314-323 (2012).

18. Feng, X., Krebs, L.T. & Gridley, T. Patent ductus arteriosus in mice with smooth muscle-specific Jag1 deletion. *Development* (2010).

19. Varshavsky, A. The N-end rule pathway of protein degradation. *Genes Cells* **2**, 13-28 (1997).

20. Tasaki, T., Sriram, S.M., Park, K.S. & Kwon, Y.T. The N-End Rule Pathway. *Annu. Rev. Biochem.* **81**, 261-289 (2012).

21. Banaszynski, L.A., Chen, L.-chun, Maynard-Smith, L.A., Ooi, A.G.L. & Wandless, T.J. A Rapid, Reversible, and Tunable Method to Regulate Protein Function in Living Cells Using Synthetic Small Molecules. *Cell* **126**, 995-1004 (2006).

Chapter 4

Engineering and characterization of a synthetic Notch signaling-mediated lateral induction feedback circuit in cell culture

This section contains my unpublished experimental work showing that lateral induction coupled with positive feedback on Notch signaling drives a ligand-dependent transition between signaling states.

Letter

Spatial pattern formation is an essential element of multicellular development. As a coordinated process among groups of cells, the generation of spatial patterns requires some mechanism of intercellular communication. A small number of signaling pathways are known to be employed in patterning processes, including juxtacrine signaling via Notch signaling [1]. In canonical mammalian Notch signaling, a member of the Notch family of receptors (Notch1-4) is bound by a member of the Delta or Jagged (Delta-like1/3-4, Jagged1-2) families of membrane-bound ligands. This interaction occurs in one of two orientations: in *cis* on the surface of the same cell, or in *trans* between molecules on the surfaces of neighboring cells [2]. Binding of Notch with ligand on the same cell surface is not productive (*cis*-inhibition), while by contrast binding with ligand on a neighboring cell leads to signal transduction by cleavage and nuclear translocation of the Notch intracellular domain (*trans*-

activation) (Fig. 1a). The Notch signaling system integrates these positive and negative inputs in a manner that we have previously reported is consistent with strong mutual *cis*-inactivation of Notch and Delta [3]. Models of mutual inactivation in the context of boundary formation and lateral inhibition patterning processes have suggested potential roles in affecting developmental patterning [4]. Studies in model organisms have obtained evidence for the developmental relevance of *cis*-inhibition in natural contexts [5,6].

The outcome of a spatial patterning process depends on the combination of signaling system properties and downstream regulatory network function. For instance, in the canonical example of pattern formation using the Notch system, lateral inhibition, downstream of Notch signaling lies some mechanism by which Delta is downregulated [7]. Processes in which Notch signaling has the opposite downstream effect, increasing the level of ligand rather than decreasing it, are referred to as lateral induction [8]. Notch-mediated lateral induction has been implicated in a number of mammalian developmental contexts. In the *Gallus* inner ear, lateral induction between Notch and Jagged1 contributes to the formation of prosensory patches limiting the domain within which sensory organs may arise [9,10]. The layers of smooth muscle in the walls of certain arteries are specified by lateral induction between Notch and Jagged1 [11,12]. The lateral induction feedback models proposed in these contexts have not incorporated the potential role of *cis*-inhibition in their function.

We developed an *in vitro* model of lateral induction by creating a mammalian cell line implementing a synthetic Notch-Delta lateral induction feedback circuit, along with fluorescent readouts of both Notch signaling and Delta levels to characterize its behavior (Fig. 1) (a similar effort has been published in [13]). The parental cell line was Chinese Hamster Ovary K1 (CHO-K1), which we have previously established expresses negligible levels of Notch receptors and ligands but is nonetheless capable of supporting Notch signaling if the receptor is supplied exogeneously [3]. Into the parent line we stably transfected a diverted form of the Notch receptor consisting of the extracellular and transmembrane domains of human Notch1 fused to a minimal version of the yeast Gal4 transcriptional activator (Gal4esn) [14] constitutively expressed under the pEF-1α promoter [15], generating

the receptor line. This replacement of the normal Notch intracellular domain diverts pathway activation away from whatever feedbacks may normally occur in response to Notch signaling, ensuring that our obervations are not confounded by endogenous regulation that may be cell type-specific. To the receptor line we stably transfected a Gal4-inducible (UAS) bicistronic construct (Fig. 1b) consisting of a rat Delta1-mCherry fusion (Delta-mCh) and a histone-tagged Citrine (H2B-Citrine) separated by the T2A sequence. The 2A family of sequences, taken from viruses, are processed normally by the ribosome and then automatically but the developing peptide then automatically cleaves at the 2A sequence [16]. The T2A sequence in particular has seen frequent use in the literature to express multiple proteins from a single transcript [17-19]. This construct therefore simultaneously provides a nuclear-localized fluorescent readout of integrated Notch signal activity due to the stability of H2B-Citrine and implements the basic "lateral induction" feedback interaction (Fig. 1b). We also further modified the feedback circuit architecture by adding a positive feedback element, implemented as a construct expressing Gal4 under UAS control, generating the "amplifier" line (Fig. 4a).

Results

The fundamental behavior of a lateral induction feedback is upregulation of *cis* ligand upon stimulation by *trans* ligand (Fig. 1b). Because activation of the Notch receptor requires a force exerted on the molecule [20], ligand in *trans* cannot merely be provided in the medium but must be adsorbed onto the cell culture surface. Following a standard protocol for *trans* stimulation we incubated 24-well cell culture plates with a solution containing a protein fusion of the extracellular domain of rat Dll1 and immunoglobulin-G (together referred to as D_{plate} or D_p). After incubation we passaged lateral induction cells to treated (D_p+) and untreated (D_p—) culture surfaces in media containing *N*-[*N*-(3,5-difluorophenacetyl)-L-alanyl]- *S*-phenylglycine t-butyl ester (DAPT), which inhibits Notch signaling by blocking γ-secretase cleavage of the receptor. We allowed cells to settle for 24 hours, after which the inhibitor was washed out with fresh media. Forty-eight hours later the cells were trypsinized, and we measured the fluorescent readouts of Notch signaling (Citrine) and *cis* ligand expression (mCherry) by FACS analysis. As desired, plate-bound ligand increased both Cit-

rine and mCherry fluorescence, indicating ligand-dependent Notch signal activation and induction of Delta expression.

If *cis*-inhibition of Notch by Delta is strong, we expect that the same amount of plate-bound Delta should lead to less Notch signaling in lateral induction cells than in reporter cells. This concept is visualized in FIG 2a, where we see that the additional *cis* Delta expressed in lateral induction cells should inactivate surface Notch and decrease the cells' overall sensitivity to Delta in *trans* relative to reporter cells that never express *cis* Delta. To make this comparison we used the plate-bound Delta *trans*-activation assay to stimulate lateral induction and reporter cells with the same amount of *trans* ligand for the same duration of time. Our data are consistent with strong *cis*-inhibition, as identical stimuluation by D_{plate} drives reporter cells to higher levels of Citrine expression than lateral induction cells (approximately four-fold, FIG 2b).

In addition to this static population-level behavior we also predict a single-cell dynamical signature of *cis*-inhibition (Fig. 3a). At the initial time when the Notch signaling inhibitor is removed, the *cis* ligand levels of both lateral induction and reporter cells are both near zero. Thus, the instantaneous level of Notch signaling, provided by the rate at which Citrine fluorescence levels increase, should be comparable in both lines at early times. However, as time passes lateral induction cells accumlate more *cis* ligand the rate of Notch signaling in those cells should decrease. By contrast, pure reporter cells lacking the positive feedback should remain devoid of *cis* ligand and thus signaling should continue at close to the initial rate (Fig. 3a).

To test for this dynamical signature we employed time-lapse fluorescence microscopy of lateral induction and reporter cells exposed to plate-bound Delta, using the protocol described in our previous work quantifying the Notch signaling input/output relationship [Nature REF]. The data yielded the dynamics as predicted in Fig. 3a. Immediately after washout of the inhibitor the median Citrine slope of lateral induction cells reached its maximum, after which it diminished. Reporter cells quickly reached and maintained a high level of Notch signaling throughout (Fig. 3b). The exaggerated difference between the initial Citrine fluorescence slopes of the lateral induction and reporter cell lines could be explained by the temporal resolution of our time-lapse imaging, which

would integrate over time during which the lateral induction cells are accumulating *cis* Delta and therefore underestimate the true initial instantaneous Notch signaling level in those cells.

We then asked how modifying the lateral induction circuit architecture by adding a positive feedback element (UAS-Gal, an "amplifier", Fig. 4a) would affect the behavior of the system. We obtained several stably integrated clones incorporating the amplifier that displayed a bimodal distribution of Citrine fluorescence both with and without *trans* Delta stimulation (FIG 4b). Cells in the less fluorescent population are in a low-signaling state (referred to simply as "low"), with both little Citrine indiciating low levels of Notch signal and low mCherry indicating low levels of *cis* Delta. Cells in the more fluorescent population are in a high-signaling state ("high"), with greater levels of Citrine indicating a combination of Notch signal and positive feedback from the amplifier and high mCherry indicating high levels of *cis* Delta.

Because the behavior we seek is a maximally *trans* ligand-dependent transition to a high-signaling state, we assessed the bimodal candidate lines on a quantitative standard of this property. We quantified the extent of ligand-dependent and ligand-independent transitions to the high-signaling state by plotting the fraction of high-signal cells in populations exposed to plate-bound *trans* Delta versus the fraction of high-signal cells in unstimulated populations (Fig. 4c). From these we chose the clone closest to the ideal behavior, which would be the top-left corner of Fig. 4c in which no cells spontaneously generate high levels of Notch signaling (zero on the x-axis) but all cells are driven into the high Notch signaling state when exposed to plate-bound Delta (one on the y-axis).

We probed the behavior of the chosen amplifier clone by obtaining a FACS timecourse of its fluorescent response to plate-bound Delta over 100 hours. Our data indicate that under both conditions with/without plate-bound Delta the fraction of cells in the high-signaling state plateaus at approximately 50/70 hours, respectively, at a higher final level with plate-bound Delta than without (85% vs 50%, Fig 5b). We suggest that the high-signal cells in the unstimulated condition represent a sequential combination of (i) sporadic spontaneous transitions to the high state due to leakiness in the Notch system followed by (ii) *trans* signaling from the spontaneously high cells to their neighbors. A striking feature of the data, the delay in the unstimulated timecourse (which only begins

to appreciably increase between 24 and 48 hours by contrast with the stimulated timecourse which begins rising within the first 24 hours), is consistent with this suggestion. Turnoff dynamics from the maximally-induced high population under Notch signaling-inhibited conditions (DAPT treatment) are slow, with very little change in the fraction of cells in the high state over 48 hours, approximate equality between high- and low-state cells at 72 hours, and recovery of a fully-off population at 120 hours.

Finally, in order to claim a lateral induction process with the potential to spatially propagate a signal, we must establish that the high state of these amplifier cells is capable of sending signal to neighboring cells. To achieve this we co-cultured pre-induced (by plate-bound Delta) amplifier cells at low density among a high density of reporter cells, and after 48 hours of growth in Notch signaling-permissive conditions we imaged the culture (Fig. 6a). Reporter cells are distinguishable from amplifier cells by constitutive Cerulean fluorescence. The pre-induced amplifier cells are visualized with bright green (Citrine) nuclei and punctate red cytosol (Delta-mCherry). Reporter cells in which Notch signaling has been induced appear with cyan nuclei, as a combination of the constitutive H2B-Cerulean and Notch signaling-driven H2B-Citrine. We appreciated visually that reporter cells in proximity to patches of pre-induced amplifier cells display high levels of Notch signaling, while reporter cells far from pre-induced amplifier cells display very little. We quantified this relationship (Fig. 6b), and found that only within two cell diameters of an mCherry-positive high-state amplifier cell was there any reporter expression of Citrine above background. This constitutes strong evidence that the amplifier cells in the high state have produced Delta that is capable of activating Notch in their neighbors, the prerequisite for spatial propagation of Notch signaling by lateral induction.

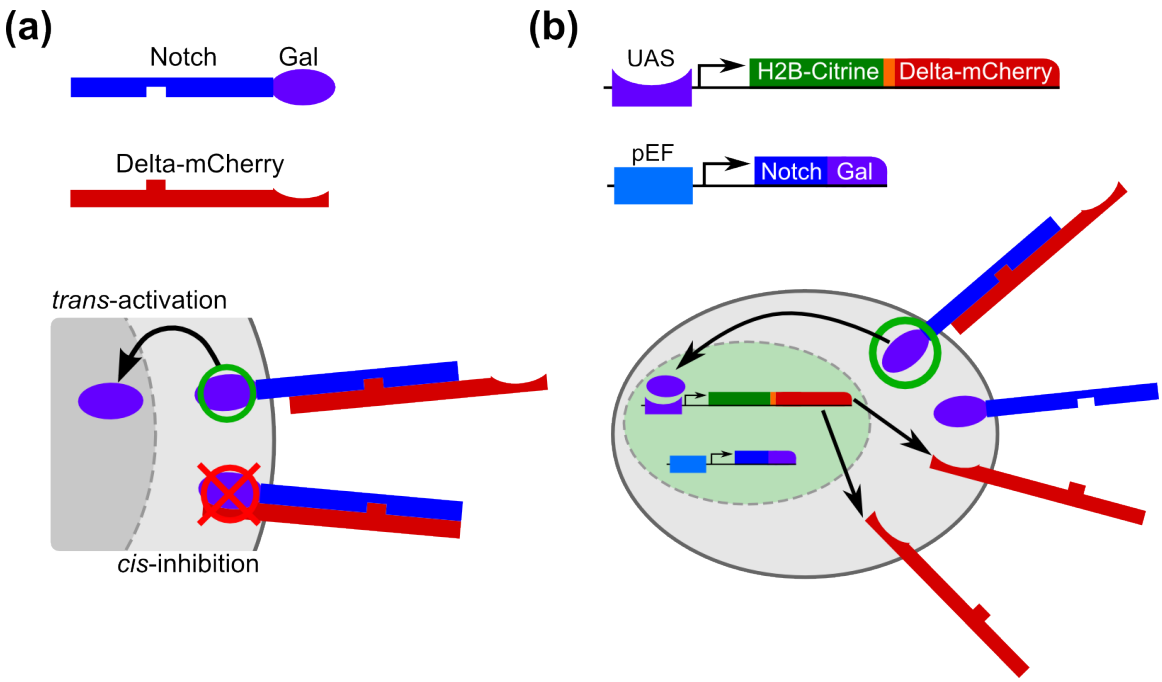

Figure 1: System for analyzing Notch signaling-mediated lateral induction (a) Notch is a transmembrane receptor, which upon *trans*-activation by ligand (upper arrow, green circle) releases its intracellular domain (replaced here with a minimal Gal4, purple) to the nucleus. Notch also interacts with ligand cell-autonomously, leading to mutual *cis*-inactivation (red circle/cross). (b) We implement synthetic Notch-mediated lateral induction in a genetically-engineered CHO-K1 cell line. The lateral induction cell line stably expresses a diverted form of Notch (the extracellular domain of human NOTCH1 fused to a minimal transcriptional activator Gal4esn) constitutively expressed under the control of the pEF1-α promoter. Activation of the Notch receptor induces expression from a stably-integrated UAS-driven bicistronic construct containing (i) a stable nuclear-localized fluorescent reporter of Notch signaling (histone 2B-Citrine) and (ii) a fusion of the Notch ligand rat Delta-like 1 to mCherry (Delta-mCherry), separated by the T2A sequence to allow coordinated expression of the two proteins from a single mRNA transcript.

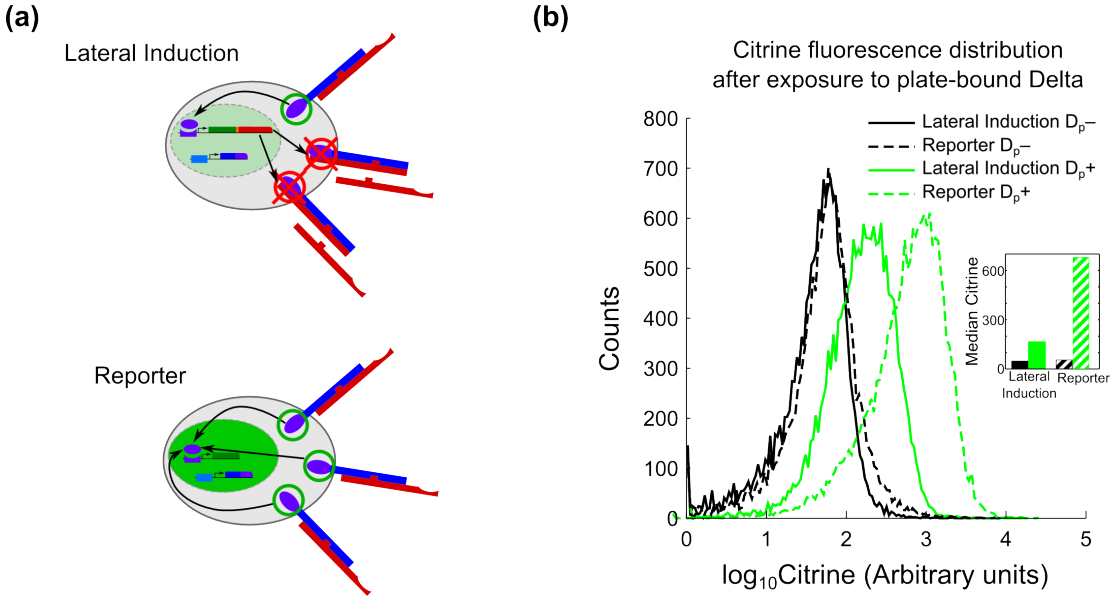

Figure 2: *Cis*-inhibition between Notch and Delta limits the magnitude of signaling in lateral induction cells. (a) Schematic comparision of a lateral induction cell and a feedback-free reporter cell illustrates the predicted limitation of Notch signaling due to the lateral induction feedback and *cis*-inhibition. In a lateral induction cell line (upper) stimulated with a specific quantity of extracellular ligand, the feedback generates inhibitory intracellular *cis*-Delta which decreases the quantity of Notch receptor available to transduce signal. In the absence of this feedback, the simple Notch reporter line (lower) has all of its Notch available to participate in productive signaling, and thus when stimulated by the same quantity of extracellular Delta should generate a response of greater magnitude (stronger green nucleus). (b) Population-level measurement of Notch signaling confirms the expected relationship between the magnitude of Notch signaling in a lateral induction line and feedback-free reporter cells. The inserted bar chart compares the population Citrine fluorescence medians of lateral induction and reporter cell lines with (D_p^+) and without (D_p^-) *trans* Delta

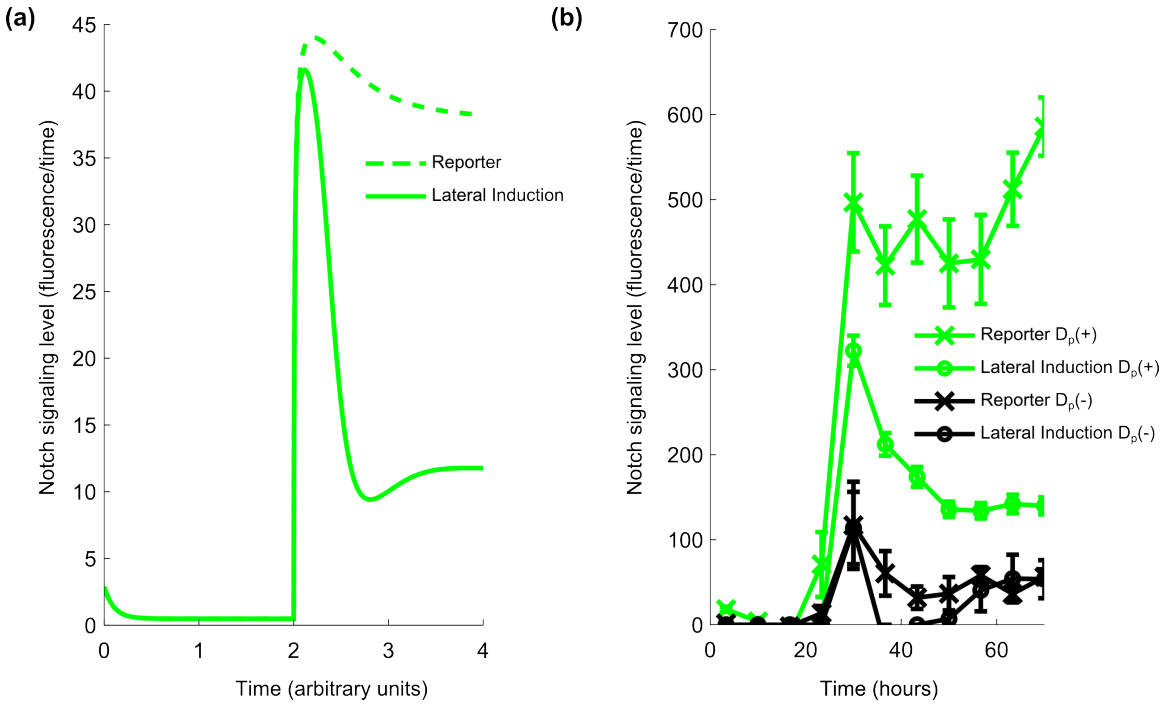

Figure 3: Dynamics of Notch signaling in the lateral induction cell line are consistent with *cis*-inhibition. (a) At the initial time when Notch signaling is allowed to commence, both lateral induction and reporter cells should express no *cis* ligand and therefore the level of Notch signaling activity (the rate of fluorescence increase) in both lines should be comparable. As signaling continues the lateral induction cells accumulate *cis* ligand which decreases the level of available receptor, so the Notch signaling activity diminishes. In the absence of feedback, the reporter cell Notch signaling activity remains near the high initial level. (b) Notch signal dynamics of lateral induction cells obtained by time-lapse microscopy are consistent with the expectation of Fig. 3a, with a transient high level of Notch signaling after inhibitor removal followed by a decrease to a lower level of Notch signaling. Reporter cells lacking the feedback do not show this decrease.

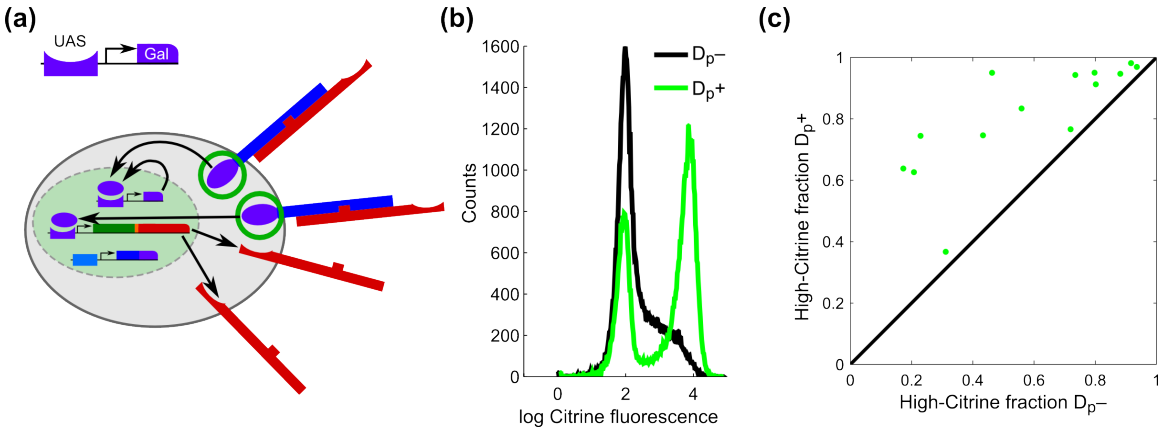

Figure 4: Addition of a positive-feedback amplifier to the regulatory circuit leads to a bimodality in Notch signaling levels. (a) We added a positive-feedback amplifier to the lateral induction circuit, consisting of UAS driving expression of the minimal Gal4. As diagrammed, in these cells Notch signaling not only drives the Citrine reporter and Delta-mCherry *cis* ligand but also activates the expression of Gal, which activates its own expression in a positive feedback loop. (b) Several clones stably integrating the amplifier construct demonstrated a ligand-dependent transition between low- and high-signaling states. After 48 hours of growth in Notch signaling-permissive conditions, both with (green) and without (black) exposure to *trans* ligand, FACS data show that the population of cells displays a bimodal distribution of Citrine fluorescence. (c) For each of these clones we plot the fraction of cells in the high Citrine state with *trans* ligand stimulation versus the fraction of cells in the high Citrine state without *trans* ligand stimulation. Points representing cell lines at the top-right of the plot report high levels of Notch signaling plus feedback regardless of *trans* ligand, indicating undersirable constitutive activation of the positive feedback system. Cell lines closer to the top-left of the plot are those with fewer transitions to the high-Citrine state in the absence of *trans* ligand, and more transitions to the high-Citrine state when stimulated by *trans* ligand.

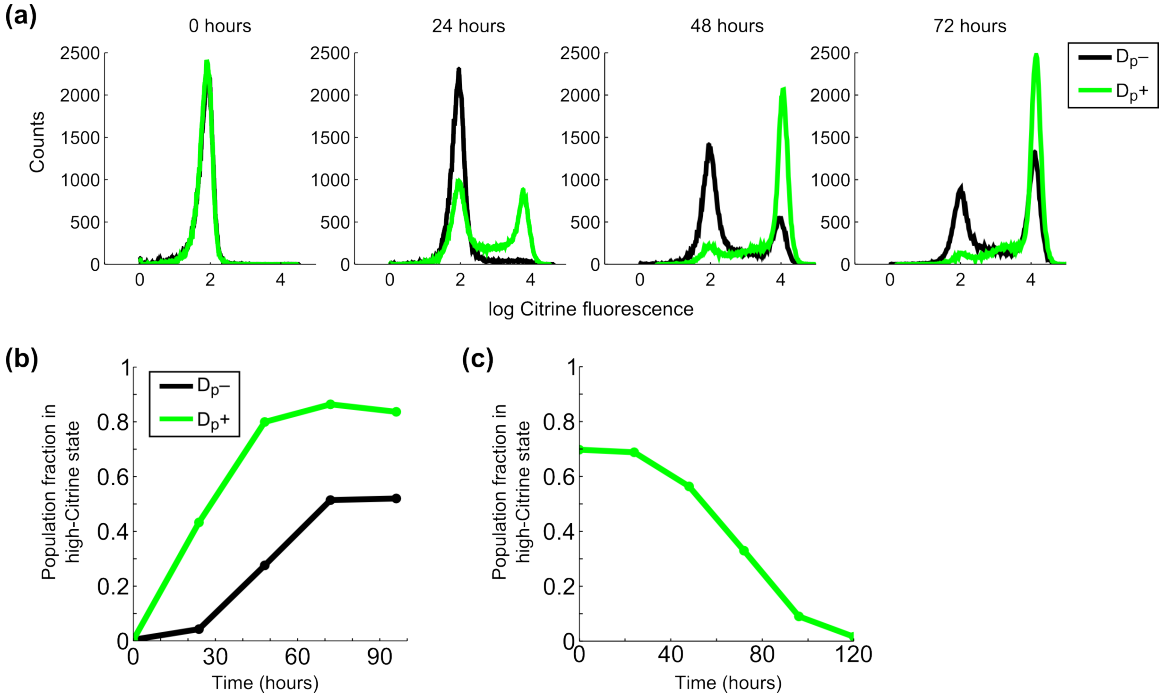

Figure 5: Timecourse of amplifier cell line response to *trans* ligand (a) FACS analysis of amplifier cell populations exposed to *trans* ligand or untreated control surfaces reveals the dynamics of ligand-dependent and ligand-dependent transitions to the high-signal state. Cells were initially prepared in a homogeneously low-Citrine state by growth for several generations in Notch signaling-inhibited (DAPT positive) conditions. At various times after removal of DAPT inhibition the distribution of fluorescence shifts toward the high-Citrine state, but at a higher rate when stimulated with *trans* ligand than without. (b) Timecourses of transitions to the high-Citrine state with and without *cis* ligand stimulation. (c) Timecourse of transition away from the high-Citrine state when a maximally *trans*-activated population is treated with the Notch inibitor DAPT.

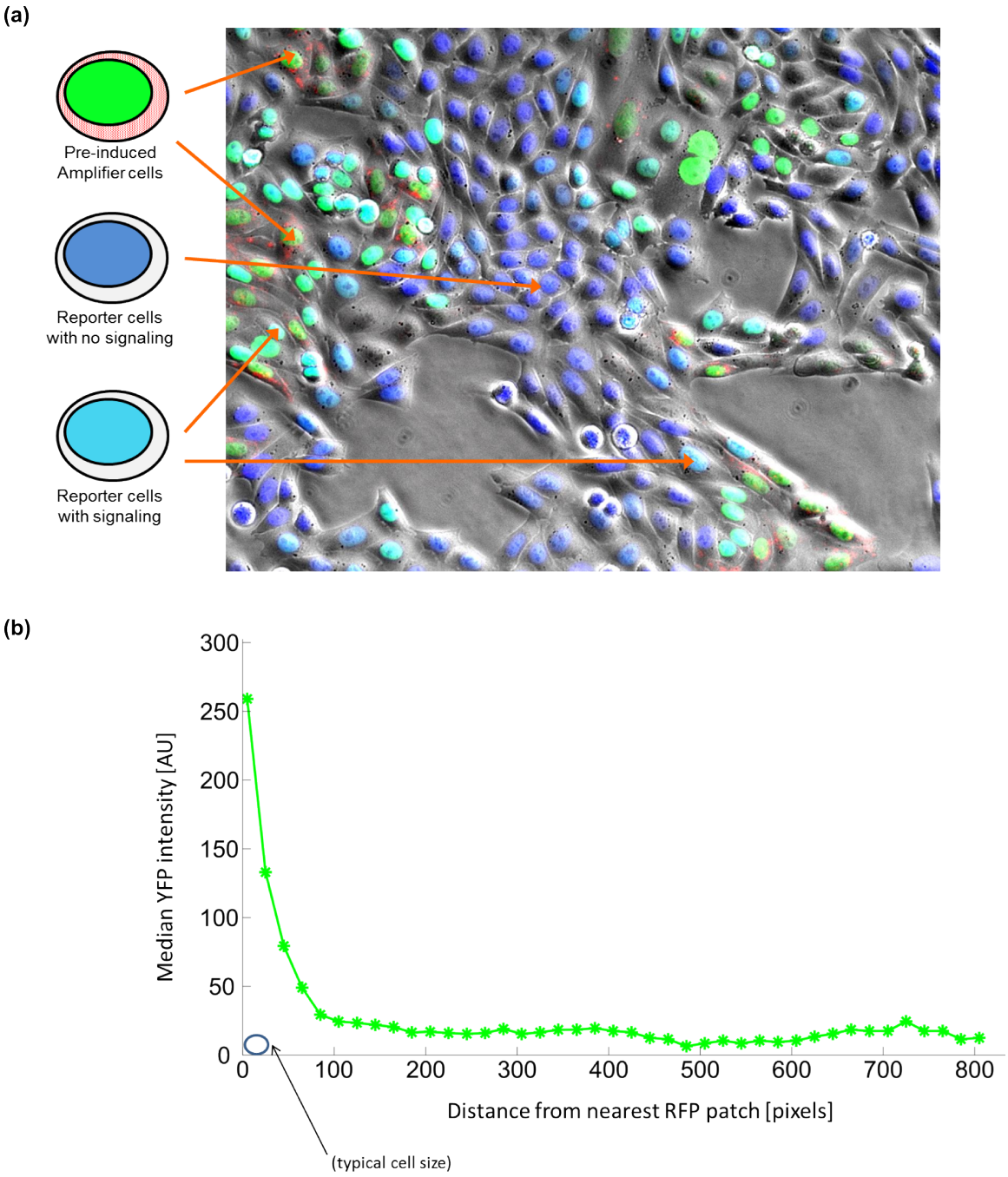

Figure 6: The high-Citrine/high-ligand state of the amplifier cell line is capable of activating Notch in neighboring cells. (a) Composite fluorescence and phase microscopy image of a co-culture with pre-induced amplifier cells (green nuclei with red cytosol) and Notch signaling reporter cells (blue nuclei), allowed to grow for 48 hours in Notch signaling-permissive conditions. Reporter cells that have high levels of Notch activity appear cyan, as the combination of Cerulean and Citrine. Only reporter cells near patches of pre-induced amplifier cells appear to be activated. (b) Profile of Citrine fluorescence as a function of distance from the nearest patch of pre-induced amplifier cells. Localization of Citrine fluorescence above background to regions within one or two cell diameters of pre-induced amplifier cell pathches indicates that surface ligand on the pre-induced amplifier cells is effectively activating Notch on neighboring cells.

Methods

The genetic constructs used in this work were created by standard molecular biology techniques. The lateral induction construct, pEV-UAS-H2B-Citrine-T2A-Delta-mCherry, was generated by combining (i) a PCR fragment of the TO-Delta-mCherry construct described in [Nature REF] including the Delta-mCherry ORF with a 3' T2A sequence replacing the start codon, and (ii) a restriction digest of the pEV-UAS-H2B-Citrine construct also described in [3]. A second step replaced the parent construct's Zeocin resistance cassette with a constitutively-expressed Hygromycin resistance also taken from TO-Delta-mCherry. The amplifier construct, pEV-UAS-Gal4esn, was generated by combining (i) a PCR fragment of the pcDNA4-hN1ecd-Gal4esn construct described in [3] with (ii) a restriction digest of the pEV-UAS-H2B-Citrine construct to remove the H2B-Citrine ORF. A second step replaced the Zeocin resistance cassette with a constitutively-expressed Puromycin resistance from the Invitrogen pExchange system.

Protocols for generating cell lines with stably integrated genetic constructs were performed as described in [3]. All lines in this work descended from the pEF-Notch-Gal line, provided by Lauren LeBon and selected for high levels of available surface Notch receptor, which was resistant to the selection markers Blasticidin at 10 μg mL^{-1} and Geneticin at 600 μg mL^{-1}. The lateral induction line was generated by stably transfecting pEF-Notch-Gal with the UAS-H2B-Citrine-T2A-Delta-mCherry construct, selecting with 500 μg mL^{-1} Hygromycin, and isolating by FACS single cells most highly induced in Citrine and mCherry on transient trasfection with a constitutive activator of UAS. At the same time a pure reporter line was generated from the same pEF-Notch-Gal background by transfection with pEV-UAS-H2B-Citrine modified to express a Hygromycin resistance maker. The lateral induction line was further modified to the amplifier line by transfecting the UAS-Gal construct, selecting in 3 μg mL^{-1} Puromycin, and screening several clones isolated by limiting dilution for Citrine and mCherry activation with and without *trans* ligand (plate-bound Delta, D_p) stimulation.

Imaging and flow cytometry data were obtained as described in [3], with the exception of substituting an LED light source (X-Cite XLED1, Lumen Dynamics) for the fluorescent source used in the

reference. Image analysis was executed in MATLAB R2012a (Mathworks) with a pipeline including nuclear segmentation based on fluorescence intensity and edge detection and cell tracking between frames using the Jonker-Volgenant algorithm [21] for the Linear Assignment Problem as coded by [22].

References

1. Artavanis-Tsakonas, S., Rand, M.D. & Lake, R.J. Notch Signaling: Cell Fate Control and Signal Integration in Development. *Science* **284**, 770 -776 (1999).

2. D'Souza, B., Meloty-Kapella, L. & Weinmaster, G. Canonical and Non-Canonical Notch Ligands. *Current Topics in Developmental Biology* **92**, 73-129 (2010).

3. Sprinzak, D. et al. Cis-interactions between Notch and Delta generate mutually exclusive signalling states. *Nature* **465**, 86-90 (2010).

4. Sprinzak, D., Lakhanpal, A., LeBon, L., Garcia-Ojalvo, J. & Elowitz, M.B. Mutual Inactivation of Notch Receptors and Ligands Facilitates Developmental Patterning. *PLoS Comput Biol* **7**, e1002069 (2011).

5. Becam, I., Fiuza, U.-M., Arias, A.M. & Miln, M. A Role of Receptor Notch in Ligand cis-Inhibition in Drosophila. *Current Biology* **20**, 554-560 (2010).

6. Li, Y. & Baker, N.E. The roles of cis-inactivation by Notch ligands and of neuralized during eye and bristle patterning in Drosophila. *BMC Dev Biol* **4**, 5-5

7. Collier, J.R., Monk, N.A.M., Maini, P.K. & Lewis, J.H. Pattern Formation by Lateral Inhibition with Feedback: a Mathematical Model of Delta-Notch Intercellular Signalling. *Journal of Theoretical Biology* **183**, 429-446 (1996).

8. Lewis, J. Notch signalling and the control of cell fate choices in vertebrates. *Seminars in Cell & Developmental Biology* **9**, 583-589 (1998).

9. Hartman, B.H., Reh, T.A. & Bermingham-McDonogh, O. Notch signaling specifies prosensory domains via lateral induction in the developing mammalian inner ear. *Proceedings of the National Academy of Sciences* **107**, 15792-15797 (2010).

10. Neves, J., Parada, C., Chamizo, M. & Giraldez, F. Jagged 1 regulates the restriction of Sox2 expression in the developing chicken inner ear: a mechanism for sensory organ specification. *Development* **138**, 735-744 (2011).

11. Feng, X., Krebs, L.T. & Gridley, T. Patent ductus arteriosus in mice with smooth muscle-specific Jag1 deletion. *Development* **137**, 4191-4199 (2010).

12. Manderfield, L.J. et al. Notch activation of Jagged1 contributes to the assembly of the arterial wall. *Circulation* **125**, 314-323 (2012).

13. Matsuda, M., Koga, M., Nishida, E. & Ebisuya, M. Synthetic Signal Propagation Through Direct Cell-Cell Interaction. *Sc. Signal.* **5**, ra31 (2012).

14. Kakidani, H. & Ptashne, M. GAL4 activates gene expression in mammalian cells. *Cell* **52**, 161-167 (1988).

15. Wakabayashi-Ito, N. & Nagata, S. Characterization of the regulatory elements in the promoter of the human elongation factor-1 alpha gene. *Journal of Biological Chemistry* **269**, 29831-29837 (1994).

16. Ryan, M.D. & Flint, M. Virus-encoded proteinases of the picornavirus super-group. *J. Gen. Virol.* **78**, 699-723 (1997).

17. Ibrahimi, A. et al. Highly Efficient Multicistronic Lentiviral Vectors with Peptide 2A Sequences. *Human Gene Therapy* **20**, 845-860 (2009).

18. Szymczak, A.L. et al. Correction of multi-gene deficiency in vivo using a single "self-cleaving" 2A peptide-based retroviral vector. *Nat. Biotech.* **22**, 589-594 (2004).

19. Carey, B.W. et al. Reprogramming of murine and human somatic cells using a single polycistronic vector. *Proceedings of the National Academy of Sciences* **106**, 157-162 (2008).

20. Musse, A.A., Meloty-Kapella, L. & Weinmaster, G. Notch ligand endocytosis: Mechanistic basis of signaling activity. *Seminars in Cell & Developmental Biology* **23**, 429-436 (2012).

21. Cao, Yi. LAPJV - Jonker-Volgenant Algorithm for Linear Assignment Problem, MATLAB Central File Exchange (2010).

22. Jonker, R. & Volgenant, A. A shortest augmenting path algorithm for dense and spare linear assignment problems. *Computing* **38**, 325-340 (1987).

Chapter 5

Conclusion

We have succeeded in using the path toward synthetic reconstitution of developmental spatial pattern to elucidate the operation of natural systems. In the first place, we quantified the relationship between signaling through Notch1 and the combination of activating *trans* Dll1 and inhibitory *cis* Dll1. We achieved this by time-lapse microscopy to measure fluorescent readouts of Notch signaling and levels of *cis* Dll1. The finding, that by contrast with gently graded *trans* activation the *cis* interaction varies sharply with the quantity of *cis* ligand, led us to conclude that *cis*-inhibition is strong and mutually inhibitory. We further came to understand that this property of the signaling system leads it to drive cells into exclusive signal 'sending' or 'receiving' states and thus function effectively as an amplifier of small differences on short lengthscales, shedding light on why it might be involved in certain types of developmental pattern and not in others.

Based on this finding, we see that the signaling system does not merely serve as a conduit for transmitting information but in itself encodes a type of logic that shapes the message. Thus, in order to have any reasonable expectation of anticipating the outcome of a given feedback circuit downstream of Notch signaling we must consider not only the feedback properties but how they interact with, or are interpreted by, the signaling system. Due to a lack of awareness of *cis* inhibition's nature, previous theoretical studies have been incomplete in this regard. Our modeling allowed us to arrive at a number of conclusions regarding the potential role of Notch in several developmental patterns. By showing that the Notch system without feedback converts a shallow gradient of ligand expression into a sharply-defined band of signal activity, we have suggested an explanation for the

ratiometric dependence on Notch and Delta dosages in the sharpening of *Drosophila* wing vein boundaries. Additionally, we discovered that mutual *cis* inhibition relaxes constraints on feedbacks driving a lateral inhibition pattern, and allows an especially simple feedback of Notch signaling upregulating Notch expression to generate lateral inhibition patterning. Lastly, in modeling a lateral induction feedback downstream of Notch signaling, we have proposed a possible mechanism for generating uniform spatially-limited populations of cells and identified a spatiotemporal pattern that may be experimentally accessible because of the *cis* inhibition of receptor and ligand.

These insights simultaneously provide guidance for synthetic reconstitution attempts that might use them to make choices in feedback architecture, and to researchers in model systems for whom the properties of regulation our theoretical work finds potentially influential in spatial patterning can serve as motivation for specific experiments. Along the lines of the former, we have implemented a pattern-forming feedback downstream of the Notch signaling system in mammalian cell culture: upregulation of Delta by Notch signaling, referred to as lateral induction. We were able to conclude that the dynamics of signaling in lateral induction cells are consistent with the negative influence of *cis* inhibition, limiting the amount of ligand produced. The addition of an amplifier generated a cell line with three crucial properties: (i) bimodality in the amount of ligand, (ii) transitions to the high-ligand state induced by exposure to *trans* ligand, and (iii) a high-ligand state that sends signal in *trans* to neighboring cells. Taken together, we conclude that this cell line incorporating both lateral induction and a positive feedback amplifier is capable of spatially propagating a Notch signal in cell culture.

Altogether, we have quantitatively characterized a widely-used signaling system, elucidated an element of its signal transduction mechanism, and computed the expected effects of the mechanism in developmentally-relevant contexts. Using this system we have implemented a lateral induction feedback, and by adding an intracellular positive feedback to the circuit generated a cell line that by our characterization is capable of spatially propagating Notch signal.

Future directions

The Notch system is considerably more complex than a single pair of receptor and ligand. Specific combinations of the four mammalian Notch family members and the five canonical mammalian DSL ligands are used in any given developmental context — for instance, the lateral induction processes around the artery to specify smooth muscle [1] and in the inner ear to define prosensory patches [2] are both mediated by the Jagged1 ligand. With the knowledge that different Notch/DSL receptor/ligand pairs have different affinities for one another, both in *cis* and in *trans*, and the indications from our modeling that those parameters are important determinants of pattern outcomes, it would be a logical extension of this program to expand the repertoire of Notch receptors and DSL ligands. In a similar vein, modulators of the Notch signaling pathway can also be used to tune system parameters to access different patterning regimes.

Beyond the Notch system, there is work ongoing in the lab on the study and potential uses of other signaling systems in other patterning processes. In light of our findings that the Notch system is in a sense optimized for certain type of pattern by its particular mechanism (juxtacrine, with mutual *cis* inactivation), one could ask if other signaling systems are similarly suited to the functions they perform. Furthermore, while in this work we have implemented intracellular feedback circuits exclusively through transcriptional regulation, utilizing other modes of regulation in the feedback may alter the system dynamics and permit another level of control over the patterning outcome. It would be very interesting to see to what extent regulatory mechanisms that operate exclusively or predominantly in one type of organism might translate to others, and what kinds of processes are enabled by those combinations.

The potential for efficiently manipulating mammalian cells in culture with arbitrary constructs encoding any of the diverse regulatory mechanisms known to occur, or yet to be discovered, and using those to achieve desired patterning outcomes is tremendously exciting for the opportunities it will allow. In basic science it will provide us with fundamental insights into understanding how natural systems operate, by allowing us to probe patterning behaviors in more experimentally accessible conditions with a greater degree of control. In the longer term, the insights we gain can potentially

lead to translational applications where generating spatially-structured populations of cells might be clinically applied in efforts such as artificial organ generation.

References

1. Manderfield, L.J. *et al.* Notch activation of Jagged1 contributes to the assembly of the arterial wall. *Circulation* **125**, 314-323 (2012).

2. Hartman, B.H., Reh, T.A. & Bermingham-McDonogh, O. Notch signaling specifies prosensory domains via lateral induction in the developing mammalian inner ear. *PNAS* **107**, 15792-15797 (2010).